frontiers | Research Topics

Case reports in PET imaging

Edited by
Silvia Taralli, Natale Quartuccio and Gaurav Malviya

Published in
Frontiers in Medicine

ISSN 1664-8714
ISBN 978-2-83251-071-1
DOI 10.3389/978-2-83251-071-1

About Frontiers

Frontiers is more than just an open access publisher of scholarly articles: it is a pioneering approach to the world of academia, radically improving the way scholarly research is managed. The grand vision of Frontiers is a world where all people have an equal opportunity to seek, share and generate knowledge. Frontiers provides immediate and permanent online open access to all its publications, but this alone is not enough to realize our grand goals.

Frontiers journal series

The Frontiers journal series is a multi-tier and interdisciplinary set of open-access, online journals, promising a paradigm shift from the current review, selection and dissemination processes in academic publishing. All Frontiers journals are driven by researchers for researchers; therefore, they constitute a service to the scholarly community. At the same time, the *Frontiers journal series* operates on a revolutionary invention, the tiered publishing system, initially addressing specific communities of scholars, and gradually climbing up to broader public understanding, thus serving the interests of the lay society, too.

Dedication to quality

Each Frontiers article is a landmark of the highest quality, thanks to genuinely collaborative interactions between authors and review editors, who include some of the world's best academicians. Research must be certified by peers before entering a stream of knowledge that may eventually reach the public - and shape society; therefore, Frontiers only applies the most rigorous and unbiased reviews. Frontiers revolutionizes research publishing by freely delivering the most outstanding research, evaluated with no bias from both the academic and social point of view. By applying the most advanced information technologies, Frontiers is catapulting scholarly publishing into a new generation.

What are Frontiers Research Topics?

Frontiers Research Topics are very popular trademarks of the *Frontiers journals series*: they are collections of at least ten articles, all centered on a particular subject. With their unique mix of varied contributions from Original Research to Review Articles, Frontiers Research Topics unify the most influential researchers, the latest key findings and historical advances in a hot research area.

Find out more on how to host your own Frontiers Research Topic or contribute to one as an author by contacting the Frontiers editorial office: frontiersin.org/about/contact

Case reports in PET imaging

Topic editors

Silvia Taralli — UOC di Medicina Nucleare, Dipartimento di Diagnostica per Immagini, Radioterapia Oncologica ed Ematologia, Fondazione Policlinico Universitario A. Gemelli IRCCS, Italy

Natale Quartuccio — Azienda Ospedaliera Ospedali Riuniti Villa Sofia Cervello, Italy

Gaurav Malviya — University of Glasgow, United Kingdom

Citation

Taralli, S., Quartuccio, N., Malviya, G., eds. (2023). *Case reports in PET imaging*. Lausanne: Frontiers Media SA. doi: 10.3389/978-2-83251-071-1

Table of contents

frontiers | Frontiers in Medicine

TYPE Editorial
PUBLISHED 02 December 2022
DOI 10.3389/fmed.2022.1087583

OPEN ACCESS

EDITED AND REVIEWED BY
Michel Goldman,
Université Libre de Bruxelles, Belgium

*CORRESPONDENCE
Silvia Taralli
silvia.taralli@hotmail.it

SPECIALTY SECTION
This article was submitted to Nuclear Medicine, a section of the journal Frontiers in Medicine

RECEIVED 02 November 2022
ACCEPTED 16 November 2022
PUBLISHED 02 December 2022

CITATION
Taralli S, Quartuccio N and Malviya G (2022) Editorial: Case reports in PET imaging. *Front. Med.* 9:1087583. doi: 10.3389/fmed.2022.1087583

Editorial: Case reports in PET imaging

Silvia Taralli[1]*, Natale Quartuccio[2] and Gaurav Malviya[3]

[1]Nuclear Medicine Unit, Dipartimento di Diagnostica per Immagini, Radioterapia Oncologica ed Ematologia, Fondazione Policlinico Universitario Agostino Gemelli IRCCS, Rome, Italy, [2]Nuclear Medicine Unit, Ospedali Riuniti Villa Sofia-Cervello, Palermo, Italy, [3]Translational Molecular Imaging, Cancer Research UK Beatson Institute, Glasgow, United Kingdom

KEYWORDS

cancer, diagnostics, case report, PET imaging, ^{18}F-FDG

Editorial on the Research Topic
Case reports in PET imaging

Advanced hybrid nuclear imaging technology, including Positron Emission Tomography together with Computed Tomography (PET/CT) or Magnetic Resonance Imaging (PET/MRI), allowing the simultaneous collection of anatomical and functional information, has been gaining significant attention in recent years and has spurred clinical research interests. This Research Topic comprises 12 unique case reports that highlight the role of ^{18}F-FDG PET imaging (mostly using PET/CT, with PET/MRI used in a number of cases) in addressing correct differential diagnosis of malignant and benign lesions, guiding the clinical management of patients with an uncommon disease, a challenging diagnosis, or an atypical presentation.

Primary cardiac tumors are very rare (0.001–0.03%), with cardiac paraganglioma (CPGL) representing only 1–3% of cardiac tumors. In this Research Topic, a multimodality imaging case report on unusual CPGL is included, demonstrating that the combination of ^{18}F-FDG PET/CT and cardiac magnetic resonance (CMR) offers a useful, non-invasive tool for pre-operative detection and staging of CPGL, which may increase prognosis rates and decrease post-operative complications (Huang et al.). Degrauwe et al. (1) recently demonstrated a similar finding, with CMR and ^{18}F-FDG PET/CT providing a unique combination for the proper characterization of morphological and metabolic features in such a tumor. ^{18}F-FDG PET/CT can also help in challenging cases of paraganglioma arising at uncommon primary sites such as the bladder (Taninokuchi Tomassoni et al.). Although ^{68}Ga-DOTANOC is the most suitable PET radiotracer for identifying bladder paragangliomas (BPGs), ^{18}F-FDG may still be a valid and more easily accessible alternative. In the case described in this article, dynamic ^{18}F-FDG PET/CT was used to reach a correct diagnosis, with BPG showing early ^{18}F-FDG uptake and wash-out in the delayed 1-h acquisition phase.

Similarly, pheochromocytoma is another rare neuroendocrine tumor (2). The case presented by Feng et al. is a good clinical example of the usefulness of PET/CT for detecting pathological findings in patients with pheochromocytoma. The patient evaluated had a history of resected bilateral malignant adrenal pheochromocytoma. After dizziness, hypertension, and bilateral iliac pain for 2 months, a PET/CT was performed, detecting nodal and bone ^{18}F-FDG-avid metastases, along with an increased uptake

in brown fat in the intercostal muscles, consistent with high levels of catecholamine serum secretion.

Another relatively rare disease, reported in a 3-year-old child, is alveolar rhabdomyosarcoma (ARMS) (Zhang et al.), which is characterized by its aggressive behavior, poor prognosis, and unfavorable outcome. ARMS may be present in critical organs and can invade the spinal canal that leads to the central nervous system; nevertheless, clinical symptoms can be variable, depending on the size and site of the retroperitoneal mass and distant metastases (3). In this patient, a post-operative biopsy and FKHR gene rupture confirmed ARMS, while PET imaging helped to reveal retroperitoneal lymphatic metastases, which was not detected by CT imaging or ultrasound. The authors also emphasized that retroperitoneal ARMS requires careful differentiation, potentially being misdiagnosed as neuroblastoma, which is a very common pediatric extra-cranial, solid tumor. The advantage of using ^{18}F-FDG PET/CT for pediatric patients lies in the possibility to evaluate disease activity and therefore guide therapy and prognostication, as is the case for Kaposiform hemangioendothelioma (KHE), a rare vascular neoplasm mostly appearing in infancy or early childhood. A 13-month-old girl with KHE presented with limited movement of the lower extremity caused by spinal involvement and a normal platelet count (Qiu et al.). ^{18}F-FDG PET/CT allowed documentation of mild hypermetabolism in the lesion, consistent with a low-grade tumor, as subsequently confirmed by KHE bioptical diagnosis. Treatment with 6-month sirolimus monotherapy reduced the retroperitoneal lesion's size, alleviating clinical symptoms.

As the diagnosis of occult cancers with unknown primary sites is very complicated and challenging, a biopsy is essential for a confident diagnosis; nevertheless, PET/CT or PET/MRI imaging can contribute, in most cases, to the planning of personalized treatment, precise staging, and improved risk-estimation. Zeng et al. reported a case of rare retroperitoneal clear-cell carcinoma with an unknown primary focus. Although no obvious abnormality was observed in either kidney, *via* imaging (PET/CT and MRI) or surgical exploration, interestingly, immunohistochemistry results confirmed a renal origin of the carcinoma. PET/CT revealed enormous ^{18}F-FDG activity in the retroperitoneal clear-cell carcinoma (as observed in high-grade renal clear-cell carcinomas), likely due to its pathological grade, suggesting that high ^{18}F-FDG uptake could be related to low tumor differentiation.

Besides its widespread oncological application, ^{18}F-FDG PET/CT also plays a key role in inflammatory and infectious settings, where its ability to quantify disease extent, evaluate treatment response, and identify inflammatory occult sites, which remain undetermined after clinical and/or conventional imaging assessment, are exploited (4). In this regard, Tsai et al. demonstrated the additional diagnostic value of ^{18}F-FDG PET imaging for resolving a challenging case of right-sided persistent lower-back pain after an L5-S1 laminectomy, refractory to several different therapies. When initial spinal root MRI imaging was considered inconclusive to support a surgical intervention, a subsequent ^{18}F-FDG PET/MRI revealed increased tracer uptake exclusively along the right S1 root, consistent with the clinical presentation; this metabolic finding allowed the final diagnosis and localization of an inflammatory neuropathy, secondary to epidural fibrosis, with sacral root entrapment. This case highlights the diagnostic value of simultaneous PET/MRI imaging for soft-tissue and spinal cord abnormalities, by combining metabolic and anatomic information.

As stated above, since most tumors demonstrate an increased ^{18}F-FDG uptake (greater than background tissues and benign lesions), metabolic information provided by ^{18}F-FDG PET imaging often plays a crucial role in correctly differentiating malignant and benign diseases. However, the chance of misinterpreting a hypermetabolic benign finding as malignant requires extreme caution from PET readers, particularly in cases of rare diseases or uncommon presentations, which can potentially lead to unnecessary diagnostic or therapeutic procedures, thereby negatively affecting patients' care (5). In this regard, the occurrence of a benign lesion mimicking malignancy was reported in a patient with fast-growing soft tissue nodules confined to the left groin. This was initially suspected as malignant due to conventional imaging features and an increased ^{18}F-FDG uptake at PET/CT (Hu et al.). Unexpectedly, subsequent surgical excision revealed an uncommon localization of Kimura's disease, a rare benign chronic lympho-granulomatous disease. Based on the overall patient history, as well as clinical, laboratory, and imaging data, this case highlights the need to consider differential diagnoses for ^{18}F-FDG-avid lymph nodes, ranging from malignant to inflammatory or infectious diseases, such as lymphoma, nodal metastases, active tuberculosis, sarcoidosis, or benign lympho-proliferative disorders, all of which can show a similar degree of tracer uptake (6). Similarly, Borè et al. reported a paramediastinal hypermetabolic lesion detected by ^{18}F-FDG PET/CT, initially performed for staging in a patient with ovarian cancer and suspected for metastasis or synchronous primitive tumor. After a subsequent biopsy, mediastinal Schwannoma was instead diagnosed, allowing the patient to undergo chemotherapy and ovarian surgery, as initially planned. This case represents a warning for the risk of PET false positives that, particularly in oncological patients, may result in incorrect upstaging, in turn potentially leading to changes in the planned therapeutic management and consequently, exposing patients to overtreatment and associated toxicity risks. Conversely, the chance of misinterpreting a low ^{18}F-FDG-avid tumor as a benign lesion requires careful consideration, with low metabolic activity in malignant lesions mainly related to low glucose metabolism (reflecting histologically and clinically less-aggressive tumor behavior), low cellularity, or small size (7). For example, oligo-vertebral plasma cell myeloma localizations, characterized by the coexistence of mild ^{18}F-FDG uptake and morpho-structural

changes, may overlap with the morpho-functional features of a vertebral hemangioma, potentially delaying tumor diagnosis and treatment (Hu et al.).

Author contributions

ST, NQ, and GM drafted the manuscript and critically revised the final version. All authors gave their final approval for manuscript submission.

Acknowledgments

We wish to thank all authors who contributed articles to this Research Topic and all those who participated as reviewers.

Conflict of interest

The authors declare that the research was conducted in the absence of any commercial or financial relationships that could be construed as a potential conflict of interest.

Publisher's note

References

1. Degrauwe S, Monney P, Qanadli SD, Prior J, Beigelmann-Aubry C, Masci P, et al. Intrapericardial paraganglioma: the role of integrated advanced multi-modality cardiac imaging for the assessment and management of rare primary cardiac tumors. *Cardiol J.* (2017) 24:447–9. doi: 10.5603/CJ.2017.0091

2. Garcia-Carbonero R, Matute Teresa F, Mercader-Cidoncha E, Mitjavila-Casanovas M, Robledo M, Tena I, et al. Multidisciplinary practice guidelines for the diagnosis, genetic counseling and treatment of pheochromocytomas and paragangliomas. *Clin Transl Oncol.* (2021) 23:1995–2019. doi: 10.1007/s12094-021-02622-9

3. Fayolle H, Jehanno N, Lauwers-Cances V, Castex M-P, Orbach D, Mognetti T, et al. PET metabolic tumor volume as a new prognostic factor in childhood rhabdomyosarcoma. *PLoS ONE.* (2022) 17:e0261565. doi: 10.1371/journal.pone.0261565

4. Treglia G. Diagnostic performance of 18F-FDG PET/CT in infectious and inflammatory diseases according to published meta-analyses. *Contrast Media Mol Imaging.* (2019) 2019:3018349. doi: 10.1155/2019/3018349

5. Metser U, Even-Sapir E. Increased (18)F-fluorodeoxyglucose uptake in benign, nonphysiologic lesions found on whole-body positron emission tomography/computed tomography (PET/CT): accumulated data from four years of experience with PET/CT. *Semin Nucl Med.* (2007) 37:206–22. doi: 10.1053/j.semnuclmed.2007.01.001

6. Zeman MN, Green C, Akin EA. Spectrum of [^{18}F]FDG-PET/CT findings in benign lymph node pathology. *Mol Imaging Biol.* (2021) 23:469–80. doi: 10.1007/s11307-020-01576-8

7. Kwee TC, Cheng G, Lam MG, Basu S, Alavi A. SUVmax of 2.5 should not be embraced as a magic threshold for separating benign from malignant lesions. *Eur J Nucl Med Mol Imaging.* (2013) 40:1475–7. doi: 10.1007/s00259-013-2484-x

frontiers in Medicine

CASE REPORT
published: 15 May 2018
doi: 10.3389/fmed.2018.00143

Impact of an 18F-FDG PET/CT Radiotracer Injection Infiltration on Patient Management—A Case Report

Jackson W. Kiser[1]*, *James R. Crowley*[1], *David A. Wyatt*[1] and *Ronald K. Lattanze*[2]

[1] Carilion Clinic, Roanoke, VA, United States, [2] Lucerno Dynamics, Cary, NC, United States

Major management decisions in patients with solid tumors and lymphomas are often based on 18F-fluorodeoxyglucose (18F-FDG) PET/CT. The misadministration of 18F-FDG outside the systemic circulation can have an adverse impact on this test's sensitivity (1) and is not uncommon (2–7). This report describes how an 18F-FDG misadministration led to a repeat PET/CT study, resulting in the visualization of distant metastases that changed the original treatment plan. The findings suggest that routine injection monitoring is indicated whenever sensitivity is critical, and support claims that infiltrations can confound interpretation of semi-quantitative PET outcome measures in patients who are followed longitudinally (2).

Keywords: PET-CT, extravasation of diagnostic and therapeutic materials, SUV, FDG, time activity curve

OPEN ACCESS

Edited by:
Ronan Abgral,
Centre Hospitalier Regional Universitaire (CHU) de Brest, France

Reviewed by:
Vikram R. Lele,
Jaslok Hospital, India
Xavier Palard-Novello,
University of Rennes 1, France

***Correspondence:**
Jackson W. Kiser
jwkiser@carilionclinic.org

Specialty section:
This article was submitted to Nuclear Medicine, a section of the journal Frontiers in Medicine

Received: *12 February 2018*
Accepted: *25 April 2018*
Published: *15 May 2018*

Citation:
Kiser JW, Crowley JR, Wyatt DA and Lattanze RK (2018) Impact of an 18F-FDG PET/CT Radiotracer Injection Infiltration on Patient Management—A Case Report. Front. Med. 5:143. doi: 10.3389/fmed.2018.00143

Precision medicine has been increasingly in the news[1]. A year-by-year review of The New England Journal of Medicine shows the term "precision medicine" has increased over 15-fold from 2012–2013 to 2016. Positron Emission Tomography (PET), a crucial imaging tool in oncology care (8), plays a vital role in precision medicine. In 2017, it had been projected that nearly 3 million PET/CT scans would be performed in the US, with ∼2.9 million scans used for oncology applications (9). While coordinated efforts to develop and encourage the adoption of guidelines and standards continue to minimize variability in molecular imaging results (10, 11), the radiotracer injection process remains susceptible to error.

The seminal quantitative 18F-FDG PET studies in the 1970's and 1980's were based on bolus injections (12). This practice continues today with an emphasis on precision. Guidelines continue to prescribe quality assurance procedures that have relatively small influence on variability such as: measuring residual activity after injection and synchronizing clocks (11). However, errors in the physical delivery of the 18F-FDG have the potential to introduce significant variability (1). These para-venous injections are known as infiltrations or extravasations. While only a few centers have published or presented on infiltrations, a critical review shows their aggregated rate is about 15% (423 infiltrations in 2,802 patients (2–7).

In an 18F-FDG administration that conforms to expectations, the entire injected dose is delivered to systemic circulation, and therefore, is the same dose used in the Standardized Uptake Value (SUV) calculation. An infiltration creates an unknown mismatch between the calculated injected dose and the actual dose delivered in circulation. Some of the infiltrated dose remains near the injection site and returns to systemic circulation largely through lymphatic reabsorption at an unknown rate during the prescribed uptake period. These problems alter the supply and clearance of the radiotracer to the tissue in an unknown way and reduces the calculated SUV. The quality of the image can also be degraded by an infiltration through the delivery of an inadequate 18F-FDG

[1]Google Trends Search. Available online at https://trends.google.com/trends/explore?date=all&q=precision%20medicine (Accessed August 27, 2017).

dose and through the continuous recovery of the radiotracer from the infiltration site, without enough time for subsequent clearance in the circulation.

Appropriately characterizing the quality of the radiotracer injection is difficult. While abnormal uptake at the injection site is evidence of an infiltration (11), the PET/CT field of view (FOV) often excludes the injection site (2). When an injection site is in the FOV, visualization and measurement of abnormal uptake may underestimate the true extent of an infiltration, since PET/CT static images are acquired ∼60 min post-injection and cannot represent the state of infiltration as it resolved during the uptake period (13). A recent presentation, demonstrating dynamic PET/CT images and time-activity curves (TACs) from the uptake period, highlighted "invisible infiltrations" and how their visual evidence resolves completely before the acquisition of static PET/CT images (14). These invisible infiltrations appear as prolonged venous stasis and also contribute to the difficulty in characterizing 18F-FDG administrations using the PET/CT image. These issues suggest that the field needs an effective means to monitor the quality of the administration.

Our nuclear imaging facility is participating in a multi-center quality improvement project that uses a novel device to characterize each 18F-FDG injection. The goal is to reduce the overall infiltration rate. The device provides real-time quality control and addresses these issues that tend to confound proper injection assessment by providing TACs from the injection site during the uptake period. After a period of extended use, the device's quality assurance software provides an analysis of injection techniques and factors that can help improve a facility's performance. We encountered this case during this project.

CASE PRESENTATION

In 2017, a 60–70 year-old male who never smoked tobacco presented with chest pain and weight loss, which prompted a chest X-ray and subsequent CT. The CT revealed a left upper lobe mass with no evidence of nodal involvement or metastases. A staging 18F-FDG PET/CT scan confirmed the presence of a single, large, lung mass; however, the quality and quantification of the image was potentially impacted by a relatively severe infiltration in the right antecubital fossa (**Figure 1**). The patient was immediately repositioned on the imaging table with their arms over their head for another PET imaging session. This image confirmed the presence of the single, large, lung mass. Biopsy of the mass revealed a non-small cell lung cancer.

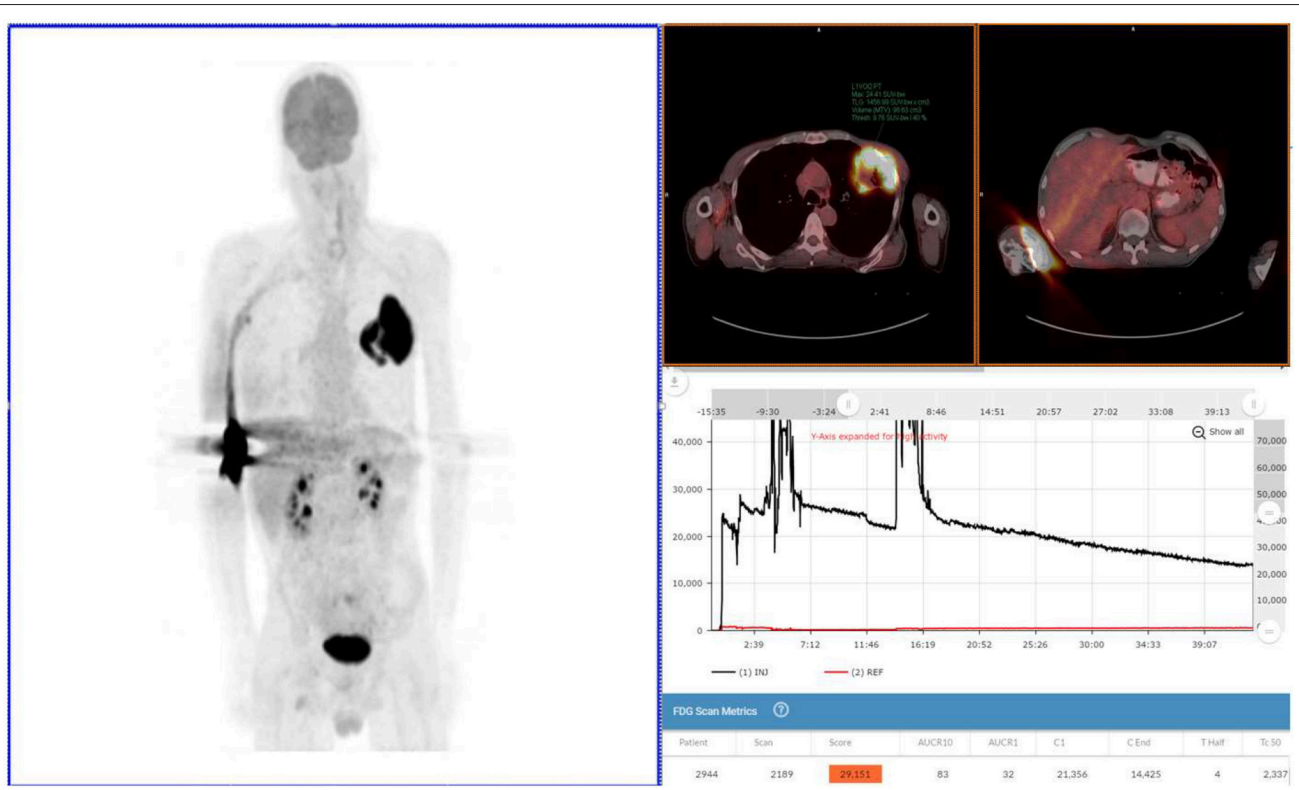

FIGURE 1 | Exam 1—maximum intensity projection image, fused axial images, and time-activity curves of baseline PET/CT scan. MIP image (above left image), taken 61 min post-injection, reveals lung mass, and abnormal uptake at right antecubital fossa (radiotracer injection site) and right axilla uptake thought to be the result of the infiltration. Black time-activity curve (lower right image) from injection arm sensor reveals severe infiltration during the first 40 min of the uptake period. Red time-activity curve (also lower right image) from contralateral arm sensor reveals minimal uptake. Fused PET/CT images (upper right images) reveal left upper lobe mass (SUV_{max} 24) and infiltration artifacts at adrenal level. No evidence of metastatic disease.

The patient was invited back for a repeat scan 3 days later to confirm initial staging of T3N0M0. The repeat scan (**Figure 2**) revealed more information about the single lung lesion and also showed new disease: a right adrenal lesion and also a potential prostate lesion, not seen in Exam 1. Based on the new information from the repeated PET/CT scan, staging was revised to T3N0M1.

DISCUSSION

Exam 1

The patient received the standard of care pre-PET/CT scan instructions, fasted appropriately and presented with blood glucose levels of 4.7 mmol/L (85 mg/dL). A Certified Nuclear Medicine Technologist (CNMT) gained access in the right antecubital fossa using a 24-gauge needle and IV cannula. A sensor, comprised of a single scintillating crystal paired with silicon photomultiplier, (Lucerno Dynamics, Cary, NC) was placed topically ∼7 cm proximal to the access site and a second sensor was placed on the opposite arm in a mirrored location. The patient was manually injected with 635 MBq (∼17 mCi) of 18F-FDG and the IV was flushed with 14 mL of saline. After ∼40 min, the sensors were removed and the injection data were downloaded. The resulting injection arm TAC revealed a severe infiltration. At the 61 min post-injection mark, emission images were acquired (Exam 1) on a PET/CT scanner (Siemens Biograph 40, Knoxville, TN) with 3D acquisition. A 3-min per bed acquisition time was performed in a cranial to caudal direction. After review of the PET images, the patient was positioned back on the imaging table with arms over their head. At the 92 min post-injection mark, emission images were acquired.

The patient was invited back for a repeat scan 3 days later in accordance with our center's standard practice to repeat scans that may have been moderately or severely infiltrated.

Exam 2

After fasting appropriately, the patient presented with blood glucose levels of 4.8 mmol/L (87 mg/dL). A CNMT, different from the one 3 days earlier, gained access in the left hand using a 24-gauge needle and IV cannula. Sensors were placed ∼7 cm proximal to the access site and on the opposite arm in a mirrored location. The patient was then manually injected with 572 MBq (∼15.5 mCi) of 18F-FDG. The IV was flushed with 20 mL of saline. After ∼30 min the sensors were removed from the patient and the injection data downloaded. The resulting injection arm TAC revealed a satisfactory 18F-FDG injection. At the 65 min post-injection mark, Exam 2 was performed with identical acquisition, processing parameters, and image analysis software using the same PET/CT scanner.

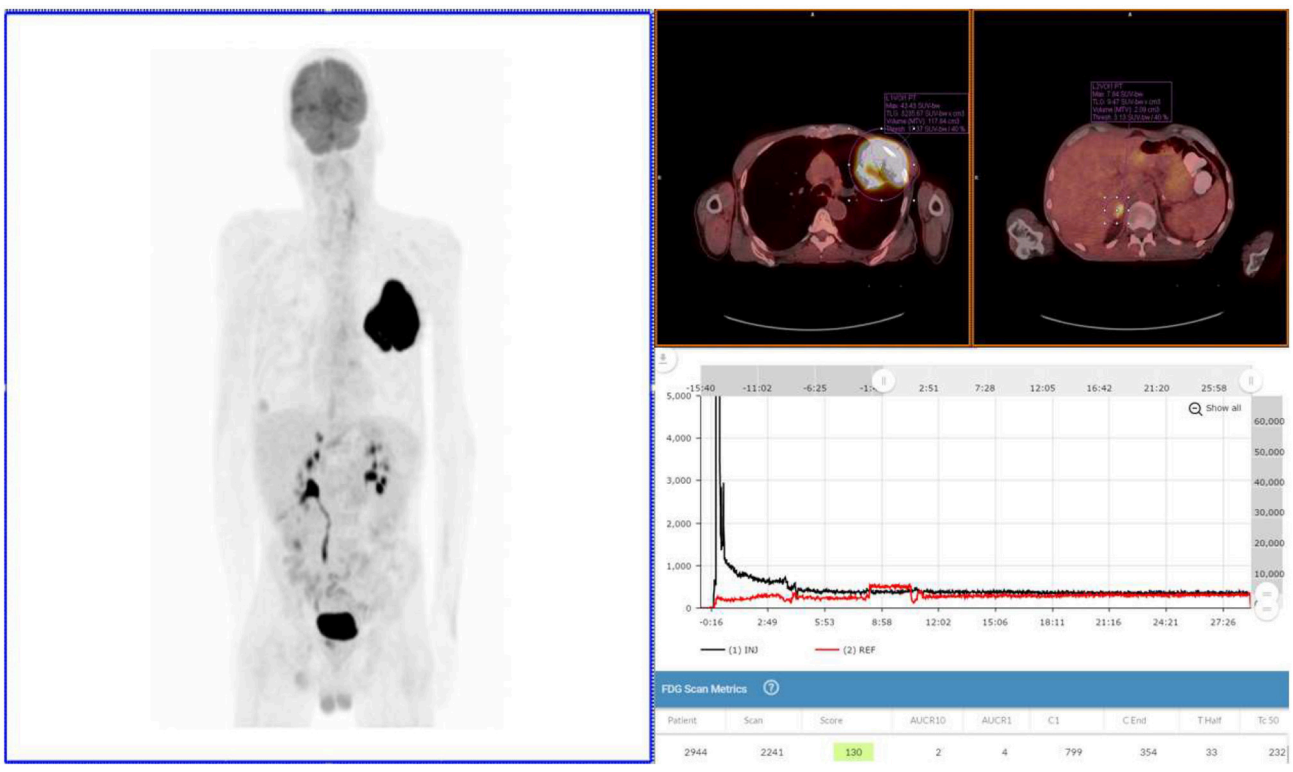

FIGURE 2 | Exam 2—maximum intensity projection image, fused axial images, and time-activity curves of repeat PET/CT Scan. Repeat PET/CT MIP image (above left image), taken 3 days after first PET/CT and 65 min post-injection, reveals lung mass, right adrenal lesion, prostate lesion, and some minimal abnormal uptake in left forearm (radiotracer injection site was left hand). Black time-activity curve (lower right image) from injection arm sensor reveals a nearly ideal injection. Red time-activity curve (also lower right image) from contralateral arm sensor reveals expected uptake. Fused PET/CT images (upper right images) reveal left lobe mass (SUV_{max} 43) and adrenal lesion.

TABLE 1 | Comparison of exam 1 and exam 2.

18F-FDG PET/CT Exam 1	18F-FDG PET/CT Exam 2 (~73 h later)
Blood sugar: 4.7 mmol/L (85 mg/dL)	Blood sugar: 4.8 mmol/L (87 mg/dL)
Injection to scan time: 61 min	Injection to scan time: 65 min
Lung lesion SUV_{max}: 24	Lung lesion SUV_{max}: 43
Adrenal: not initially observed and indeterminate in retrospect	Adrenal: SUV_{max}: 11
Staging: T3N0M0	Staging: T3N0M1
Surgical candidate: Possibly	Surgical candidate: No

SUV, Standardized uptake value.

RESULTS

Exam 1 revealed abnormal uptake at the right antecubital fossa, indicative of a severe infiltration, and a lung lesion with a SUV_{max} of 24. Right axilla uptake was noted, but suspected to be associated with infiltration. No other lesions were noted in the 61 min post-injection images nor in the 92 min post-injection images with arms over the head. Based on biopsy results and the image review, the patient was diagnosed with squamous cell lung cancer and staged as T3N0M0. Surgical debulking and adjuvant therapy were considered as options after discussion with a cardiothoracic surgeon.

Exam 2 revealed the lung lesion with a SUV_{max} of 43, an 80% increase from the Exam 1. A right adrenal lesion was highly suspicious with a SUV_{max} of 11. Another lesion was detected in the prostate region with a SUV_{max} of 5. The significance of the prostate lesion was uncertain in the setting of lung cancer and not strongly considered to represent metastatic disease in this case. No activity was noted in the right axilla, confirming the impact of the infiltration in Exam 1. Based on the image review, staging was altered to T3N0M1, and the planned patient management was changed. A comparison of Exam 1 and Exam 2 can be found in **Table 1**.

CONCLUDING REMARKS

18F-FDG PET/CT has played an increasingly important role in the initial staging of cancer and the assessment of tumor response (15). In precision medicine, this tool will play an even more significant role, using semi-quantitative, or quantitative PET/CT data for single or multi-time-point assessments (e.g., diagnosis, staging, eligibility assessment, or investigation of predicative or prognostic biomarkers) (10).

An infiltration will negatively affect image quality and underestimate an SUV. Depending on the purpose of the scan and awareness of an infiltration, a clinician may be able to salvage some infiltrated scans by delaying imaging 120–180 min post-injection. The extended uptake period may yield better images. However, since an infiltration will confound quantification measures based on the severity of the infiltration, repeating the scan may be a better option. Since multiple PET/CT scans—each requiring an 18F-FDG injection—are used to assess response, the cumulative probability an infiltration will impact the assessment increases with the number of scans. In the current nuclear medicine practice, injections sites that are out of the FOV, invisible infiltrations, and visible infiltrations underestimated due to the static nature of images, can all contribute to the interpreting and treating physicians reaching the wrong conclusion about staging and tumor response to treatment. This single case report demonstrates the major impact an 18F-FDG infiltration can have on PET/CT SUV values and on patient staging; it also suggests that routine injection monitoring is indicated whenever sensitivity of PET/CT scanning is critical.

ETHICS STATEMENT

Extensive efforts were made by the authors to contact the next of kin for consent to the publication of this case report, however this could not be obtained. Efforts have therefore been made to ensure that the case is presented with the minimal amount of potentially identifiable information.

AUTHOR CONTRIBUTIONS

JK: provided images, image analysis, and helped draft the initial submission; JC: provided details of the patient imaging sessions and provided the initial draft of the submission; DW: provided patient details and staging information, and staging considerations; RL: provided time activity curves, created subsequent drafts of the submissions, and coordinated the editing process.

REFERENCES

1. Boellaard R. Standards for PET image acquisition and quantitative image analysis. *J Nucl Med.* (2009) **50**:11S−20S. doi: 10.2967/jnumed.108.057182
2. Osman M, Muzaffar R, Altinyay M, Teymouri C. FDG dose extravasations in PET/CT: frequency and impact on SUV measurements. *Front Oncol.* (2011) **1**:41. doi: 10.3389/fonc.2011.00041
3. Hall N, Zhang J, Reid R, Hurley D, Knopp M. Impact of FDG extravasation on SUV measurement in clinical PET/CT. Should we routinely scan the injection site? *J Nucl Med.* (2006) **47**(Suppl. 1):115P.
4. Krumrey S, Frye R, Tran I, Yost P, Nguyen N, Osman M. FDG manual injection versus infusion system: A comparison of dose precision and extravasation. *J Nucl Med.* (2009) **50**(Suppl. 2):2031.
5. Bains A, Botkin C, Oliver D, Nguyen N, Osman M. Contamination in 18F-FDG PET/CT: An initial experience. *J Nucl Med.* (2009) **50**(Suppl. 2):2222.
6. Silva-Rodriguez J, Aguiar P, Sanchez M, Mosquera J, Luna-Vega V, Cortés J, et al. Correction for FDG PET dose extravasations: Monte Carlo validation and quantitative evaluation of patient studies. *Med Phys.* (2014) **41**:052502. doi: 10.1118/1.4870979
7. McMunn A, Lattanze R. Pilot quality improvement study for PET/CT radiotracer injection process. *J Nucl Med.* (2017) **58**(Suppl. 1):788.

8. Kinahan PE, Mankoff DA, Linden HM. The value of establishing the quantitative accuracy of PET/CT Imaging. *J Nucl Med.* (2015) **56**:1133–34. doi: 10.2967/jnumed.115.159178
9. Daher NM. *US Nuclear Medicine and PET Imaging Systems Market.* Market Engineering Reports 2014 (Accessed August 17, 2017).
10. Graham M, Wahl R, Hoffman J, et al. Summary of the UPICT protocol for ^{18}F-FDG PET/CT imaging in oncology clinical trials. *J Nucl Med.* (2015) **56**:955–61. doi: 10.2967/jnumed.115.158402
11. FDG-PET/CT Technical Committee. *FDG-PET/CT as an Imaging Biomarker Measuring Response to Cancer Therapy, Quantitative Imaging Biomarkers Alliance, Version 1.05*. QIBA. Available from: RSNA.ORG/QIBA (Accessed December 11, 2013).
12. Alavi A, Reivich M. The conception of FDG-PET imaging. Sem Nucl Med. (2002) **32**:2–5. doi: 10.1053/snuc.2002.29269
13. Williams JM, Arlinghaus LR, Rani SD, et al. Towards real-time topical detection and characterization of FDG dose infiltration prior to PET imaging. *Eur J Nucl Med Mol Imag.* (2016) **43**:2374–80. doi: 10.1007/s00259-016-3477-3
14. Osman M, Townsend D, Frye S, Lattanze R, Muzzafar R. Prolonged venous stasis: invisible intravenous FDG infiltrations and potential negative implications in PET/CT examination. *J Nucl Med.* (2017) **58**(Suppl. 1):699.
15. Jones T, Townsend D. History and future technical innovation in positron emission tomography. *J Med Imaging* (2017) **4**:011013. doi: 10.1117/1.JMI.4.1.011013

Conflict of Interest Statement: RL was employed by company Lucerno Dynamics.

The other authors declare that the research was conducted in the absence of any commercial or financial relationships that could be construed as a potential conflict of interest.

frontiers in Medicine

CASE REPORT
published: 08 October 2018
doi: 10.3389/fmed.2018.00275

False Positive 18F-FDG Positron Emission Tomography Findings in Schwannoma—A Caution for Reporting Physicians

Paul Boré[1], Renaud Descourt[1], Luc Ollivier[2], Pierre-Yves Le Roux[3] and Ronan Abgral[3]*

[1] Service d'Oncologie Médicale, Centre Hospitalier Régional et Universitaire de Brest, Université de Bretagne Occidentale, Brest, France, [2] Service de Radiothérapie, Centre Hospitalier Régional et Universitaire de Brest, Université de Bretagne Occidentale, Brest, France, [3] Service de Médecine Nucléaire, EA 3878 (GETBO) IF 148, Centre Hospitalier Régional et Universitaire de Brest, Université de Bretagne Occidentale, Brest, France

Schwannoma is a rare source of false-positive 18F-fluorodeoxyglucose (18F-FDG) uptake in Positron-emission tomography (PET/CT), inducing potential errors in staging of several solid cancer, with implications for patient management. This clinical case reports the situation of a patient undergoing an 18F-FDG-PET/CT for initial staging of an ovarian adenocarcinoma. We found a high paramediastinal hypermetabolic mass suspicious of remote extension or secondary synchronous primitive tumor. The biopsy finally reveals a histopathology of Schwannoma, allowing the patient to be eligible for a surgical procedure of her ovarian adenocarcinoma by rejecting the hypothesis of malignancy.

Keywords: positron-emission tomography, schwannoma, neoplasm staging, ovarian neoplasms, mediastinal neoplasms

OPEN ACCESS

Edited by:
Anil Kumar Mishra, Institute of Nuclear Medicine & Allied Sciences (DRDO), India

Reviewed by:
Baljinder Singh, Post Graduate Institute of Medical Education and Research (PGIMER), India
Ramin Sadeghi, Mashhad University of Medical Sciences, Iran

****Correspondence:***
Paul Boré
paul.bore@chu-brest.fr

Specialty section:
This article was submitted to Nuclear Medicine, a section of the journal Frontiers in Medicine

Received: *26 July 2018*
Accepted: *10 September 2018*
Published: *08 October 2018*

Citation:
Boré P, Descourt R, Ollivier L, Le Roux P-Y and Abgral R (2018) False Positive 18F-FDG Positron Emission Tomography Findings in Schwannoma—A Caution for Reporting Physicians. Front. Med. 5:275. doi: 10.3389/fmed.2018.00275

BACKGROUND

Even if they are considered as benign tumors, high FDG uptake can be seen in schwannomas, providing a risk of false-positive interpretation with consequences on tumor staging and also management of patient.

For example Martinez-Esteve et al. (1) have reported the case of a patient with a locally advanced HER2 overexpressed breast tumor treated by chemotherapy and Trastuzumab showing a hypermetabolic retro-tracheal lymphadenopathy [15 × 17 mm and standardized uptake value (SUVmax) 4.5]. On the 18F-FDG PET-CT intermediate therapeutic assessment, there was a complete metabolic response except for the retro tracheal lymphadenopathy. The histopathological analysis of this finally excluded a metastatic lesion related to breast cancer and revealed a benign Schwannoma, allowing to continue initial therapeutic strategy.

Moreover, Gorospe et al. (2) have published a case of difficult initial staging of a pulmonary adenocarcinoma of the right upper lobe. Indeed, 18F-FDG PET/CT findings concluded to a suspicious supraclavicular right lymph node (SUVmax 2.6 vs. 2.8 for the primary) and the patient's tumor was restaged into a T3N3M0 IIIB lung cancer vs. T3N0M0 IIB according to WHO classification (3). Before modifying treatment management of patient based on 18F-FDG PET/CT findings, a surgical biopsy was performed and finally concluded again to a schwannoma.

Several other case reports show that schwannomas are usually associated with a high 18F-FDG uptake on PET-CT (4–6). But, cases of schwannomas with low uptake exist even if they are less frequent (7).

Only few cases of schwannoma located in the mediastinum with an 18F-FDG uptake have already been reported in literature.

CASE PRESENTATION

A 75-year-old female patient with previous hystory of active smoking at 75 year-package associated with other cardiovascular risk factors (hypertension, hypercholesterolemia, non-insulin-dependant diabetes, and obesity) has been sent to our university hospital for a suspicion of strangulated umbilical hernia. An abdomen and pelvis CT scan was then performed and found a diffuse infiltration of mesenteric fat evoking a peritoneal carcinosis without primary tumor clearly identified.

An exploring laparoscopy showed a visual aspect of inflammatory peritoneum with a thickened epiploon and non-tumorous ovaries. On the contrary, histopathological examinations (biopsy and cytology) suggested an immunohistochemical profile compatible with high-grade serous papillary carcinoma of ovarian or peritoneal origin. The therapeutic strategy included neo-adjuvant chemotherapy by CARBOPLATIN-PACLITAXEL and interval surgery after 3 cycles.

Moreover, an 18F-fluorodeoxyglucose (18F–FDG) Positron-emission tomography (PET/CT) was performed not to ignore a supra-diaphragmatic remote extension of disease that would exclude surgery indication. In addition to multiple hypermetabolic known peritoneal carcinomatosis lesions (**Figure 1**), PET CT found fortuitly a pathological 18F-FDG uptake upon a high paramediastinal tissue 3 cm mass located at the left pulmonary apex (SUV max: 12.8) (**Figures 2**–**4**). Due to this suspicion of remote extension of disease or secondary primary tumor, a biopsy under CT scan was performed. The histolopatological analysis concluded with an appearance of Schwannoma, without any sign suggestive of malignancy.

While awaiting the histological characterization of this mass, the patient finally benefited from 6 cycles of chemotherapy before surgery by laparotomy. Unfortunately due to carcinomatosis extended to the entire abdominal cavity with a peritoneal index at 19 (8) a complete resection surgery was not possible and new courses of CARBOPLATIN TAXOL were scheduled.

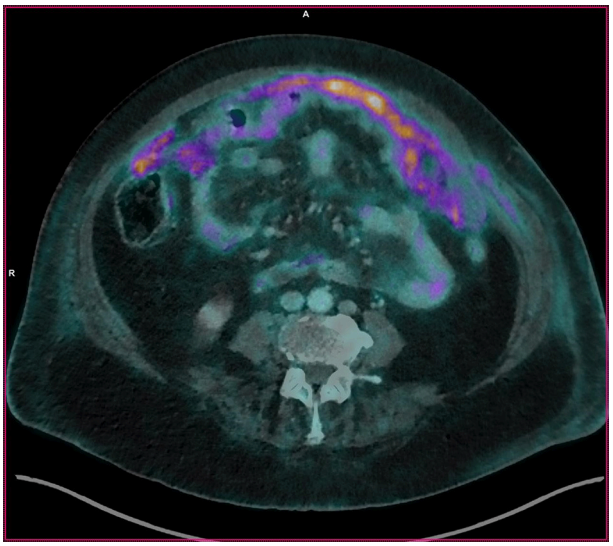

FIGURE 1 | Fusion image in cross section. Image of peritoneal carcinomatosis of the patient.

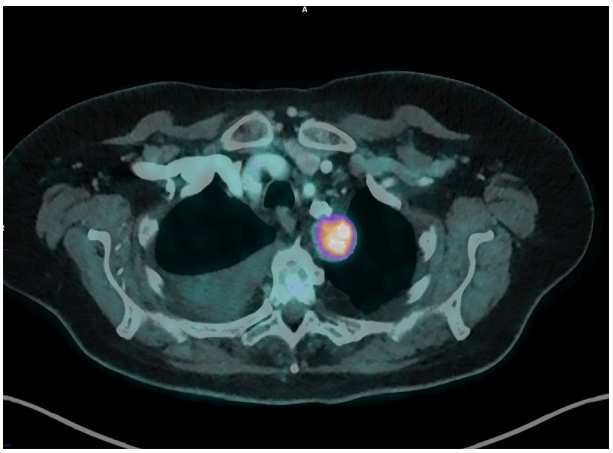

FIGURE 2 | Fusion image in axial cut. It is found that the mass is well-located behind the tracheabronchial axis.

DISCUSSION

Schwannomas are the most common nerve sheath tumors (9) and are usually solitary. Majority of lesions are benign tumors that usually grow slowly [only 2% of them may evolve into a malignant form (10, 11)]. They are often asymptomatic and fortuitly revealed. Microscopically they are well circumscribed with a surrounding capsule and are composed by a clonal population of Schwann cells. There are two components, a highly ordered cellular called Antoni A area (hypercellular area) and a looser myxoid component called Antoni B area. In immunohistochemistry they express the S100 protein (12). Most of them are sporadic tumors. However in few cases, they are associated with neurofibromatosis type 2 disease, Carney's complex, or schwannomatosis. There are also some variants of schwannomas which are cellular schwannoma, plexiform schwannoma, and melanotic schwannoma (13).

This tumor consists of an abnormal proliferation of Schwann cells developped from nerves. The most frequent locations of schwannomas are the brachial plexus or the large nerve trunks of the limbs (particularly elbow, wrist, or knee). Deep forms in retroperitoneum or mediastinum exist and are often of large size (14). In the mediastinum, nerve tumors such as schwannoma are located in the posterior compartment where they account for two-third to 80% of tumors in this localization (15–17). The other most common masses of the posterior mediastinum are meningoceles, para esophageal cysts, goiter, and lymphoma. Three compartments are described in the

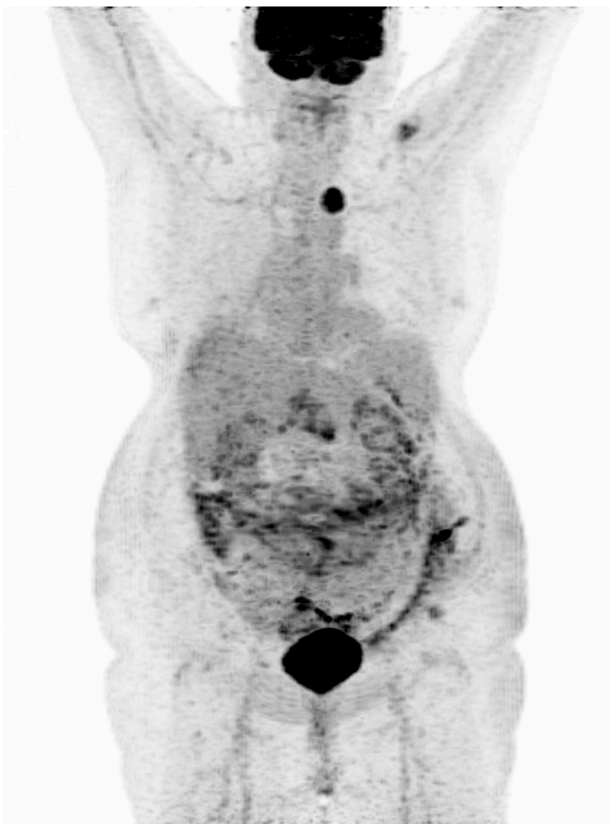

FIGURE 3 | Maximal intensity projection of our patient. Acquisition of broadcoast images realized 60 min after injection of 252 Megabecquerels of FDG-IBA in a vein of the right wrist. Visualization of the supra-diaphragmatic isolated hypermetabolism.

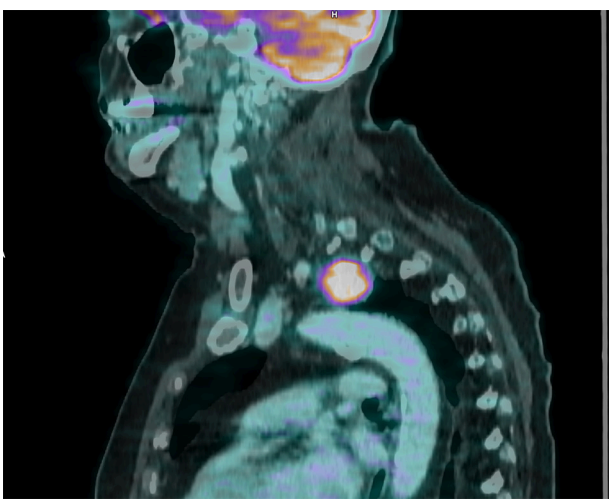

FIGURE 4 | Sagittal cut, fusion image, 30 mm mass above aortic stock, maximum standardized uptake value of 12.8.

mediastinum. The posterior mediastinum is the paravertebral zone bounded by the posterior trachea and pericardium, the diaphragm, the vertebral column, and the thoracic inlet (18). The anterior mediastinum is the prevascular zone and the middle mediastinum is the peri-tracheoesophageal zone (17). Regarding the other compartments, lymphoma, germinal tumor, and thymic tumors are typically located in the anterior (19) and lymphadenopathy and lymphoma in the middle mediastinum.

On imaging, schwannomas occur on the path of a nerve, are well-limited, often oval and unique. The metabolic characteristics of schwannomas on 18F-FDG PET-CT are not well-described in literature to differentiate benign or malignant forms. Ahmed et al. did not found an association between SUV and benign schwannoma or malignant tumor (20).

Beaulieu et al. (21) compared the FDG uptake with Schwannoma cellularity, tumor size and tumor proliferation rate (Ki-67 index). The SUVmax varied from 1.9 to 7.2 (mean = 4.6; $n = 9$). They found that the SUV max of the hypocellular tumors was significantly lower than the SUV max of the hypercellular tumors (composed by a larger; $p = 0.010$). They did not found an association between SUVmax and tumor size or Ki-67 index. They did not find why there is a high FDG accumulation in benign tumors such as schwannoma.

In a study of 22 histologically proven schwannomas, Miyake et al. (22) did not find a correlation between expression of glucose transporters (GLUTs) and SUVmax of the lesions that could explain why there is a high FDG accumulation in this tumors. Moreover, SUVmax ranged from 1.5 to 17.3 with a median of 3.7 and factors significantly associated with higher SUVmax were gastrointestinal origin ($p = 0.007$) and the presence of peri-tumor lymph nodes ($p < 0.001$).

More recently it has been showed that schwannomas with18F-Dihydroxyphenylalanine (DOPA) uptake (23) and also in 68Ga-Prostate-specific membrane antigen (PSMA) PET-CT (24).

It therefore seems difficult to conclude to a diagnosis of Schwannoma only based on SUV characteristics on PET-CT since their SUVmax seems to vary enormously. There is also several other causes of known false positives such as infectious and inflammatory processes.

Several cases reporting masses to PET-CT with hypermetabolism in follows-up of tumoral pathologies have been described, and these hypermetabolisms are generally associated with malignant tumors. However as described earlier that is not always true. Schwannomas with an 18F-FDG uptake have been described but especially outside the mediastinum. To our knowledge only few publications report this situation in the mediastinum. This case confirms the necessity to be aware of a neurogenic tumor when the PET reader concludes to a hypermetabolic mass of the posterior mediastinum and especially if it can lead to a change in patient care.

CONCLUDING REMARKS

Schwannoma is a potential cause of 18F-FDG false positive uptake in PET-CT, inducing risk of worse staging or therapeutic assessment, with consequences on patient management. Currently there are no reliable argument to differentiate a benign Schwannoma from a malignant tumor only on 18F-FDG-PET-CT imaging. This case report also recalls the need to biopsy

doubtful lesions fortuitly discovered on 18F-FDG-PET-CT in order to avoid a loss of chance and possible complications related to unnecessary treatment toxicities.

ETHICS STATEMENT

All procedures performed in this study were in accordance with the ethical standards of the institutional research committee on human experimentation and with the Helsinki Declaration of 1975, as revised in 2008. Ethical review and approval was not required in accordance with the national and institutional requirements. The patient provided written informed consent.

AUTHOR CONTRIBUTIONS

PB provided details of the patient and provided initial draft of submission. RD provided details of the patient and helped draft the initial submission. P-YL and RA provided images, image analysis, and helped draft the initial submission. LO helped draft the initial submission.

REFERENCES

1. Martínez-Esteve A, Álvarez-Pérez RM, Pachón-Garrudo VM, González-Mancha R, Borrego-Dorado I. Mediastinal schwannoma mimicking lymph node metastasis from locally advanced breast cancer in a (18)F-FDG PET/CT study. *Rev Esp Med Nucl Imagen Mol.* (2016) 35:272–3. doi: 10.1016/j.remn.2015.11.001
2. Gorospe L, Rioja-Martín ME, Santos-Carre-o AL, Pacios-Blanco RE, Muoz-Molina GM. Supraclavicular schwannoma mimicking a lymphadenopathy in a lung cancer patient: PET/CT findings. *Lung Cancer* (2017) 110:74–6. doi: 10.1016/j.lungcan.2017.06.001
3. Goldstraw P. The 7th Edition of the TNM Classification for Lung Cancer: Proposals from the IASLC Staging Project. *Eur J Cancer Suppl*. (2007) 5:15–22. doi: 10.1016/S1359-6349(07)70018-6
4. Wang S, Luo D, Chen G, Liu E, Wang S. FDG PET/CT of intercostal schwannoma. *Clin Nuclear Med*. (2016) 41:e310–2. doi: 10.1097/RLU.0000000000001151
5. Yap J, Huang Y, Lin M. Detection of synchronous gastric schwannoma on FDG PET/CT aided by discordant metabolic response. *Clin Nuclear Med*. (2015) 40:e287–9. doi: 10.1097/RLU.0000000000000724
6. Perniola G, Tomao F, Fischetti M, Lio S, Pecorella I, Benedetti Panici P. Benign schwannoma in supraclavicular region: a false-positive lymph node recurrence of breast cancer suspected by PET scan. *Arch Gynecol Obstetr*. (2014) 290:583–6. doi: 10.1007/s00404-014-3241-5
7. Roger PA, Berna P, Merlusca G, Joly JP, Auquier MA, Sevestre H, et al. [Schwannoma of the vagus nerve: diagnostic strategy and therapeutic approach]. *Rev Mal Respir*. (2012) 29:70–3. doi: 10.1016/j.rmr.2011.06.016
8. Sugarbaker PH. *Pritoneal Carcinomatosis: Principles of Management*. Boston, MA: Springer (1996).
9. Bouvier C, Maues de Paula A, Roche PH, Chagnaud C, Figarella-Branger D. Tumeurs du système nerveux périphérique. *EMC Neurol*. (2013) 10:1–11. doi: 10.1016/S0246-0378(12)58206-0
10. Woodruff JM, Selig AM, Crowley K, Allen PW. Schwannoma (Neurilemoma) with malignant transformation a rare, distinctive peripheral nerve tumor. *Am J Surg Pathol*. (1994) 18:882–95. doi: 10.1097/00000478-199409000-00003
11. Enzinger FM. *Soft Tissue Tumor*. 2nd ed. Washington, DC: SWCMC (1988).
12. Mordant P, Le Pimpec-Barthes F, Riquet M. Tumeurs nerveuses du médiastin de l'adulte. *Rev Pneumol Clin*. (2010) 66:81–94. doi: 10.1016/j.pneumo.2009.12.010
13. Hilton DA, Hanemann CO. Schwannomas and their pathogenesis. *Brain Pathol*. (2014) 24:205–20. doi: 10.1111/bpa.12125
14. Lapierre F, Rigoard P, Wager M. Tumeurs des nerfs périphériques. *Neurochirurgie* (2009) 55:413–20. doi: 10.1016/j.neuchi.2009.09.004
15. Davis RD Jr, Oldham HN Jr, Sabiston DC Jr. Primary cysts and neoplasms of the mediastinum: recent changes in clinical presentation, methods of diagnosis, management, and results. *Ann Thorac Surg*. (1987) 44:229–37. doi: 10.1016/S0003-4975(10)62059-0
16. Pavlus J, Carter B, Tolley M, Keung E, Khorashadi L, Lichtenberger J. Imaging of thoracic neurogenic tumors. *Am J Roentgenol*. (2016) 207:552–61. doi: 10.2214/AJR.16.16018
17. Fujimoto K, Hara M, Tomiyama N, Kusumoto M, Sakai F, Fujii Y. Proposal for a new mediastinal compartment classification of transverse plane images according to the Japanese Association for Research on the Thymus (JART) general rules for the study of mediastinal tumors. *Oncol Rep*. (2013) 31:565–72. doi: 10.3892/or.2013.2904
18. Whitten C, Khan S, Munneke G, Grubnic S. A diagnostic approach to mediastinal abnormalities. *Radiographics* (2007) 27:657–71. doi: 10.1148/rg.273065136
19. Jeanbourquin D. Diagnostic des masses médiastinales de l'adulte. *Radiol Imagerie Méd*. (2010) 5:1–29. doi: 10.1016/S1169-7768(10)52870-4
20. Ahmed A, Watanabe H, Aoki J, Shinozaki T, Takagishi K. Schwannoma of the extremities: the role of PET in preoperative planning. *Eur J Nucl Med Mol Imaging* (2001) 28:1541–51. doi: 10.1007/s002590100584
21. Beaulieu S, Rubin B, Djang D, Conrad E, Turcotte E, Eary JF. Positron emission tomography of schwannomas: emphasizing its potential in preoperative planning. *Am J Roentgenol*. (2004) 182:971–4. doi: 10.2214/ajr.182.4.1820971
22. Miyake KK, Nakamoto Y, Kataoka TR, Ueshima C, Higashi T, Terashima T, et al. Clinical, morphologic, and pathologic features associated with increased fdg uptake in schwannoma. *Am J Roentgenol*. (2016) 207:1288–96. doi: 10.2214/AJR.15.14964
23. Berends A, Kerstens M, Bolt J, Links T, Korpershoek E, de Krijger R et al. False-positive findings on 6-[18F]fluor-l-3,4-dihydroxyphenylalanine PET (18F-FDOPA-PET) performed for imaging of neuroendocrine tumors. *Eur J Endocrinol*. (2018) 179:127–135. doi: 10.1530/EJE-18-0321
24. Dias A, Bouchelouche K. Prostate-specific membrane antigen PET/CT incidental finding of a schwannoma. *Clin Nuclear Med*. (2018) 43:267–8. doi: 10.1097/RLU.0000000000001988

Conflict of Interest Statement: The authors declare that the research was conducted in the absence of any commercial or financial relationships that could be construed as a potential conflict of interest.

frontiers in Medicine

CASE REPORT
published: 12 November 2021
doi: 10.3389/fmed.2021.733553

18F-FDG PET/CT in a Patient With Malignant Pheochromocytoma Recurrence and Bone Metastasis After Operation—Case Report and Review of the Literature

Bei Feng[1], *Maojia Chen*[2], *Yanghongyan Jiang*[1], *Yongfeng Hui*[1] *and Qian Zhao*[1]*

[1] Department of Nuclear Medicine, General Hospital of Ningxia Medical University, Yinchuan, China, [2] West China Hospital of Sichuan University, Chengdu, China

Introduction: Bone metastasis of malignant pheochromocytoma is a rare disease. We report a patient with a 10-year history who underwent 18F-FDG PET/CT to detect bone metastasis and receive radiotherapy and chemotherapy with complete response for bilateral iliac pain.

Case presentation: A 48-year-old male patient complained of dizziness, hypertension, and bilateral iliac pain for 2 months. The patient had a history of resection of bilateral malignant adrenal pheochromocytoma 10 years earlier, and all complaints were relieved immediately after operation. 18F-FDGPET/CT showed abdominal lymph node uptake and multiple bone uptake, as well as multiple brown fat uptake. A biopsy of the left ilium confirms the metastasis of malignant pheochromocytoma.

Discussion: In our literature review, we discuss the metastasis of pheochromocytoma reported by some scholars, and the role of radionuclides such as 18F-FDG PET/CT, 18F-DOPA PET/CT, I-123MIBG, and 68Ga-DOTATATE PET, in the diagnosis of malignant pheochromocytoma. The patient above is a good case for clinicians in the diagnosis and treatment of metastatic pheochromocytoma, especially in some hospitals with only 18F-FDG imaging agents.

Conclusion: A review of this case and similar rare cases in the literature illustrates the importance of 18F-FDG PET/CT in the diagnosis of malignant pheochromocytoma.

Keywords: 18F-FDG, malignant pheochromocytoma, brown fat, recurrence, bone metastasis

OPEN ACCESS

Edited by:
Désirée Deandreis, University of Turin, Italy

Reviewed by:
Maria Gazzilli, Civil Hospital of Brescia, Italy
Luca Camoni, University of Brescia, Italy

***Correspondence:**
Qian Zhao
cecilia_hh@126.com

Specialty section:
This article was submitted to Nuclear Medicine, a section of the journal Frontiers in Medicine

Received: *30 June 2021*
Accepted: *13 October 2021*
Published: *12 November 2021*

Citation:
Feng B, Chen M, Jiang Y, Hui Y and Zhao Q (2021) 18F-FDG PET/CT in a Patient With Malignant Pheochromocytoma Recurrence and Bone Metastasis After Operation—Case Report and Review of the Literature. Front. Med. 8:733553. doi: 10.3389/fmed.2021.733553

INTRODUCTION

According to the classification of tumors of the World Health Organization, 3–13% of patients with adrenal pheochromocytoma are diagnosed as malignant lesions (1). The 5-year survival rate was 34–60%, depending on the site of tumor metastasis. Patients with liver and lung metastasis were shown shorten survival time, while those with only bone metastasis showed the best prognosis (2). Unfortunately, it is extremely rare that the pheochromocytoma metastasizes to the bone.

Currently, the commonly used imaging for detecting bone metastasis is CT, MRI, PET/CT, and SPECT/CT. Among them, PET/CT or SPECT/CT is a "one-stop" examination, which displays not only morphological but also metabolic information of the whole body by one test. 18F-FDG is the analog of glucose, which reflects the metabolism of glycolysis inside the tumors. 18F-FDG PET/CT has been widely used in the detection, staging, prognosis, and therapeutic assessment of various kinds of tumors. Besides the primary lesions, all metastatic lesions can be shown, including osteogenic and osteolytic bone destructions (3). Pacak et al. (4) found that 18F-FDG PET/CT imaging is helpful for the localization and diagnosis of pheochromocytoma with high sensitivity and specificity.

Here, we report a rare case of 10-year postoperative bone metastasis of malignant pheochromocytoma detected by 18F-FDG PET/CT. The patient has provided a written informed consent form and agreed to publish this manuscript and any identifiable images or data.

CASE PRESENTATION

We report a 48-year-old male patient with dizziness, hypertension, bilateral iliac pain, and elevated blood pressure for 2 months. Bilateral adrenalectomy and splenectomy were performed in 2009. Postoperative pathology confirmed bilateral adrenal pheochromocytoma. All the symptoms were completely relieved, and the blood pressure returns to a normal level after operation. No antitumor and antihypertension therapy were needed. In April 2020, the patient visited the hospital and complained bone pain in the left hip, accompanied by palpitation, shortness of breath, and dizziness. The highest blood pressure was 200/120 mmHg, cortisol 4PM was 6.54 μg/dl (3.44–16.76), cortisol 8PM was 13.64 μg/dl (5.27–22.45), and serum corticotropin was 167.9 pg/ml (7.20–63.30). Chest X-ray showed no abnormality, UCG: left ventricular diastolic function decreased (Grade I), aortic sinus widened. T3, T4, TSH, CEA, CA125, CA199, PSA, HCG, NSE, CY-FRA21-1, and other tumor-related markers were normal. Urapidil sustained-release tablets were not effective, and the blood pressure control was not satisfied. The bone pain was obviously aggravated in nearly half a month.

In order to further find out the cause of bone pain, the patient underwent 18F-FDG PET/CT examination in our hospital. After fasting for more than 4 h, 7.91 mCi was injected intravenously, and 18F-FDG PET/CT brain body tomography was performed after 60-min rest.

An 18F-FDG PET/CT scan reported abdominal lymph node metastasis (SUVmax, 5.2) and multiple bone metastasis (SUVmax, 20.3) (**Figure 1**), accompanied by FDG uptake of bilateral vertebrae and intercostal muscles (SUVmax, 6.5) related to brown fat uptake (**Figure 2**). The bone biopsy of left iliac (**Figure 3**) considered metastasis of malignant pheochromocytoma. Combined with medical history of bilateral adrenal pheochromocytoma and immunohistochemical results: Cha (-), Vim (+ +), AE1/AE3 (-), the case was finally confirmed malignant pheochromocytoma metastasis.

The patients received cyclophosphamide, vincristine, and dacarbazine (CVD) chemotherapy for three cycles. Then, bilateral iliac metastatic lesions were treated with high-dose-rate interstitial brachytherapy (54Gy/3Gy/18f). Finally, the pain in the ilium of the patient was completely relieved after radiotherapy and chemotherapy.

DISCUSSION

Pheochromocytoma is a benign tumor derived from chromaffin tissue adjacent to adrenal medulla or sympathetic ganglion (5). About 10% of the tumors are bilateral, 10% are non-functional, and 10% are malignant (6). The metastasis has occurred when the malignant pheochromocytoma was found. The only diagnostic criterion for malignant pheochromocytoma is the detection of tumor metastasis (7). Metastases can be isolated or multifocal, commonly in bone, and rarely metastatic to lymph, lung, and liver. The order of involvement was long bone, pelvis, skull, vertebral body and ribs, mostly osteolytic destruction (8).

Studies show that the 5-year survival rate of patients with pheochromocytoma without metastasis can reach 89.3% (9). However, the prognosis of patients with distant metastasis is very poor, with a 5-year survival rate of about 40% and a low long-term survival rate (10). Press et al. (11) believed that recurrence was difficult to treat, especially if diagnosis was not in time or disease had metastatic spread. Therefore, early diagnosis of patients with pheochromocytoma, with malignant potential and careful evaluation of the location and extent of the tumor, is of great significance for the cure of the tumor and the prolongation of survival of the patients.

We searched PubMed with the words "pheochromocytoma" and "osseousmetastasis," and a total of 35 cases have been reported. McCarthy et al. (12) reported a case of pheochromocytoma metastatic to the left femur, which was detected by X-ray in 1977. They suggested surgical treatment was a nice method for patients with isolated bone metastasis. Kasliwal et al. (13) reported a case of metastatic malignant pheochromocytoma in vertebrae with MRI SPECT imaging and 131I-MIBG therapy. Darlong et al. (14) also reported a bladder and vertebral and rib metastasis detected by 18F-DOPA PET.

In 18F-FDG PET/CT scans, the incidence of brown adipose tissue uptake is 1.44–6.7% for physiological reasons (15). The most common location of brown adipose tissue detected by adult 18F-FDG PET/CT is the blue area in **Figure 2A**. In this case, there is brown fat uptake in the intercostal muscle, suggesting a recurrence of pheochromocytoma. On the other hand, in recent years, 18F-FDGPET/CT has confirmed the existence of metabolically active brown fat under pathological conditions (16). The increase of brown adipose tissue in patients with pheochromocytoma is associated with high levels of serum catecholamine secretion (17).

More and more new molecular probes or agents were introduced to modality imaging techniques, especially PET/CT. Besides FDG, there are many new probes in

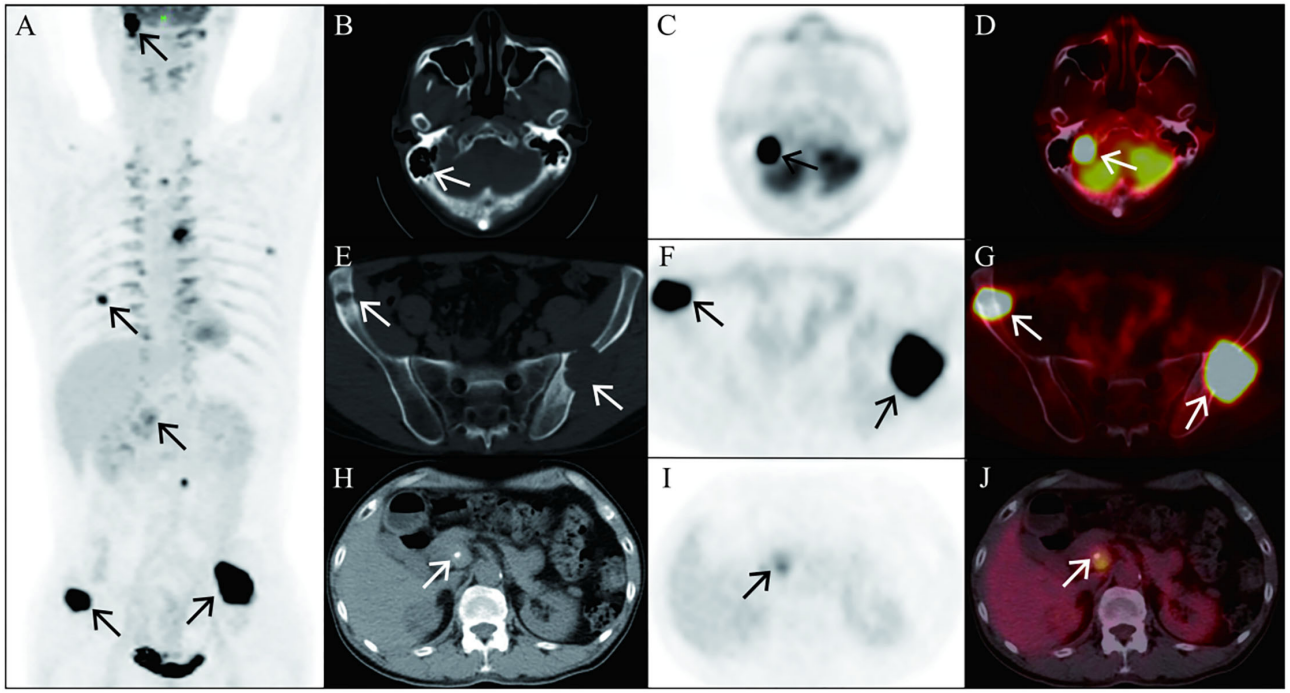

FIGURE 1 | As shown in MIP of 18F-FDG PET, 18F-FDG uptake in the petrous part of right temporal bone [**(A)**, arrows], right foramen magnum, right four anterior ribs, left five lateral ribs and posterior ribs, left eight posterior ribs [**(A)**, arrows], left pedicle of Lumbar 3 vertebral body [**(A)**, arrows], and bilateral ilium [**(A)**, arrowhead] are revealed and characterized with osteolytic bone destruction. Axial CT, PET, and fusion PET/CT images of representative involve bone lesions, including the petrous part of right temporal bone [**(B–D)**, arrows; SUVmax, 20.3] and bilateral ilium [**(E–G)**, arrowhead; SUVmax, 20.3], which are exhibited. In addition, the image shows the 18F-FDG uptake in the abdominal lymph nodes peri-pancreatic, indicating pheochromocytoma metastasis [**(H–J)**, arrow; SUVmax, 5.2].

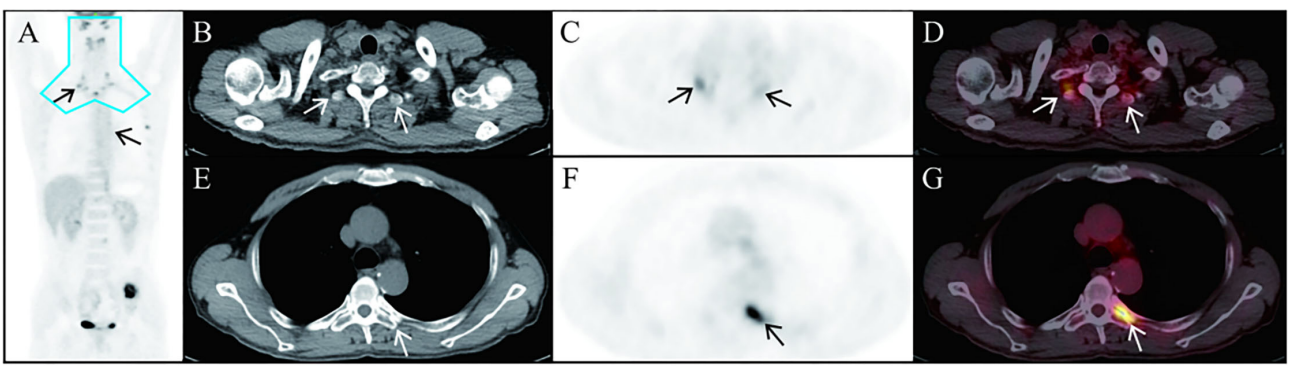

FIGURE 2 | In this case, 18F-FDG uptake (SUVmax, 6.5) is seen in the bilateral vertebrae and intercostal muscles. Representative brown adipose tissue in the thoracic vertebra transverse process [**(B–D)**, arrows] and in posterior intercostal space [**(E–G)**, arrowhead] in the axial CT, PET, and fusion PET/CT images is exhibited. The most common location for brown adipose tissue that is detectable in adults by PET/CT is the blue area in **(A)**.

radiopharmaceuticals were reported, which played an important and promising role in the diagnosis and therapeutic assessment of metastatic malignant pheochromocytoma.

A SPECT radionuclide tracer, 123I-MIBG, has high specificity in the localization and diagnosis of pheochromocytoma, and is of great significance in ectopic pheochromocytoma, postoperative reexamination, and multiple diseases (18). In addition, Grassi et al. (19) reported a patient with malignant pheochromocytoma who underwent 18F-DOPA PET/CT, I-123MIBG, and 68Ga-DOTATATE PET examinations. The results show that I-123MIBG imaging has traditionally been used to detect pheochromocytoma, but recent studies have shown that some pheochromocytoma imaging may be false negative. Therefore, in order to better display pheochromocytoma, we can consider using new imaging agents, such as 18F-DOPA PET/CT and 68Ga-DOTATATE PET.

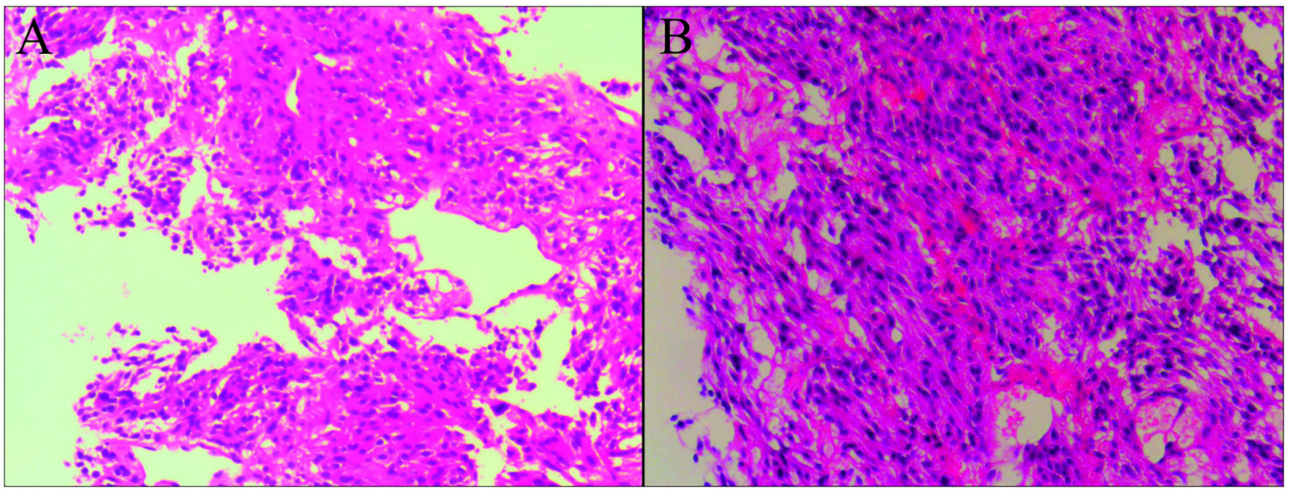

FIGURE 3 | Biopsies of the left ilium demonstrated the presence of metastasis of malignant pheochromocytoma. That tumor cells are spindle shaped and oval, with abundant cytoplasm and pink staining, and the nuclei are round, oval, and deeply stained, which are observed in the microscopic section of hematoxylin-eosin stain [**(A,B)**, original magnification × 10].

In addition, Yanagi et al. (20) reported a primary lesion of the right adrenal, illustrating low uptake due to wide centric necrosis, and metastatic lesions of liver, lumber vertebrae, ribs, and sacroiliac joint showed high uptake on the I-131 MIBG scintigraphy. 131I-MIBG can be selectively absorbed by pheochromocytoma and stored in catecholamine granules of tumor cells to release β-rays in particles and act on tumor cells to achieve therapeutic effect. 131I-MIBG palliative treatment has a certain effect (21). A recent study using FDG-PET, 18F-fluorodopamine PET, MIBG, 111In-pentetreotode, and 99mTc-methylene diphosphate scintigraphy indicated that FDG-PET was the preferable functional imaging modality for the localization of metastatic paraganglioma (22). Jaiswal et al. (23) studies show that 177Lu-DOTATATE is a safe and effective method for the treatment of metastatic pheochromocytoma. Win et al. (24) retrospectively reviewed five patients with malignant phaeochromocytoma who underwent imaging with CT and 123I-MIBG and compared the results with those of PET imaging using 68Ga-DOTATATE. The results showed that, compared with 123I-MIBG, 68Ga-DOTATATE showed more lesions, a higher uptake rate, and better resolution.

The patient above is a good case for clinicians in the assessment of metastatic pheochromocytoma, especially in some hospitals with only 18F-FDG imaging agents.

CONCLUDING REMARKS

Bone metastasis of malignant pheochromocytoma is a rare disease with poor prognosis. For patients with the potential for malignant recurrence, it is necessary to screen valuable predictors of recurrence, strengthen follow-up, and find recurrent diseases. This will help to completely cure and improve the prognosis of patients. Our case shows that 18F-FDG PET/CT has a good value in the localization diagnosis and clinical staging of malignant chromaffin bone metastasis. In addition, brown fat imaging can evaluate the level of catecholamine secretion in diseased blood and very helpful for clinical diagnosis of recurrent malignant pheochromocytoma.

DATA AVAILABILITY STATEMENT

The original contributions presented in the study are included in the article/supplementary material, further inquiries can be directed to the corresponding author/s.

ETHICS STATEMENT

Ethical review and approval was not required for the study on human participants in accordance with the local legislation and institutional requirements. The patients/participants provided their written informed consent to participate in this study. Written informed consent was obtained from the individual(s) for the publication of any potentially identifiable images or data included in this article.

AUTHOR CONTRIBUTIONS

BF and MC initiated the idea for case reporting and prepared the final copy of the manuscript. YH and YJ took responsibility for collecting patient's data. QZ took responsibility for reviewing the CT and FDG PET/CT. All authors have read and approved the final manuscript.

REFERENCES

1. Hafnermarx A. *World Health Organization Classification of Tumors. Pathology and Genetics of Tumors of the Urinary System and Male Genital Organs.* New Haven, CT: World Health Organization (2004).
2. Pacak K. Pheochromocytoma: recommendations for clinical practice from the First International Symposium. *Nat Clin Pract Endocrinol Metabol.* (2007) 3:92. doi: 10.1038/ncpendmet0396
3. Pietrzak AK, Czepczynski R, Wierzchoslawska E, Cholewinski W. Detection of the prostate cancer bone metastases: is it feasible to compare 18F-fluorocholine PET/CT, 18F-fluorodeoxyglucose PET/CT and 99mTc–methyl diphosphonate bone scintigraphy? *Urol J.* (2018) 15:242–7. doi: 10.22037/uj.v0i0.4065
4. Pacak K, Eisenhofer G, Carrasquillo JA, Chen CC, Whatley M, Goldstein DS. Diagnostic localization of pheochromocytoma: the coming of age of positron emission tomography. *Ann N Y Acad Sci.* (2010) 970:170–6. doi: 10.1111/j.1749-6632.2002.tb04423.x
5. Lenders J, Quan-Yang D, Graeme E, Anne-Paule GR, Grebe S, Hassan MM, et al. Pheochromocytoma and paraganglioma: an endocrine society clinical practice guideline. *J Clin Endocrinol Metabol.* (2014) 1915:1498. doi: 10.1210/jc.2014-1498
6. Lorenzen J, Buchert R, Bleckmann C, Münchow N, Bohuslavizki KH. A search for the focus in patients with fever of unknown origin: is positron-emission tomography with F-18-fluorodeoxyglucose helpful? *RöFo Fortschritte auf dem Gebiet der R.* (1999) 171:49–53. doi: 10.1055/s-1999-9892
7. Sherwin RP. Present status of the pathology of the adrenal gland in hypertension. *Am J Surg.* (1964) 107:136–43. doi: 10.1016/0002-9610(64)90249-1
8. Hamidi O, Young WF, Gruber L, Smestad J, Yan Q, Ponce OJ, et al. Outcomes of patients with metastatic phaeochromocytoma and paraganglioma: a systematic review and meta-analysis. *Clin Endocrinol.* (2017) 87:440–50. doi: 10.1111/cen.13434
9. Timmers H, Brouwers FM, Hermus A, Sweep F, Verhofstad A, Verbeek A, et al. Metastases but not cardiovascular mortality reduces life expectancy following surgical resection of apparently benign pheochromocytoma. *Endocr Relat Cancer.* (2008) 15:1127–33. doi: 10.1677/ERC-08-0049
10. Lam M, Lips C, Jager PL, Dullaart R, Lentjes E, Van RPP, et al. Repeated [131I]metaiodobenzylguanidine therapy in two patients with malignant pheochromocytoma. *J Clin Endocrinol Metab.* (2005) 2005:5888–95. doi: 10.1210/jc.2004-2290
11. Press D, Akyuz M, Dural C, Aliyev S, Monteiro R, Mino J, et al. Predictors of recurrence in pheochromocytoma. *Surgery.* (2014) 156:1523–7. doi: 10.1016/j.surg.2014.08.044
12. McCarthy EF, Bonfiglio M, Lawton W. A solitary functioning osseous metastasis from a malignant pheochromocytoma of the organ of Zuckerkandl. *Cancer.* (1977) 40:3092–6. doi: 10.1002/1097-0142(197712)40:6<3092::AID-CNCR2820400650>3.0.CO;2-N
13. Kasliwal MK, Sharma MS, Vaishya S, Sharma BS. Metachronous pheochromocytoma metastasis to the upper dorsal spine-6-year survival. *Spine J.* (2008) 8:845–8. doi: 10.1016/j.spinee.2007.06.004
14. Darlong V, Pandey R, Garg R, Kumar S, Punj J. Perioperative concerns of recurrent urinary bladder phaeochromocytoma with skeletal metastasis. *Singapore Med J.* (2012) 53:e40–1.
15. Kim SH, Krynyckyi BR, Machac J, Kim CK. Temporal relation between temperature change and FDG uptake in brown adipose tissue. *Eur J Nucl Med Mol Imaging.* (2008) 35:984–9. doi: 10.1007/s00259-007-0670-4
16. Altini C, Asabella AN, Ferrari C, Rubini D, Rubini G. 18F-FDG PET/CT in ocular and orbital abnormalities not only neopastic: comparison with traditional imaging. *Recenti Prog Med.* (2015) 106:393–401. doi: 10.1701/1960.21308
17. Hadi M, Chen CC, Whatley M, Pacak K, Carrasquillo JA. Brown fat imaging with (18)F-6-fluorodopamine PET/CT, (18)F-FDG PET/CT, and (123)I-MIBG SPECT: a study of patients being evaluated for pheochromocytoma. *J Nucl Med.* (2007) 48:1077–83. doi: 10.2967/jnumed.106.035915
18. Pocaro AB, Cavalleri S, Ballista C, Righetti R, Tallarigo C. Modern imaging methods and preoperative management of pheochromocytoma: review of the literature and case report. *Archivos Espaoles De Urología.* (2000) 53:749.
19. Grassi I, Nanni C, Vicennati V, Castellucci P, Allegri V, Montini GC, et al. I-123 MIBG scintigraphy and 68Ga-DOTANOC PET/CT negative but F-18 DOPA PET/CT positive pheochromocytoma: a case report. *Clin Nucl Med.* (2011) 36:124–6. doi: 10.1097/RLU.0b013e318203bc4f
20. Yanagi Y, Asaumi J, Hisatomi M, Konouchi H, Wakasa T, Kishi K. Mandibular metastasis presenting as the initial maifestation of malignant pheochromocytoma. *Eur J Radiol.* (2002) 44:5–9. doi: 10.1016/S0720-048X(01)00366-7
21. Sisson JC. Radiopharmaceutical treatment of pheochromocytomas. *Ann N Y Acad Sci.* (2010) 970:54–60. doi: 10.1111/j.1749-6632.2002.tb04412.x
22. Takano A, Oriuchi N, Tsushima Y, Taketomi-Takahashi A, Nakajima T, Arisaka Y, et al. Detection of metastatic lesions from malignant pheochromocytoma and paraganglioma with diffusion-weighted magnetic resonance imaging: comparison with 18F-FDG positron emission tomography and 123I-MIBG scintigraphy. *Ann Nucl Med.* (2008) 22:395–401. doi: 10.1007/s12149-008-0128-1
23. Jaiswal SK, Sarathi V, Memon SS, Garg R, Malhotra G, Verma P, et al. 177Lu-DOTATATE therapy in metastatic/inoperable pheochromocytoma-paraganglioma. *Endocr Connect.* (2020) 9:864–73. doi: 10.1530/EC-20-0292
24. Win Z, Al-Nahhas A, Towey D, Todd JF, Rubello D, Lewington V, et al. 68Ga-DOTATATE PET in neuroectodermal tumours: first experience. *Nucl Med Commun.* (2007) 28:359–63. doi: 10.1097/MNM.0b013e32808ea0b0

Conflict of Interest: The authors declare that the research was conducted in the absence of any commercial or financial relationships that could be construed as a potential conflict of interest.

frontiers in Medicine

CASE REPORT
published: 09 March 2022
doi: 10.3389/fmed.2022.840795

Situs Inversus Totalis on ^{18}F-FDG PET/CT: A Case Report and a Literature Review

*Xu-Sheng Liu, Rui-Min Wu, Hua-Bing Wan, Yi-Jia Chen, Fan Tan, Dao-Bing Zeng, Yi Yang and Zhi-Jun Pei**

Department of Nuclear Medicine and Institute of Anesthesiology and Pain, Taihe Hospital, University of Medicine, Shiyan, China

A 62-year-old female patient with pathologically confirmed left lung small cell neuroendocrine carcinoma. The patient was referred to our positron emission tomography (PET)/CT center to look for possible metastatic diseases. After fasting for 8 h, the fasting blood glucose level of the patient was 7.1 mmol/L. The patient was intravenously injected with a 6.42 mCi (238 MBq) ^{18}F-fluorodeoxyglucose (FDG) imaging agent. After the patient rested for 1 h, we scanned the patient with SIEMENS Biograph mCT 64 PET/CT camera. In addition to lung tumors and lymph node diseases, abnormal tracer uptake in the patient's thyroid was also found. PET/CT also showed situs inversus totalis of the patient, including the dextrocardia, liver on the left side, stomach, and spleen on the right side of the patient's body. The identification of anatomical variations and abnormalities by PET/CT imaging is very important to develop the best treatment for lung cancer.

Keywords: 18 F-FDG, PET/CT, small cell lung cancer, situs inversus totalis, neuroendocrine carcinoma

OPEN ACCESS

Edited by:
Giorgio Treglia, Ente Ospedaliero Cantonale (EOC), Switzerland

Reviewed by:
Virginia Liberini, University of Turin, Italy
Maria Gazzilli, Civil Hospital of Brescia, Italy

****Correspondence:***
Zhi-Jun Pei
pzjzml1980@taihehospital.com

Specialty section:
This article was submitted to Nuclear Medicine, a section of the journal Frontiers in Medicine

Received: *24 January 2022*
Accepted: *07 February 2022*
Published: *09 March 2022*

Citation:
Liu X-S, Wu R-M, Wan H-B, Chen Y-J, Tan F, Zeng D-B, Yang Y and Pei Z-J (2022) Situs Inversus Totalis on ^{18}F-FDG PET/CT: A Case Report and a Literature Review. Front. Med. 9:840795. doi: 10.3389/fmed.2022.840795

INTRODUCTION

Situs inversus totalis refers to the position of the thoracic cavity, abdominal cavity, or thoracic and abdominal cavity, which is opposite to normal and presents a mirror image with healthy people (1). This kind of patient is rare in clinics (2). It is reported that situs inversus totalis (SIT) can be associated with multiple cancers, such as breast cancer (3), esophageal cancer (4), and cervical cancer (5). Lung small cell neuroendocrine carcinoma, also known as small cell lung cancer (SCLC), is a subtype of pulmonary neuroendocrine tumors (PNETs) (6). According to the classification of who in 2015, PNETs are divided into four subtypes: typical carcinoid (TC), atypical carcinoid (AC), large cell neuroendocrine carcinoma (LCNEC), and SCLC (7). PNETs are epithelial tumors derived from pulmonary neuroendocrine cells. They have unique biological and clinical characteristics, accounting for about 20% of primary lung tumors. They are a common type of neuroendocrine tumor (NETs) (8). It is rare for the same patient to have both SIT and SCLC. Positron emission tomography (PET)/CT is a molecular imaging technology able to provide both anatomical and functional information. It can obtain cross-sectional images of the whole body in all directions, to achieve the purpose of early detection of lesions and diagnosis of diseases (9). In this study, we reported the PET/CT of patients with SIT along with SCLC as follows.

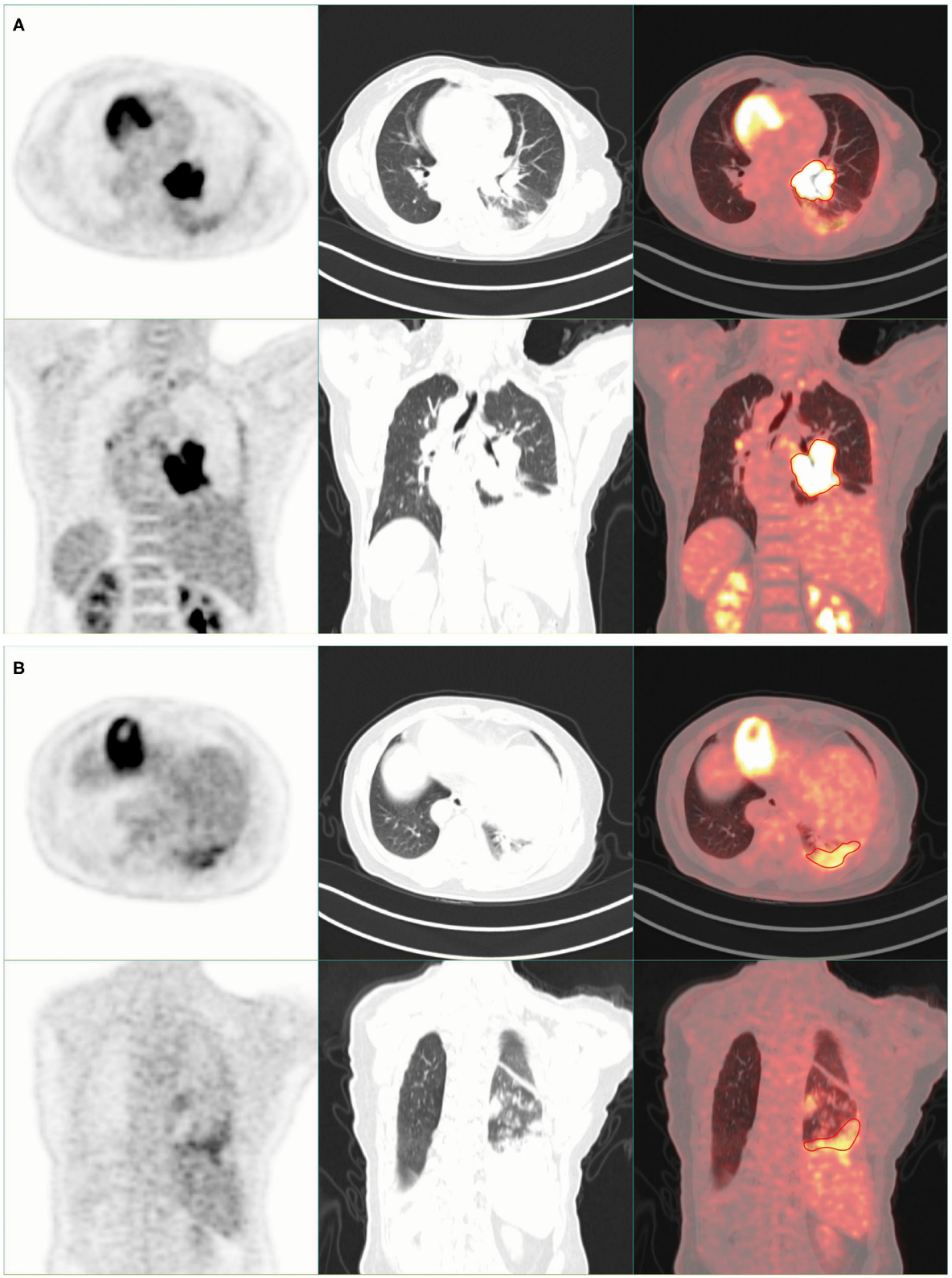

FIGURE 1 | Chest imaging of positron emission tomography (PET)/CT scan. **(A)** There was high tracer uptake in the left hilar area. **(B)** The bronchus of the lower lobe of the left lung was truncated, and high tracer uptake was observed.

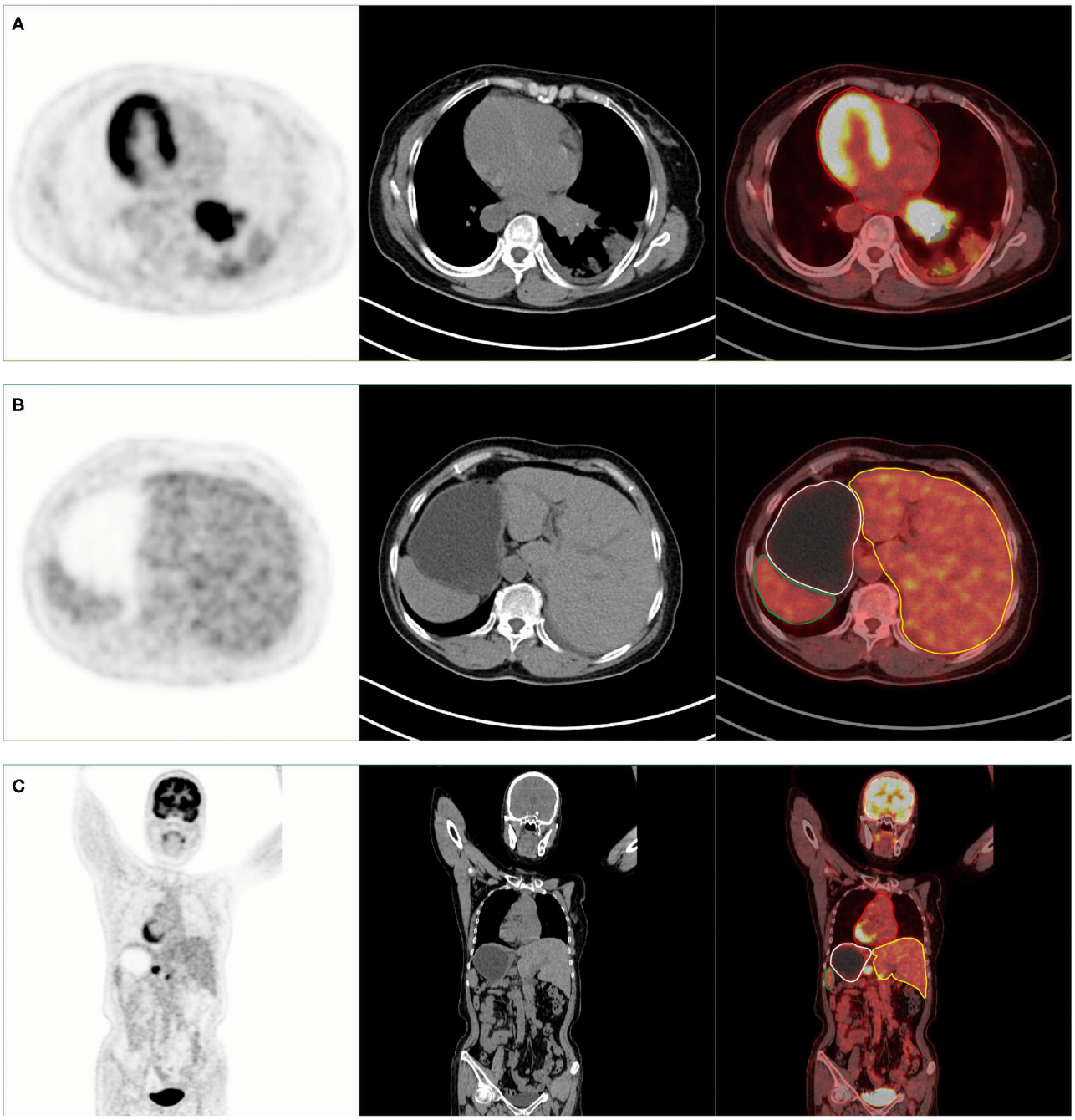

FIGURE 2 | PET/CT scan showed that this was a patient with situs inversus totalis (SIT). **(A,B)** Axial PET, CT, and PET/CT fusion images show the dextrocardia (red area), liver on the left side (yellow area), stomach (white area), and spleen (green area) on the right side of the patient's body. **(C)** Coronal PET, CT, and PET/CT fusion images show the dextrocardia (red area), liver on the left side (yellow area), stomach (white area), and spleen (green area) on the right side of the patient's body.

CASE PRESENTATION

A 62-year-old woman was admitted with a cough with intermittent coughed blood. The main performance is no obvious inducement of cough, mainly obvious at night, the weight loss of 10 kg within half a month. The patient's cough has worsened in the past day with hemoptysis. CT scan showed central lung cancer with obstructive pneumonia in the lower lobe of the left lung, and SIT was also found. The serum ferritin level was 300.73 ng/ml and the carbohydrate antigen CA125 level was 132.8 μ/ml. The pathological results of bronchoscopy biopsy confirmed that it was small cell neuroendocrine carcinoma of the

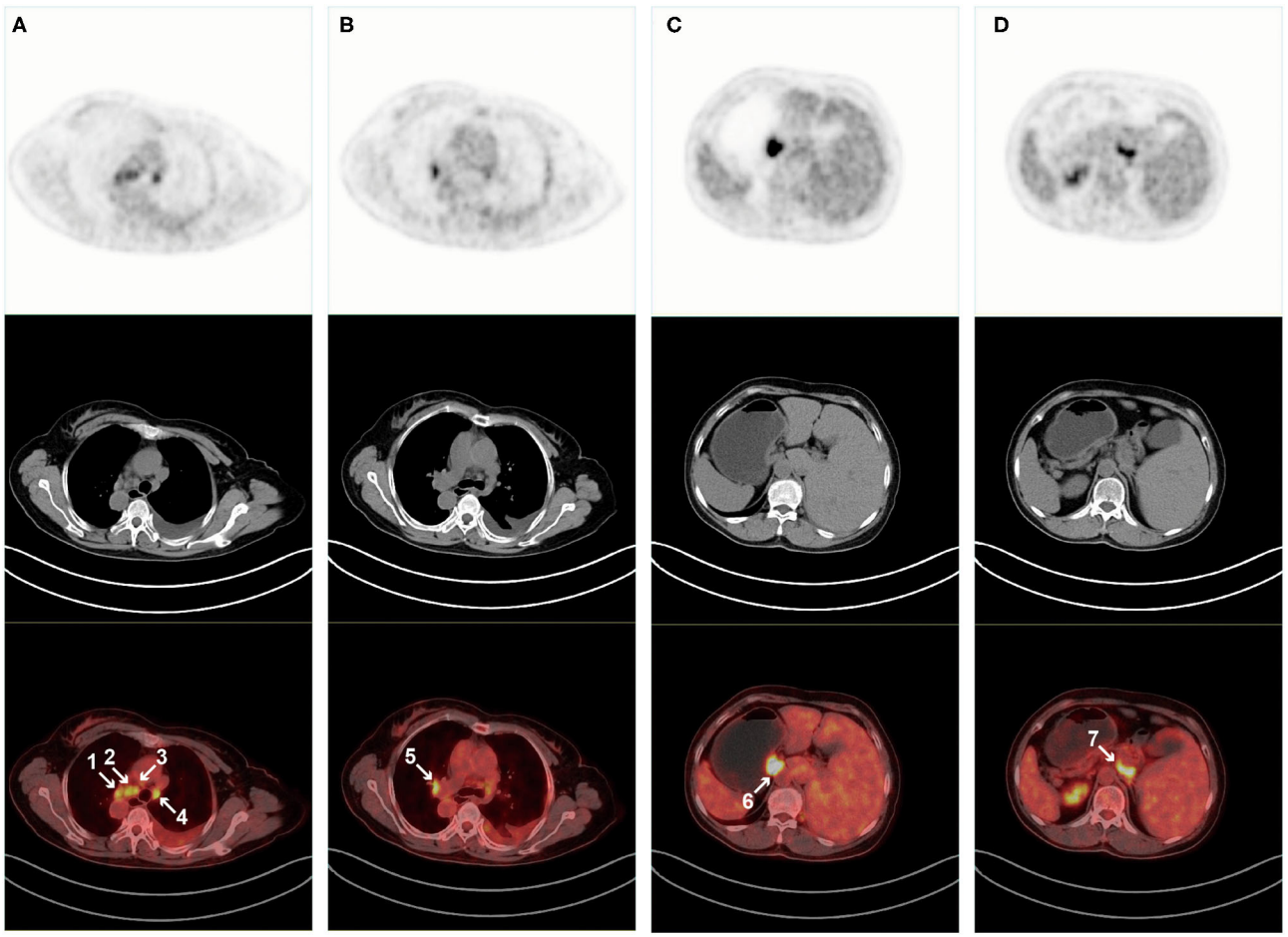

FIGURE 3 | PET/CT scan found that multiple lymph nodes also had high tracer uptake. Axial and coronal PET, CT, and PET/CT fusion images show tracer uptake in the mediastinum **(A)** Right hilar, **(B)** Gastric, **(C)** Liver, and **(D)** Lymph nodes.

lung [immunohistochemical results: CK (P) (+), CD56 (+), Cg-A (+), CK7 (–), P63 (–), P40 (–), Ki-67 (90%+), TTF-1(SPT24) (+), and Syn (+)]. The patient was referred to our department for an ^{18}F-fluorodeoxyglucose (FDG) PET/CT examination.

The PET/CT (SIEMENS Biograph, Germany) scan results showed high tracer uptake in the left hilar area (**Figure 1A**). The bronchus of the lower lobe of the left lung was truncated and significant uptake of tracer was observed (**Figure 1B**). The results of this scan were consistent with those of CT scan and pathological examination. An interesting phenomenon was found when observing the whole-body PET/CT scanning images of patients. PET/CT scan showed that this was a patient with SIT. The imaging of the heart, liver, stomach, and other organs in the patient is completely opposite to that in the normal person (**Figure 2**).

In addition to the known high tracer uptake in left lung tumors, PET/CT scan also found high tracer uptake in multiple lymph nodes. These lymph nodes were distributed in the mediastinum (**Figure 3A**), right hilum (**Figure 3B**), stomach (**Figure 3C**), and liver (**Figure 3D**). At the same time, we also found mucinous changes in the patient's left maxillary sinus, and its tracer uptake was slightly increased (**Figure 4A**). However, PET/CT showed no significant change in thyroid density, but the tracer uptake was abnormally increased (**Figure 4B**). However, the levels of thyroid-stimulating hormone (TSH, 4.57 mIU/L, 0.4–5), triiodothyronine (T3, 1.83 nmol/L, 1.07–2.6), thyroxine (T4, 117.46 nmol/L, 69–161), free triiodothyronine (FT3, 4 pmol/L, 2.76–7.65), and free thyroxine (FT4, 8.09 pmol/L, 7.98–16.02) in the patient's serum were within the normal range. Laboratory examination also found that the contents of alanine aminotransaminase (ALT, 47.3 U/L, 0–40), aspartate aminotransaminase (AST, 53.7 U/L, 0–35), γ-glutamyltransferase (GGT, 112 U/L, 0–45) and alkaline phosphatase (ALP, 157.6 U/L, 50–135) in the patient's serum were significantly increased, but PET/CT scan did not find obvious abnormalities in the liver.

DISCUSSION

Situs inversus totalis (SIT), is a rare congenital anomaly, represents a complete left to right side transposition of the

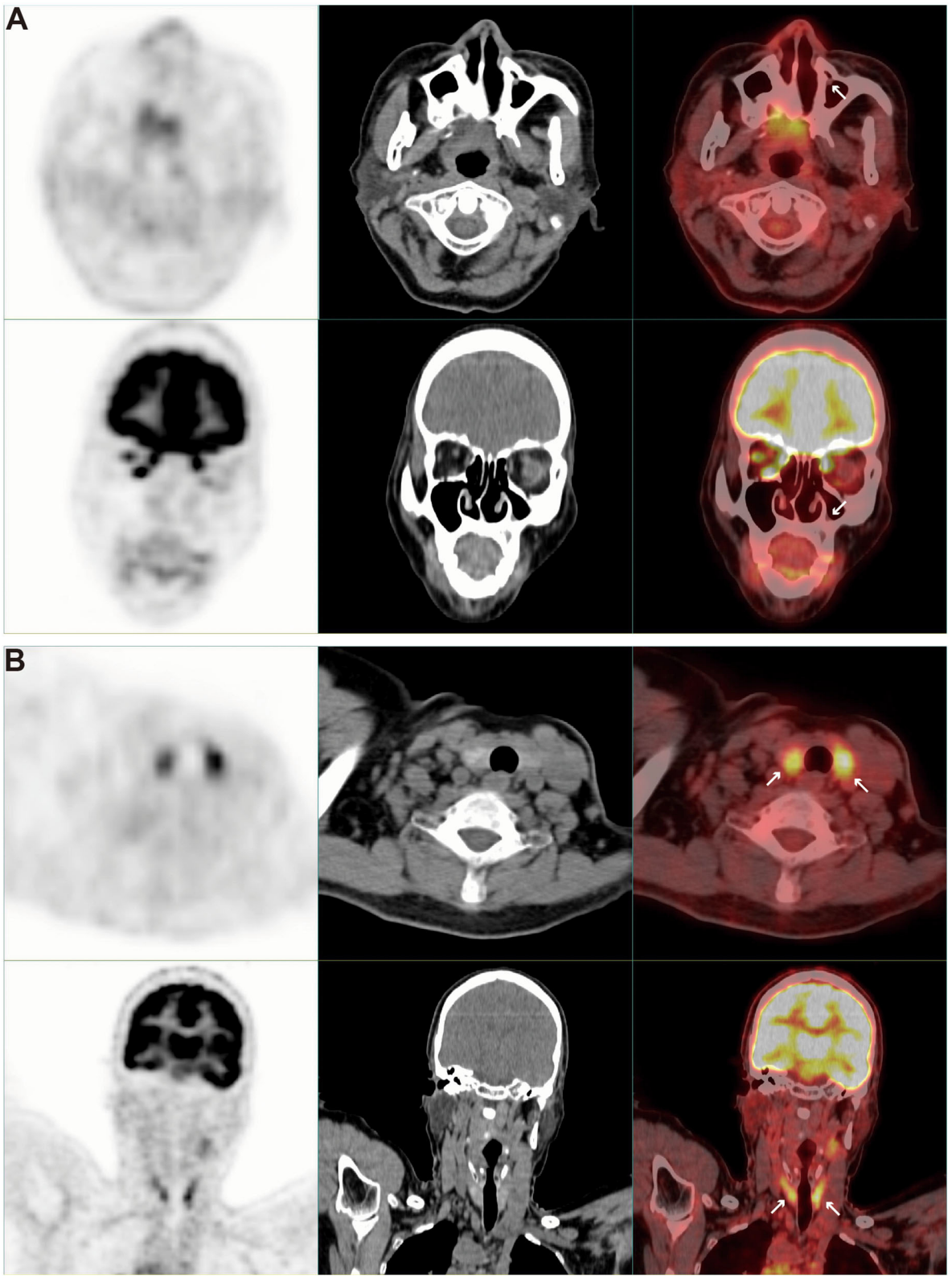

FIGURE 4 | PET / CT scan showed abnormalities of maxillary sinus and thyroid. **(A)** Axial and coronal PET, CT, and PET/CT fusion images show mucinous changes in the left maxillary sinus. **(B)** Axial and coronal PET, CT, and PET/CT fusion images showed abnormal tracer uptake in the patient's thyroid.

asymmetrical thoracic and abdominal organs, and incorporates dextrocardia (1, 3). As shown in this case, simultaneous abnormalities in the respiratory and lymphatic system often complicate SIT cases. Interestingly, the occurrence of lung small cell neuroendocrine carcinoma in patients with SIT is extremely rare. This is the first reported case of SCLC, lymph node metastasis, and SIT.

Although surgical resection is a common method for SCLC treatment, it is more difficult to stage and treat SCLC after SIT and lymph node metastasis. PET/CT not only has the characteristics of high spatial resolution and clear anatomical structure of CT but also has the advantages of PET functional imaging. At the same time, PET/CT scan can also provide information about whether there is metastasis in various organs of the whole body and provide strong evidence for the accurate staging of tumors (9).

It is well known that SIT, bronchiectasis, and sinusitis are typical features of Kartagener syndrome. Kartagener syndrome complicated with lung cancer has also been reported before (10). Although there is no pathological evidence of bronchiectasis, in this case, careful examination is still needed before the operation to rule out the possibility of Kartagener syndrome. At the same time, if surgical treatment is required, surgeons need to be very careful about SIT to avoid errors. Although SIT has been reported with solid tumors (1, 3–5, 11), whether an association between SIT and malignancies has been controversial, and further clinical and epidemiological research evidence is needed due to objective limitations such as the number of cases. It is also necessary to see if malignant metastases already exist when developing treatment options for patients with SIT with tumors. PET/CT scanning is very important to identify the abnormal biological distribution of tracers and observe anatomical variation, so as to help clinicians formulate the best treatment strategy for patients.

DATA AVAILABILITY STATEMENT

The original contributions presented in the study are included in the article/supplementary material, further inquiries can be directed to the corresponding author/s.

ETHICS STATEMENT

Written informed consent was obtained from the individual(s) for the publication of any potentially identifiable images or data included in this article.

AUTHOR CONTRIBUTIONS

X-SL conceived the project and wrote the manuscript. X-SL, R-MW, and H-BW performed image acquisition and prepared images. X-SL, Y-JC, FT, D-BZ, and YY participated in the discussion and language editing. Z-JP reviewed the manuscript. All authors contributed to the article and approved the submitted version.

REFERENCES

1. Calabria FF, Leporace M, Bagnato A. Situs inversus totalis and cholangiocarcinoma of the gallbladder detected by 18F-FDG PET/CT. *Clin Nucl Med.* (2018) 43:439–40. doi: 10.1097/RLU.0000000000002047
2. Iwamura T, Shibata N, Haraguchi Y, Hisashi Y, Nishikawa T, Yamada H, et al. Synchronous Double Cancer of the Stomach and Rectum With Situs Inversus Totalis and Polysplenia. *Syndrome.* (2001) 12:148–53. doi: 10.1097/00004836-200108000-00012
3. Halac M, Mut SS, Ylmaz S, Ergul N, Sonmezoglu K. Appearance of Situs Inversus Totalis and Polysplenia Syndrome on FDG PET/CT. *Clin Nucl Med.* (2008) 33:142–3. doi: 10.1097/RLU.0b013e31815ef836
4. Xie CL, Cai JS, Tan ZH, Yang J, Yang HX. Total minimally invasive mckeown esophagectomy in an esophageal cancer patient with situs inversus totalis: a case report. *Thorac Cancer.* (2021) 12:122–7. doi: 10.1111/1759-7714.13723
5. Zhang Y, Chen Y, Huang Z, Zhou F. Adenocarcinoma of the cervix uteri and endometrium combined with the kartagener syndrome on FDG PET/CT. *Clin Nucl Med.* (2015) 40:922-3. PubMed PMID: 26284775. doi: 10.1097/RLU.0000000000000961
6. Rekhtman N. Lung neuroendocrine neoplasms: recent progress and persistent challenges. *Modern Pathol.* (2021) 21:943. doi: 10.1038/s41379-021-00943-2
7. Travis WD, Brambilla E, Nicholson AG, Yatabe Y, Austin JHM, Beasley MB, et al. The 2015 world health organization classification of lung tumors: impact of genetic, clinical and radiologic advances since the 2004 classification. *J Thorac Oncol.* (2015) 10:1243–60. doi: 10.1097/JTO.0000000000000630
8. Sackstein PE, O'Neil DS, Neugut AI, Chabot J, Fojo T. Epidemiologic Trends in Neuroendocrine tumors: an examination of incidence rates and survival of specific patient subgroups over the past 20 years. *Semin Oncol.* (2018) 45:249–58. doi: 10.1053/j.seminoncol.2018.07.001
9. Rowe SP, Pomper MG. Molecular imaging in oncology: current impact and future directions. *CA: Cancer J Clinic.* (2021) 21:21713. doi: 10.3322/caac.21713
10. Zhou D, Tian Y, Lu Y, Yang X. Anatomical variants of pulmonary segments and uni-portal thoracoscopic segmentectomy for lung cancer in a patient with kartagener syndrome: a case report. *General Thoracic Cardiovascul Surg.* (2021) 69:1432–7. doi: 10.1007/s11748-021-01685-3
11. Huang J, Yang H, Wang M, Zhao X, Shao S, Zhang F, et al. Gallbladder adenosquamous cancer with situs inversus totalis: a case report and literature review. *Oncotargets Ther.* (2021) 14:4299–304. doi: 10.2147/OTT.S319030

Conflict of Interest: The authors declare that the research was conducted in the absence of any commercial or financial relationships that could be construed as a potential conflict of interest.

frontiers | Frontiers in Medicine

CASE REPORT
published: 25 April 2022
doi: 10.3389/fmed.2022.860545

Case Report: Nerve Root Entrapment Due to Epidural Fibrosis in a Patient With Failed Back Surgery Syndrome: Value of 2-^{18}F-Fluorodeoxyglucose Simultaneous Positron Emission Tomography-Magnetic Resonance Imaging

*Yueh-Hsun Tsai[1], Guo-Shu Huang[2,3], Chi-Tun Tang[4], Wei-Chou Chang[2] and Yi-Chih Hsu[2]**

[1] Department of Surgery, Tri-Service General Hospital, National Defense Medical Center, Taipei City, Taiwan, [2] Department of Radiology, Tri-Service General Hospital, National Defense Medical Center, Taipei City, Taiwan, [3] Department of Medical Research, Tri-Service General Hospital, National Defense Medical Center, Taipei City, Taiwan, [4] Department of Neurosurgery, Tri-Service General Hospital, National Defense Medical Center, Taipei City, Taiwan

OPEN ACCESS

Edited by:
Alberto Cuocolo, University of Naples Federico II, Italy

Reviewed by:
Domenico Albano, University of Brescia, Italy
Sikandar Shaikh, Shadan Hospital and Institute of Medical Sciences, India

***Correspondence:**
Yi-Chih Hsu
doc31578@gmail.com

Specialty section:
This article was submitted to Nuclear Medicine, a section of the journal Frontiers in Medicine

Received: *23 January 2022*
Accepted: *04 April 2022*
Published: *25 April 2022*

Citation:
Tsai Y-H, Huang G-S, Tang C-T, Chang W-C and Hsu Y-C (2022) Case Report: Nerve Root Entrapment Due to Epidural Fibrosis in a Patient With Failed Back Surgery Syndrome: Value of 2-^{18}F-Fluorodeoxyglucose Simultaneous Positron Emission Tomography-Magnetic Resonance Imaging. Front. Med. 9:860545. doi: 10.3389/fmed.2022.860545

Failed back surgery syndrome (FBSS) is a highly prevalent condition in patients after spine surgery. Although magnetic resonance imaging (MRI) is the gold standard for the diagnosis of epidural fibrosis, it is sometimes difficult to determine if epidural fibrosis contributes to radiculopathy. Herein, we share our experience in locating radiculopathy lesions using simultaneous positron emission tomography (PET)/MRI. 2-[^{18}F]-FDG (^{18}F-fluorodeoxyglucose) simultaneous PET/MRI maps of body glucose metabolism detected using PET can be used to correlate anatomical details provided by MRI to offer a very clear picture of neural inflammation due to extensive epidural fibrosis. More applications of 2-[^{18}F]-FDG simultaneous PET/MRI in low back pain and other musculoskeletal diseases should be further investigated in the future.

Keywords: epidural fibrosis, magnetic resonance imaging, failed back surgery syndrome, positron emission tomography, case report

INTRODUCTION

Failed back surgery syndrome (FBSS) is defined as persistent back or leg pain after one or more lumbar disk surgeries (1). Treatment for FBSS is often ineffective because of the difficulty in identifying the etiology (2). Magnetic resonance imaging (MRI) is the gold standard for evaluating spine lesions; contrast-enhanced MRI can differentiate between epidural fibrosis, spinal stenosis, and disk herniation (3). Although substantial intra-observer and near-perfect inter-observer agreement have been achieved for the evaluation of epidural fibrosis using MR images (4), we are still unable to determine whether epidural fibrosis causes radiculopathy (5). Positron emission tomography (PET)/computed tomography(CT) has been previously used to detect peripheral nerve pathologies, including neurolymphomatosis and neuritis (6–8). However, to our knowledge, the PET-MR findings of radiculitis after laminectomy have not been reported. Studies using PET

to assess metabolic activity showed increased binding in the spinal cord and compressed nerve roots in patients with radicular pain (9). We present a patient with FBSS who presented with refractory back pain radiating to the right leg and for whom root entrapment by epidural fibrosis was observed using PET/MRI.

CASE REPORT

The patient was a 66-year-old woman with chronic lower back pain. She denied any history of having systemic diseases, such as diabetes mellitus. She failed from conservative treatment including anti-inflammatories, muscle relaxants, analgesics and physical therapies. After a series of conservative treatments, she underwent, laminectomy of L5-S1 and posterior lumbar interbody fusion of L4–S1 was performed 20 months ago. Persistent back pain with downward radiation at the right foot (predominantly tightness and numbness) was noted after the operation; it correlated to the L5 or S1 dermatome. MRI revealed extensive scars over the sides of L4 to S1, bilaterally. However, the decision for surgical intervention was difficult to make because the patient only had symptoms on the right side. She

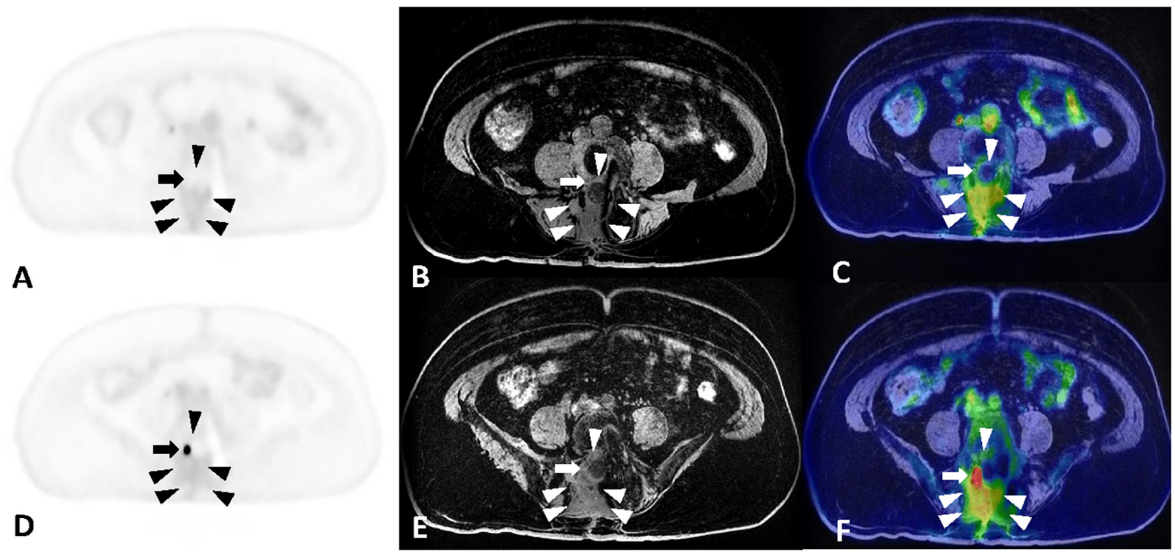

FIGURE 1 | (A–C) Maximum intensity projection, MRI and PET-MR fusion images at the level of L3-L4, separately. **(D–F)** Maximum intensity projection, MRI and PET-MR fusion images at the level of L5-S1, separately. Fat-suppression T1-weighted sequences in the axial plane without contrast showing increased and homogeneous intensity within the epidural space [arrowheads in panels **(B,E)**], indicative of extensive scar formation. The fusion images [arrowheads in panels **(C,F)**] reveal mild FDG uptake in the epidural scar with SUVmax of 2.0. The epidural fibrosis encircles the right L4 root [arrow in panel **(C)**] and right S1 root [arrow in panel **(F)**]. The FDG uptake of the right L4 root is similar to that of the adjacent epidural scar, while the right S1 root shows intense FDG uptake with SUVmax of 4.2.

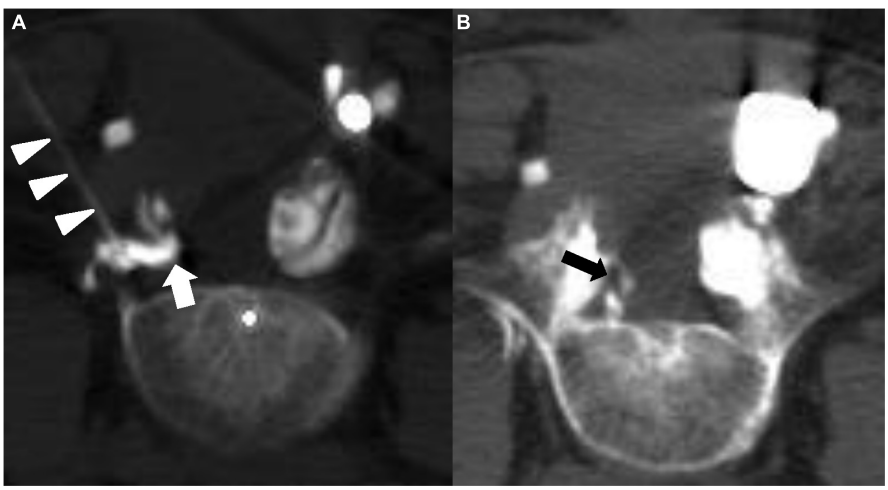

FIGURE 2 | CT-guided transforaminal injection at the level of L5-S1. Axial CT for the extent of contrast spread. **(A)** Visualization of the needle in the epidural space (arrowheads) and the dye (thick arrow) blocked by the scar. **(B)** Contrast filling around the right S1 root (thick arrow) at the ventral epidural space.

underwent right pedicle screw removal and decompression but did not have any improvement after surgery. She was also treated with radiofrequency ablation and nerve block, but the effect was only transient and it lasted less than one day. The lower back pain and right leg claudication worsened after 3 months, with a visual analog scale (VAS) score of 9. The patient visited our outpatient department due to persistent symptoms. 2-[^{18}F]-FDG PET-MRI scans were arranged and performed on a 3T PET/MRI scanner (Signa PET/MRI, GE Healthcare, Waukesha, WI, United States), which combines 3T MRI with time-of-flight capable silicone photomultiplier-based PET. The result revealed a faint FDG uptake (standard uptake value [SUV] = 1–2) over the right lateral epidural scar at the level of L5/S1; the scar was located along the course of the right S1 root, which revealed a nodular FDG uptake (maximal SUV = 4.2). Multiple epidural scars were seen over the sides of L4 to S1, bilaterally; however, no abnormal FDG uptake other than at the right S1 root was observed. The tentative diagnosis was entrapment neuropathy secondary to epidural fibrosis (**Figure 1**). We arranged CT-guided transforaminal injection of a lidocaine and contrast dye mixed injectate for the pre-operative diagnosis of right s1 root entrapment by an epidural scar (**Figure 2**). There was a good response to lidocaine injection for 2–3 hours, however, the symptoms recurred the following day. The diagnosis of epidural fibrosis with right S1 root entrapment was confirmed.

DISCUSSION

Failed back surgery syndrome has become a common problem in recent years, given the increasing rate of spine operations to treat back pain due to the aging population. It was found in a systematic review that the number of patients reporting recurrent back or leg pain after discectomy ranged from 5 to 36% (10). The post operative pain at the beginning can be caused by the degenerative changes, hematoma formation in the epidural or subdural space, infection, nerve injury. The progression of these etiologies can lead to formation of the epidural fibrosis, which worsened the symptoms due to traction of the fibrotic tissue on adjacent nerve roots. Epidural fibrosis is reported as a contributing factor to postoperative pain in 20–36% of FBSS cases (11). Although patients with extensive epidural fibrosis were shown to be 3.2 times more likely to experience recurrent radicular pain than those with less extensive epidural fibrosis in a previous study (4). we are still unable to determine whether radiculopathy is caused by epidural fibrosis (5).

Positron emission tomography is a sensitive tool for identifying hypermetabolic activity in cells, with broad utility in cancer surveys (12). PET has unique capabilities to provide quantitative information about the molecular and metabolic activity of tissues, but a higher resolution of anatomic information is needed to localize lesions (13). Hence, simultaneous PET/MRI has been more valuable because of the integration of metabolic activity and the detailed anatomy of the spinal root (9). Simultaneous PET/MRI provides better information about soft-tissue, spinal cord, and spinal disk abnormalities than PET/CT (14). The clinical applications of PET/MRI in the musculoskeletal system have been recently reported (13). A study reported the role of PET in identifying inflammation in peripheral nerves in various neuropathies (8) in which multiple epidural scars were seen over the sides of L4 to S1, bilaterally. However, these findings did not correlate with the patient's clinical symptoms. The decision for surgical intervention was difficult to make because of the difficulty in identifying the primary site of the radiculopathy. PET/MRI in our case revealed increased FDG uptake at the right S1 root, which was correlated to the epidural scar found entrapping the right S1 root on MRI. Epidural injections were administered using a fluoroscopic-guided transforaminal approach at the level of the involved nerve root to confirm the primary lesion, as described in a previous study.

In our case, contrast enhanced MRI was not performed. According to previous study (15), although contrast enhancement in MRI improved the visualization of nerve roots lying in scar tissue among 16% cases and better defined the extent of epidural fibrosis. However, it rarely altered final diagnosis. In our cases, the epidural fibrosis over was clearly defined in L3-L4 and L5-S1 with non-contrast MRI. But only PET/MRI revealed the distinct nerve root lesion. Study performed by Passavanti et al. (16) also concluded that Gadolinium enhanced MRI images compared with unenhanced MRI increased diagnostic confidence and agreement only in differentiating epidural fibrosis from disk herniation mainly in the first 6 months After 18 months, Gadolinium enhanced MRI did neither improve confidence nor agreement. In our case, the patient received the spine surgery 20 months before the PET/MRI scan. Therefore, whether performing a gadolinium MRI should show no difference.

Our case is the first to identify neural inflammation due to extensive epidural fibrosis after laminectomy. Using PET/MRI maps, body glucose metabolism detected using PET to correlate anatomical details provided by MRI can offer a very clear picture of the neural inflammation caused by extensive epidural fibrosis (9). In our experience, simultaneous PET/MRI can aid in the diagnosis of radiculitis in a patient with FBSS, not only for anatomic evaluation, but also for the metabolic assessment of the spinal roots in extensive epidural fibrosis.

DATA AVAILABILITY STATEMENT

The original contributions presented in the study are included in the article/**Supplementary Material**, further inquiries can be directed to the corresponding author.

ETHICS STATEMENT

The studies involving human participants were reviewed and approved by the Institutional Review Board of Tri-Service General Hospital. The patients/participants provided their written informed consent to participate in this study. Written informed consent was obtained from the individual(s)

for the publication of any potentially identifiable images or data included in this article.

AUTHOR CONTRIBUTIONS

Y-HT and W-CC reviewed the literature and contributed to manuscript drafting and revision. G-SH analyzed and interpreted the imaging findings. C-TT and Y-CH were responsible for the revision of the manuscript. All authors issued final approval for the version to be submitted.

ACKNOWLEDGMENTS

We would like to thank all colleagues and students who contributed to this study.

SUPPLEMENTARY MATERIAL

The Supplementary Material for this article can be found online at: https://www.frontiersin.org/articles/10.3389/fmed.2022.860545/full#supplementary-material

REFERENCES

1. Baber Z, Erdek MA. Failed back surgery syndrome: current perspectives. *J Pain Res.* (2016) 9:979–87. doi: 10.2147/jpr.S92776
2. Rigoard P, Gatzinsky K, Deneuville JP, Duyvendak W, Naiditch N, Van Buyten JP, et al. Optimizing the management and outcomes of failed back surgery syndrome: a consensus statement on definition and outlines for patient assessment. *Pain Res Manag.* (2019) 2019:3126464. doi: 10.1155/2019/3126464
3. Hussain A, Erdek M. Interventional pain management for failed back surgery syndrome. *Pain Pract.* (2014) 14:64–78. doi: 10.1111/papr.12035
4. Ross JS, Obuchowski N, Modic MT. MR evaluation of epidural fibrosis: proposed grading system with intra- and inter-observer variability. *Neurol Res.* (1999) 21:S23–6. doi: 10.1080/01616412.1999.11758604
5. Annertz M, Jönsson B, Strömqvist B, Holtås S. No relationship between epidural fibrosis and sciatica in the lumbar postdiscectomy syndrome. A study with contrast-enhanced magnetic resonance imaging in symptomatic and asymptomatic patients. *Spine (Phila Pa 1976).* (1995) 20:449–53. doi: 10.1097/00007632-199502001-00007
6. Roy SG, Parida GK, Tripathy S, Das CJ, Kumar R. Active leprosy neuritis detected on FDG PET/CT. *Clin Nucl Med.* (2018) 43:132–3. doi: 10.1097/rlu.0000000000001946
7. Salm LP, Van der Hiel B, Stokkel MP. Increasing importance of 18F-FDG PET in the diagnosis of neurolymphomatosis. *Nucl Med Commun.* (2012) 33:907–16. doi: 10.1097/MNM.0b013e3283561881
8. Xie X, Cheng B, Han X, Liu B. Findings of multiple neuritis on FDG PET/CT imaging. *Clin Nucl Med.* (2013) 38:67–9. doi: 10.1097/RLU.0b013e3182708916
9. Albrecht DS, Ahmed SU, Kettner NW, Borra RJH, Cohen-Adad J, Deng H, et al. Neuroinflammation of the spinal cord and nerve roots in chronic radicular pain patients. *Pain.* (2018) 159:968–77. doi: 10.1097/j.pain.0000000000001171
10. Parker SL, Mendenhall SK, Godil SS, Sivasubramanian P, Cahill K, Ziewacz J, et al. Incidence of low back pain after lumbar discectomy for herniated disc and its effect on patient-reported outcomes. *Clin Orthop Relat Res.* (2015) 473:1988–99. doi: 10.1007/s11999-015-4193-1
11. Chan CW, Peng P. Failed back surgery syndrome. *Pain Med.* (2011) 12:577–606. doi: 10.1111/j.1526-4637.2011.01089.x
12. Tsurusaki M, Okada M, Kuroda H, Matsuki M, Ishii K, Murakami T. Clinical application of 18F-fluorodeoxyglucose positron emission tomography for assessment and evaluation after therapy for malignant hepatic tumor. *J Gastroenterol.* (2014) 49:46–56. doi: 10.1007/s00535-013-0790-5
13. Gholamrezanezhad A, Basques K, Batouli A, Matcuk G, Alavi A, Jadvar H. Clinical nononcologic applications of PET/CT and PET/MRI in musculoskeletal, orthopedic, and rheumatologic imaging. *AJR Am J Roentgenol.* (2018) 210:W245–63. doi: 10.2214/ajr.17.18523
14. Andersen KF, Jensen KE, Loft A. PET/MR imaging in musculoskeletal disorders. *PET Clin.* (2016) 11:453–63. doi: 10.1016/j.cpet.2016.05.007
15. Murray JG, Stack JP, Ennis JT, Behan M. Digital subtraction in contrast-enhanced MR imaging of the postoperative lumbar spine. *AJR Am J Roentgenol.* (1994) 162:893–8. doi: 10.2214/ajr.162.4.8141014
16. Passavanti Z, Leschka S, Wildermuth S, Forster T, Dietrich TJ. Differentiating epidural fibrosis from disc herniation on contrast-enhanced and unenhanced MRI in the postoperative lumbar spine. *Skeletal Radiol.* (2020) 49:1819–27. doi: 10.1007/s00256-020-03488-8

Conflict of Interest: The authors declare that the research was conducted in the absence of any commercial or financial relationships that could be construed as a potential conflict of interest.

frontiers | Frontiers in Medicine

CASE REPORT
published: 30 June 2022
doi: 10.3389/fmed.2022.942558

Multimodality Imaging Evaluation of Primary Right Atrial Paraganglioma: A Case Report and Literature Review

Wen-peng Huang[1†], Ge Gao[2†], Zhao Chen[1], Yong-kang Qiu[1], Jian-bo Gao[3] and Lei Kang[1]*

[1] Department of Nuclear Medicine, Peking University First Hospital, Beijing, China, [2] Department of Radiology, Peking University First Hospital, Beijing, China, [3] Department of Radiology, The First Affiliated Hospital of Zhengzhou University, Zhengzhou, China

Background: Cardiac paraganglioma (CPGL) accounts for 1–3% of cardiac tumors and is usually benign. In total, 35–50% of CPGL lesions secrete catecholamines, causing hypertension, excessive sweating, palpitations, headache, and other symptoms. Preoperative imaging evaluation is important to determine the location of the cardiac mass, its blood supply vessels, and the relationship with surrounding structures. Multimodal imaging techniques combine with morphological and functional information to provide powerful methods for preoperative diagnosis and lesion localization. Furthermore, they can assist to reduce the incidence of intraoperative and postoperative complications and improve patient prognosis.

Case Report: A 67-year-old woman suffered from paroxysmal palpitations with a heart rate of 110 beats per minute 1 month ago. Urine catecholamine and methoxyepinephrine levels were significantly increased. The patient had a 5-year history of hypertension with a maximum blood pressure of 160/100 mmHg. Computed tomography (CT) examination found a soft tissue mass in the right atrium with heterogeneous and significant enhancement, whose blood supply was from the left ileal branch artery. The patient then underwent cardiac magnetic resonance (CMR). The lesion showed inhomogeneous iso signals on the T1-weighted image (T1WI), slightly high signals on the T2 fat-suppression image, inhomogeneous high signals on the diffusion-weighted imaging (DWI), and apparent diffusion coefficient (ADC) images. The mass exhibited heterogeneous and significant enhancement on the first perfusion and delayed scans after intravenous contrast injection. However, abnormal signals were surprisingly found in the patient's right lung, and the possibility of metastatic lesions could not be excluded. The patient underwent F-18 fluorodeoxyglucose-positron emission tomography/computed tomography (^{18}F-FDG PET/CT) to rule out metastatic lesions. A fluorodeoxyglucose (FDG)-avid soft tissue mass was shown in the right atrium, with the maximum standardized uptake value (SUVmax) at about 15.2, as well as a pathological intake of brown fat throughout the body. Combined with clinical symptoms, CPGL was considered without significant sign of metastasis in ^{18}F-FDG PET/CT.

OPEN ACCESS

Edited by:
Silvia Taralli,
Fondazione Policlinico Universitario A. Gemelli (IRCCS), Italy

Reviewed by:
Giorgio Treglia,
Ente Ospedaliero Cantonale (EOC), Switzerland
Maria Gazzilli,
Civil Hospital of Brescia, Italy

****Correspondence:***
Lei Kang
kanglei@bjmu.edu.cn

† These authors have contributed equally to this work

Specialty section:
This article was submitted to Nuclear Medicine, a section of the journal Frontiers in Medicine

Received: *12 May 2022*
Accepted: *03 June 2022*
Published: *30 June 2022*

Citation:
Huang W-p, Gao G, Chen Z, Qiu Y-k, Gao J-b and Kang L (2022) Multimodality Imaging Evaluation of Primary Right Atrial Paraganglioma: A Case Report and Literature Review. Front. Med. 9:942558. doi: 10.3389/fmed.2022.942558

Finally, the patient underwent surgical resection and the post-operative pathology confirmed a CPGL.

Conclusion: The combination of ^{18}F-FDG PET/CT with the CMR containing different image acquisition sequences provides a powerful aid for preoperative non-invasive diagnosis, localization, and staging of CPGL, which helps to reduce intraoperative and postoperative complications and improve patient prognosis.

Keywords: heart neoplasms, 18F-FDG, PET/CT, magnetic resonance imaging, x-ray computed tomography, paraganglioma, case report

INTRODUCTION

Primary cardiac tumors are very rare, with a prevalence ranging from 0.001 to 0.03%, of which about 20–30% are malignant (1, 2). Cardiac paraganglioma (CPGL) is extremely rare as it only accounts for 1–3% of cardiac tumors. In total, 35–50% of CPGL lesions secrete catecholamines, causing hypertension, excessive sweating, palpitations, headache, and other symptoms, most of which can be cured by complete surgical resection. Preoperative imaging evaluation is important to determine the exact location of CPGL, the blood supply vessels, and the relationship with surrounding structures. The use of multimodality imaging techniques, combined with morphological and functional information, is helpful in the preoperative diagnosis, localization of tumors, reduction of the incidence of intraoperative and postoperative complications, and improvement of patient prognosis.

CASE PRESENTATION

A 67-year-old woman came to the hospital with 1-month paroxysmal palpitations and 1-week bilateral lower limb edema with aggravation for 2 h. The patient presented with paroxysmal palpitations with a heart rate of 110 beats per minute 1 month ago and received no treatment. The patient had a 5-year history of hypertension and a 4-year history of diabetes mellitus, with a maximum blood pressure of 160/100 mmHg, and usually took oral antihypertensive medication to maintain her blood pressure. Physical examination revealed that the patient had no symptoms of dyspnea, hemoptysis, cyanosis, or abnormal sensation. Urine catecholamine and methoxyepinephrine levels were significantly increased (**Table 1**). An electrocardiogram (ECG) showed sinus tachycardia and echocardiography found an enlarged left atrium and a hypoechoic mass of about 4.6 cm × 4.6 cm at the top of the right atrium near the superior vena cava, with clear borders and uniform internal echogenicity. Compression of the right atrium and superior vena cava is demonstrated in **Figure 1**. Computed tomography (CT) examination indicated a soft tissue mass in the right atrium, about 4.7 cm × 4.4 cm in size, with a CT attenuation value of about 46 HU in plain view and a significant heterogeneous enhancement with a CT attenuation value of about 142 HU after enhancement. Its blood was supplied by the left circumflex branch of the coronary artery with a nutrient vessel visible in the lesion and a draining vein connected to the superior vena cava (**Figure 2**). The patient then underwent cardiac magnetic resonance (CMR) imaging. The lesion was found in the right atrium with the inferior border reaching the entrance of the inferior vena cava, with inhomogeneous iso signal on T1-weighted image (T1WI), patchy low signal inside, and inhomogeneous slightly high signal on T2 fat-suppression image, ranging from approximately 5.2 cm × 5.0 cm × 6.0 cm [Left right diameter (LR) × Anteroposterior diameter (AP) × Superior and lower diameter (SI)]. The lesion displayed inhomogeneous high signals on the diffusion-weighted imaging (DWI) and apparent diffusion coefficient (ADC) image. Heterogeneous and significant enhancement was shown in the first-perfused and delayed phases after intravenous contrast injection (**Figure 3**). However, abnormal signals were surprisingly found in the patient's right lung, so an F-18 fluorodeoxyglucose-positron emission tomography/computed tomography (^{18}F-FDG PET/CT) scan was performed to rule out metastatic lesions. A soft tissue mass with a high fluorodeoxyglucose (FDG) uptake was seen in the right atrium, with the maximum standardized uptake value (SUVmax) at about 15.2 and a maximum dimension of approximately 4.1 cm × 5.9 cm, which was poorly demarcated from the pericardium. In the upper lobe of the right lung, a mixed-density nodule shadow with a mild FDG uptake was seen near the pleural, with an SUVmax at about 5.8 and a size of about 1.7 cm × 2.3 cm, surrounded by a multi-density nodular shadow with a slightly radioactive uptake with an SUVmax at about 1.7. Inflammatory lesions were considered. Furthermore, high FDG uptake of brown fat was

TABLE 1 | Results of laboratory test with reference values.

Variable	Value	Reference
Urine vanillylmandelic acid (μmol/24 h)	76.00	<6
Urine norepinephrine (μg/24 h)	1130.00	<70
Urine epinephrine (μg/24 h)	369.00	<20
Urea (mmol/L)	8.82	2.2–8.2
Human chorionic gonadotropin (mIU/mL)	7.68	0–5
Erythrocyte sedimentation rate (mm/h)	42.00	0–20
C-reactive protein (mg/L)	6.82	0–5
Immunoglobulin G (g/L)	16.25	5.66–14.25

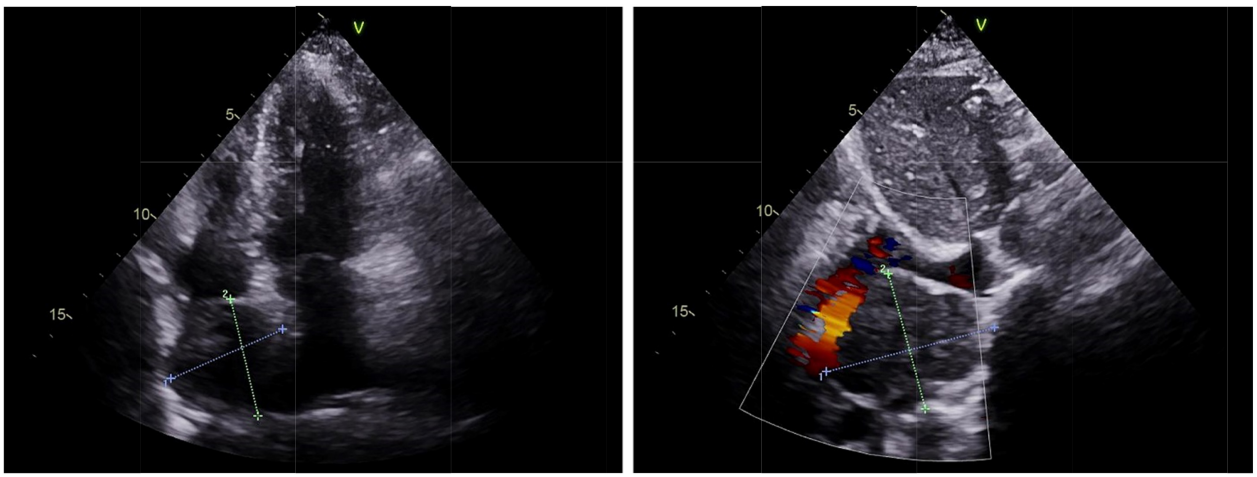

FIGURE 1 | Echocardiography of cardiac paraganglioma. An enlarged left atrium and a hypoechoic mass of about 4.6 cm × 4.6 cm at the top of the right atrium near the superior vena cava was found with clear borders and uniform internal echogenicity, as well as the compression of the right atrium and the superior vena cava.

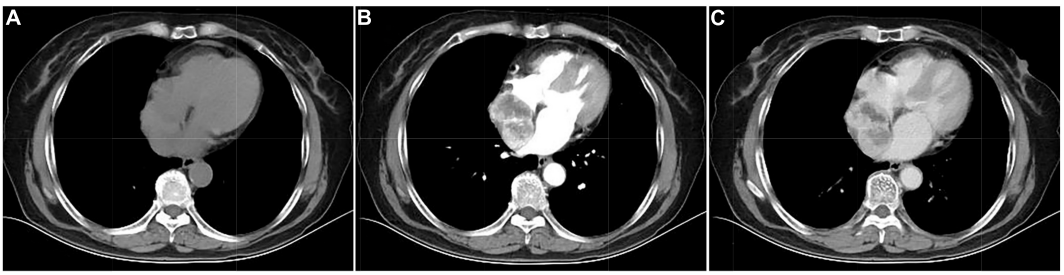

FIGURE 2 | Computed tomography images of cardiac paraganglioma. **(A)** Plain image; **(B)** arterial phase image; **(C)** venous phase image.

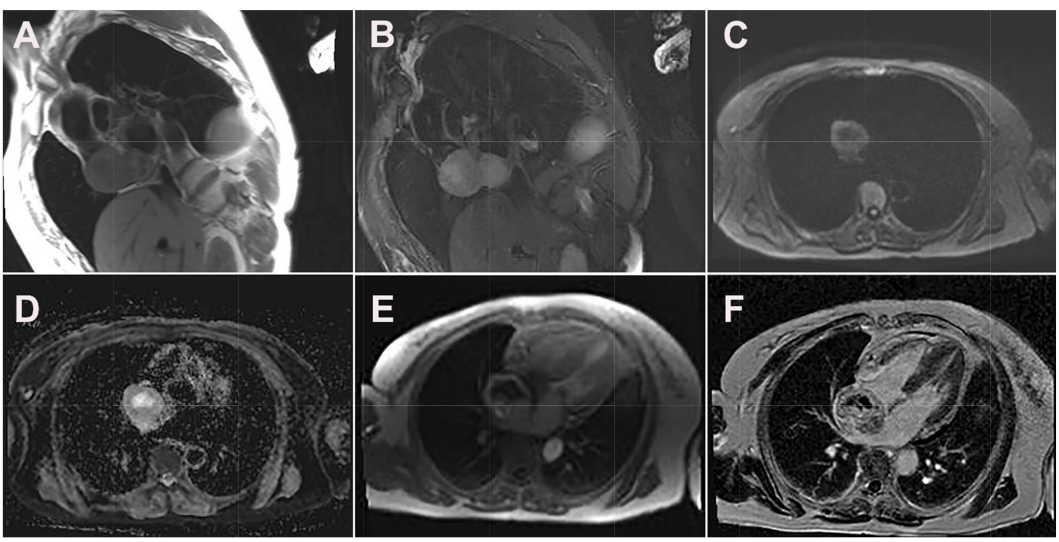

FIGURE 3 | Cardiac magnetic resonance images of cardiac paraganglioma. **(A)** T1-weighted image; **(B)** T2 fat-suppressed image; **(C)** diffusion-weighted imaging; **(D)** apparent diffusion coefficient image; **(E)** first-perfused image; **(F)** delayed scans image.

demonstrated symmetrically along the bilateral intermuscular neck, posterior cervical triangle, mediastinum, intrapericardial, sternum, spine, parasternal, perirenal, and retroperitoneal area with the SUVmax at about 34.4, which were typically related with the high secretion of catecholamine hormones from paragangliomas (**Figure 4**). Therefore, based on the clinical symptoms and multiple imaging findings, a CPGL in the right atrium was considered. The patient underwent a surgical resection under general anesthesia and extracorporeal circulation after preoperative blood pressure control with the α-blocker phenibutramine and metoprolol tartrate-extended release tablets. During surgery, the tumor was found to be grayish-yellowish-red in color, partially located in the atrial wall and the right atrium. The tumor had a short tip connected to the interatrial septum and a smooth and intact membrane, with a size of approximately 7.5 cm × 6.0 cm × 3.5 cm. Histopathological examination showed that the tumor cells were organoid and glandular vesicle-like in arrangement, with indistinct boundaries,

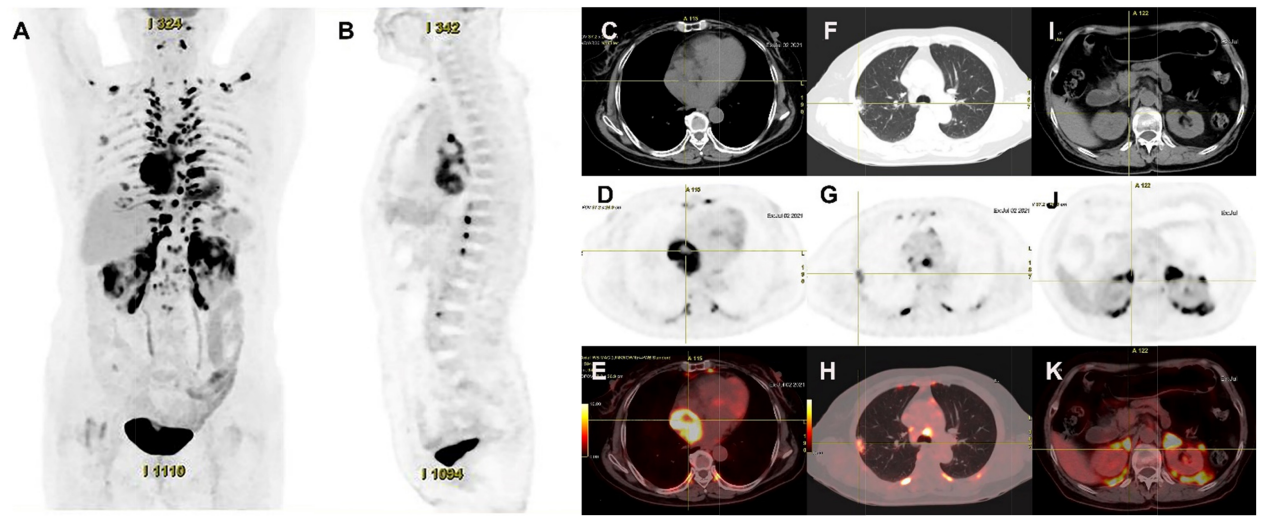

FIGURE 4 | ^{18}F-FDG PET/CT images of cardiac paraganglioma. **(A,B)** The whole-body maximum intensity projection showed an intensely hypermetabolic thoracic mass. **(C–E)** In a cardiac lesion with a high FDG uptake, the SUVmax is about 15.2. **(F–H)** In the upper lobe of the right lung, a mixed-density nodule with a mild FDG-avid was found near the pleural, with the SUVmax at about 5.8 and a size of about 1.7 cm × 2.3 cm, inflammatory lesions were considered. **(I–K)** High FDG uptake of brown fat was demonstrated symmetrically along the perirenal and retroperitoneal area with the SUVmax at about 34.4, which was usually caused by the high secretion of catecholamine hormones from paragangliomas.

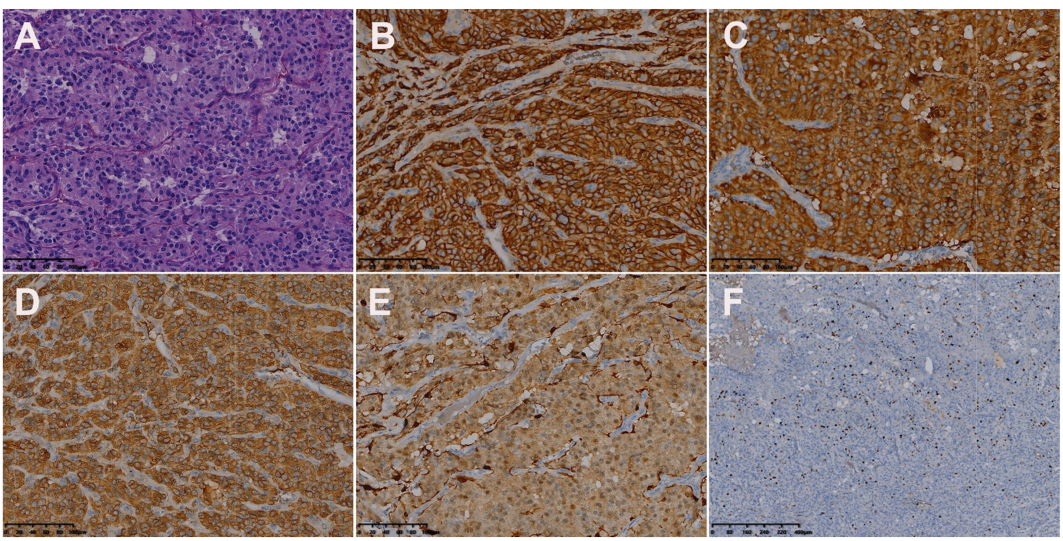

FIGURE 5 | Histologic and immunohistochemical features of cardiac paraganglioma. **(A)** Hematoxylin-eosin (HE) staining showed that the tumor cells were polygonal, with round-like nuclei and rare nuclear fission images (magnification, ×200). In immunohistochemical staining, the tumor cells were positive for CD56 **(B)**, SYN **(C)**, CgA **(D)**, and S-100 **(E)**. Moreover, 3% of them were positive for Ki-67 **(F)** [magnification **(B–F)** ×200].

an eosinophilic cytoplasm, round-like nuclei, rare nuclear fission images, abundant interstitial vessels, fibrous tissue hyperplasia, and collagenization with pigmentation. Immunohistochemistry showed Cytokeratin (CK) (−), Epithelial membrane antigen (EMA) (−), Neural cell adhesion molecules (CD56) (+), Synaptophysin (SYN) (+), Chromogranin A (CgA) (+), S-100 (+), Ki-67 (3% +), Melan-A (−), and Homatropine methyl bromide-45 (HMB45) (−). Based on the results of pathological morphology and immunohistochemistry, the tumor was diagnosed as CPGL (**Figure 5**). The patient showed a good prognosis after surgery with normal blood pressure and no complications or tumor recurrence.

DISCUSSION

We report a case of a 67-year-old female patient with primary right atrial paraganglioma and a review of the literature on imaging performed with MRI and nuclear medicine imaging. This case should be excluded from other primary cardiac tumors, such as a mucinous tumor, hemangioma, or angiosarcomas, with a different prognosis. Pheochromocytomas and paragangliomas are a series of neuroendocrine tumors originating from the adrenal medulla and chromaffin cells of the parasympathetic or sympathetic ganglia, respectively. Paragangliomas are often referred to as extra-adrenal pheochromocytomas (3). CPGL is extremely rare and occurs often in the left atrium, the left ventricle, and the left atrioventricular sulcus due to the proximity of the paraganglia cells to the left atrium and less in the right atrium, the right ventricle, and the atrial septum (4). In total, 35–50% of CPGLs secrete catecholamine hormones, which cause symptoms such as persistent or paroxysmal hypertension, headache, palpitations, and profuse sweating (5, 6). The occurrence of CPGL is associated with genetic mutations and is manifested as autosomal dominant inheritance, so the family history may provide an important diagnostic clue (7). The differentiation of benign and malignant CPGL cannot be based on the histopathological criteria but rather on the presence of distant metastases and biological behavior of recurrence (8, 9).

A literature search was performed on PubMed database from 2005 to 2022, using the keywords containing paraganglioma, cardiac, and heart. The MRI, single photon emission computed tomography (SPECT), SPECT/CT, positron emission tomography (PET)/CT, and PET/MRI manifestations of CPGL are summarized in **Tables 2**, **3** (1, 10–30). The purpose of imaging for CPGL is not only to localize and characterize the tumor but also to determine whether the surgical resection can be successfully undergone and to perform the post-treatment follow-up. CPGL, containing paraganglia cell nests and surrounding supporting cells, is a blood-rich tumor that often involves the coronary artery as the trophoblastic vessel. In this case, the left ileal branch is the blood-supplying artery. Echocardiography is the most common initial test. CPGL is mostly presented as a hypoechoic mass, suggesting the presence of a cardiac tumor. CPGL usually appears as round or ovoid in CT. When the tumor is large, cystic degeneration and necrosis, as well as hemorrhage, may occur. MRI is better than echocardiography and CT scan by providing more details of CPGL and its relationship to the surrounding structures. Due to the absence of radiation, MRI is more suitable for pediatric patients and screening. CPGL typically shows an equal or a low signal on T1WI but the signal will increase when the foci are accompanied by bleeding. High signals were found on T2WI with no reduction of signal in the antiphase. CPGL shows significant enhancement after contrast administration whereas extensive perfusion is seen in the early phase (31). Tumor necrosis can be detected on MRI and is a common feature seen in CPGL (23).

For metastatic lesions, functional imaging usually has a higher sensitivity, especially for bone metastases and distant soft tissue metastases that may be difficult to visualize on CT or MRI. Radionuclide imaging techniques are available for detecting, staging, and following up on paragangliomas. Beyond their ability to detect and localize paragangliomas, these imaging methods can provide valuable additional information (32). In SPECT imaging, ^{123}I-labeled metaiodobenzylguanidine (MIBG) is a guanethidine analog that is structurally similar to norepinephrine and is taken up by adrenergic storage cells in the adrenal gland and the paraganglia, allowing it to visualize neuroendocrine tissues. The sensitivity of ^{131}I-MIBG scintigraphy is limited, so ^{123}I-MIBG scintigraphy was introduced to improve image quality and increase sensitivity (33). Van Der Horst-Schrivers et al. (34) considered that the sensitivity of ^{123}I-MIBG scintigraphy for non-metastatic and metastatic PGL has been documented to be 96 and 79%, respectively. Timmers et al. (35) researched different functional imaging methods in the localization of pheochromocytoma and paraganglioma, the sensitivity rates to the detection rate of 6-Fluoro-(18F)-l-3,4-dihydroxyphenylalanine (^{18}F-DOPA PET), ^{18}F-fluorodopamine PET, ^{18}F-FDG PET, and ^{123}I-MIBG scintigraphy in non-metastasis PGL were 81, 77, 88, and 77%, respectively, and their sensitivity rates to the detection rate of metastatic PGL were 45, 76, 74, and 57%, respectively. ^{18}F-FDG PET/CT is recommended for patients with a biochemically established diagnosis of PGL when the aim is to localize the primary tumors and exclude metastases. In this case, the glucose metabolism of the soft tissue mass in the right atrium was high but metastatic lesions in the lung were excluded, which provided a powerful help for surgical resection. However, the FDG uptake alone cannot make an accurate judgment on the histological origin of the tumor so other imaging features from CMR should be integrated to further localize, characterize, and quantify the lesions.

Cardiac paraganglioma should be distinguished from a cardiac mucinous tumor, cavernous hemangioma, and angiosarcoma (10, 30). Mucinous tumors are the most common cardiac tumors mostly occurring in the left atrium with visible tips attached to the atrial septum or the atrial wall, and the lesions can follow the movement of the heart. Cardiac cavernous hemangiomas occur mostly in the left ventricle and showed hypodense on the CT scan. After enhancement, the lesions may show a gradual filling from the margin to the center. Angiosarcoma is the most common cardiac malignancy, which is mostly located in the right atrium, with dyspnea and chest pain as the main clinical manifestations. The imaging shows a mass with heterogeneous

TABLE 2 | Magnetic resonance imaging findings of cardiac paraganglioma.

Sr. no.	References	Age (years)	Sex	Location	T1WI	T2WI	Enhancement patter	Density characteristics
1	Duan et al. (10)	22	Woman	Left atrium	Hyperintense	Hyperintense	NA	Heterogeneous
2	Patrianakos et al. (11)	38	Man	Transverse sinus	Isointense to myocardium	Strong hyperintense	NA	NA
3	Arcos et al. (1)	22	Woman	Left atrioventricular groove	Slight hyperintense	Slight hyperintense	Focal late gadolinium enhancement	Heterogeneous
4	Berona et al. (12)	34	Woman	Left atrium	Hyperintense	Hyperintense	NA	NA
5	Degrauwe et al. (13)	43	Man	Intrapericardial	Isointense	Hyperintense	Intense enhancement	Homogenous
6	Gahremanpour et al. (14)	24	Woman	Left atrial	Hyperintense	Hyperintense	Substantial contrast enhancement	NA
7	Bhojwani et al. (15)	42	Man	Left anterior descending artery	Intermediate hyperintense	Hyperintense	Avid contrast enhancement	NA
8	Del Forno et al. (16)	46	Woman	Right atrioventricular groove	Hypointense	Hyperintense	NA	Heterogeneous
9	Beroukhim et al. (17)	16	Man	Between the aorta and the main pulmonary artery	Isointense	Hyperintense	Peripheral hyperenhancement	Heterogeneous
10	Manabe et al. (18)	46	Woman	Between the pulmonary artery trunk and the left atrium	NA	Hyperintense	Avid enhancement	Heterogeneous
11	Semionov and Sayegh, (19)	25	Woman	Right intrapericardial	NA	NA	Avid enhancement	NA
12	Tomasian et al. (20)	25	Woman	Left atrial	Hypointense	Hyperintense	Intense enhancement	Heterogeneous
13	Alghamdi et al. (21)	39	Man	Between the left atrial appendage and the main pulmonary artery	NA	NA	Avid enhancement	Heterogeneous
14	Thomas et al. (22)	32	Woman	Right atrioventricular groove	NA	NA	Avid enhancement	Heterogeneous
15	McGann et al. (23)	54	Man	Right atrium	NA	NA	Thin, circumferential rim of contrast-enhanced tissue	Heterogeneous

TABLE 3 | The single photon emission computed tomography (SPECT) and positron emission tomography (PET) findings of cardiac paraganglioma.

Sr.no.	References	Age (years)	Sex	Location	Imaging methods	Metabolism	Distant metastasis
1	Duan et al. (10)	22	Woman	Left atrium	^{18}F-FDG PET/CT	Hypermetabolic (SUVmax 29.5)	None
2	Michałowska et al. (24)	25	Man	Atrioventricular groove	^{99m}Tc-HYNICTOC SPECT/CT	Hypermetabolic	None
3	Huot Daneault et al. (25)	47	Man	Right atrium	^{18}F-FDG PET/CT	Marked hypermetabolism (SUVmax 36)	Diffuse bone metastatic
3	Huot Daneault et al. (25)	47	Man	Right atrium	^{68}Ga-DOTATATE PET/CT	Hypermetabolic (SUVmax 14)	Diffuse bone metastatic
4	Wu et al. (26)	21	Man	Right atrioventricular sulcus	^{18}F-FDG PET/CT	Hypermetabolic	None
4	Wu et al. (26)	21	Man	Right atrioventricular sulcus	^{123}I- MIBG scintigraphy	Hypermetabolic	None
5	Arcos et al. (1)	22	Woman	Left atrioventricular groove	^{18}F-FDG PET/CT	Hypermetabolic	None
6	Gahremanpour et al. (14)	24	Woman	Left atrial	^{123}I-MIBG scintigraphy	Hypermetabolic	None
7	Almenieir et al. (27)	24	Woman	Right ventricle	^{18}F-FDG PET/CT	Hypermetabolic	None
8	Bhojwani et al. (15)	42	Man	Abutting the left anterior descending artery	^{18}F-FDG PET/MRI	Hypermetabolic (SUVmax 16)	None
9	Manabe et al. (18)	46	Woman	Between the pulmonary artery trunk and the left atrium	^{123}I-MIBG scintigraphy	Obvious focal hypermetabolic	None
9	Manabe et al. (18)	46	Woman	Between the pulmonary artery trunk and the left atrium	^{18}F-FDG PET/CT	Hypermetabolic (SUVmax 15.6)	None
10	Semionov and Sayegh (19)	25	Woman	Right intrapericardial	^{18}F-FDG PET/CT	Hypermetabolic (SUVmax 31)	None
11	Tomasian et al. (20)	25	Woman	Left atrial	^{18}F-FDG PET/CT	Hypermetabolic	None
12	Thomas et al. (22)	32	Woman	Right atrioventricular groove	^{18}F-FDG PET/CT	Hypermetabolic	None
13	Dhanasopon et al. (28)	24	Woman	Left atrium	^{18}F-DOPA PET/CT	Hypermetabolic	None
14	Yuan et al. (29)	15	Woman	Right atrium	^{123}I-MIBG scintigraphy	Hypermetabolic	None
15	Sheehy et al. (30)	37	Woman	Right atrioventricular groove	^{18}F-FDG PET/CT	Hypermetabolic	None

MIBG, metaiodobenzylguanidine; FDOPA, 6-18F-fluoro-L-3, 4-dihydroxyphenylalanine; HYNICTOC, hydrazinonicotinyl-Tyr3-octreotide; FDG, fluorodeoxyglucose.

density/signal and enhancement due to the existence of necrosis. Extensive pericardial involvement and hemorrhagic pericardial effusion can be found. Due to the low incidence and variety of cardiac tumors, it is easy to miss or misdiagnose them by relying on one examination alone. Therefore, in addition to imaging methods, the diagnosis of cardiac tumors should be based on clinical and pathological examinations.

Complete surgical resection is the most effective treatment modality for CPGL; in some cases of CPGL, heart transplantation might be necessary (3). The role of adjuvant therapy in CPGL is unclear. Ayala-Ramirez et al. (36) evaluated the clinical benefit of systemic chemotherapy in patients with metastatic pheochromocytoma. The study by Tanabe et al. (37) describes the response to cyclophosphamide, vincristine, and dacarbazine (CVD) in 17 patients with malignant paraganglioma. Tumor volume or biochemical markers were decreased by only 30% in 47.1% of the patients and the progression-free survival was 31–60 months (37). Patients with complete resection of the tumor have a good long-term prognosis (38). However, more than 50% of CPGL have intraoperative or postoperative complications, whereas their proximity to the vasculature and complex surrounding tissue relationships make the procedure technically challenging, and the mortality rate is quite high (29). Adequate preoperative preparation is important to prevent intraoperative life-threatening conditions, such as a hypertensive crisis (39). This case was managed as a complete resection of the tumor under extracorporeal circulation with a good postoperative prognosis.

CONCLUSION

In this case, the glucose metabolism of the right atrial soft tissue mass was high, along with pathological brown fat uptake and clinical symptoms, so CPGL was considered, which is consistent with the pathological diagnosis. The combination of ^{18}F-FDG PET/CT with the CMR containing different image acquisition sequences provides a powerful aid for preoperative non-invasive diagnosis, localization, and staging of CPGL, which helps to reduce intraoperative and postoperative complications and to

improve the patient prognosis. In addition, the combination of functional and anatomical imaging of PET/CT examination can help to find or exclude metastatic lesions in patients.

DATA AVAILABILITY STATEMENT

The raw data supporting the conclusions of this article will be made available by the authors, without undue reservation.

ETHICS STATEMENT

Written informed consent was obtained from the individual(s) for the publication of any potentially identifiable images or data included in this article.

AUTHOR CONTRIBUTIONS

W-PH: acquisition and analysis of the work, drafting of the manuscript, data collection of imaging, and data analysis. GG and ZC: manuscript editing. Y-KQ: formal analysis and resource acquisition. J-BG: review and editing. LK: supervision and writing – review and editing. All authors contributed to the article and approved the submitted version.

FUNDING

This study was funded by the Beijing Science Foundation for Distinguished Young Scholars (JQ21025) and the Peking University Medicine Fund of Fostering Young Scholars' Scientific & Technological Innovation (BMU2022PY006).

REFERENCES

1. Arcos L, Bustos J, Acuña J, Cely A, Forero J, Jaimes C. Cardiac paraganglioma: advantages of cardiovascular multimodality imaging. *CASE (Phila).* (2018) 2:266–72. doi: 10.1016/j.case.2018.07.011
2. Huang W, Li L, Gao J, Gao JB. Epithelioid hemangioendothelioma of the right atrium invaded the superior vena cava: case report and review of literature. *Int J Cardiovasc Imaging.* (2021) 37:285–90. doi: 10.1007/s10554-020-01963-w
3. Neumann HPH, Young WF Jr., Eng C. Pheochromocytoma and paraganglioma. *N Engl J Med.* (2019) 381:552–65. doi: 10.1056/NEJMra1806651
4. Hodin R, Lubitz C, Phitayakorn R, Stephen A. Diagnosis and management of pheochromocytoma. *Curr Probl Surg.* (2014) 51:151–87. doi: 10.1067/j.cpsurg.2013.12.001
5. Tahir M, Noor SJ, Herle A, Downing S. Right atrial paraganglioma: a rare primary cardiac neoplasm as a cause of chest pain. *Tex Heart Inst J.* (2009) 36:594–7.
6. Manger WM. An overview of pheochromocytoma: history, current concepts, vagaries, and diagnostic challenges. *Ann N Y Acad Sci.* (2006) 1073:1–20. doi: 10.1196/annals.1353.001
7. Young WF Jr. Paragangliomas: clinical overview. *Ann N Y Acad Sci.* (2006) 1073:21–9. doi: 10.1196/annals.1353.002
8. Romano S, Fava C, Minuz P, Farzaneh-Far A. Succinate dehydrogenase gene mutation with cardiac paraganglioma: multimodality imaging and pathological correlation. *Eur Heart J.* (2017) 38:1853–4. doi: 10.1093/eurheartj/ehx007
9. Zhang Y, Wu QL, Yun JP. [Interpretation of the fourth edition of WHO pathological classification of the thyroid tumors in 2017]. *Zhonghua Er Bi Yan Hou Tou Jing Wai Ke Za Zhi.* (2018) 53:718–20. doi: 10.3760/cma.j.issn.1673-0860.2018.09.020
10. Duan Y, Xu R, Liu W, Cui X, Li K, Yang X, et al. PET/CT in a patient with cardiac paraganglioma. *Int J Cardiovasc Imaging.* (2021) 37:1473–7. doi: 10.1007/s10554-020-02101-2
11. Patrianakos AP, Iliopoulos D, Marketou M, Skalidis EI, Parthenakis FI. Cardiac paraganglioma: multimodality imaging of a rare tumor. *JACC Case Rep.* (2021) 3:273–5. doi: 10.1016/j.jaccas.2020.11.047
12. Berona K, Joshi R, Woo YJ, Shrager J. Postpartum diagnosis of cardiac paraganglioma: a case report. *J Emerg Med.* (2021) 55:e101–5. doi: 10.1016/j.jemermed.2018.05.034
13. Degrauwe S, Monney P, Qanadli SD, Prior J, Beigelmann-Aubry C, Masci PG, et al. Intrapericardial paraganglioma: the role of integrated advanced multimodality cardiac imaging for the assessment and management of rare primary cardiac tumors. *Cardiol J.* (2017) 24:447–9. doi: 10.5603/CJ.2017.0091
14. Gahremanpour A, Pattakos G, Reul RM, Mirzai-Tehrane M. Diagnostic imaging and treatment of a left atrial paraganglioma. *Tex Heart Inst J.* (2017) 44:296–8. doi: 10.14503/THIJ-16-5749
15. Bhojwani N, Huang J, Garg V, Yang M, Oliveira GH, Rajiah P. Utility of 18F-fluorodeoxyglucose positron emission tomography/magnetic resonance imaging in the diagnosis of cardiac paraganglioma. *Indian J Nucl Med.* (2017) 32:380–2. doi: 10.4103/ijnm.IJNM_93_17
16. Del Forno B, Zingaro C, Di Palma E, Capestro F, Rescigno G, Torracca L. cardiac paraganglioma arising from the right atrioventricular groove in a paraganglioma-pheochromocytoma family syndrome with evidence of sdhb gene mutation: an unusual presentation. *Ann Thorac Surg.* (2016) 102:e215–6. doi: 10.1016/j.athoracsur.2016.01.072
17. Beroukhim RS, del Nido P, Teot LA, Janeway K, Geva T. Cardiac paraganglioma in an adolescent. *Circulation.* (2012) 125:e322–4. doi: 10.1161/CIRCULATIONAHA.111.043968
18. Manabe O, Oyama-Manabe N, Alisa K, Hirata K, Itoh K, Terae S, et al. Multimodality evaluation of cardiac paraganglioma. *Clin Nucl Med.* (2012) 37:599–601. doi: 10.1097/RLU.0b013e3182485204
19. Semionov A, Sayegh K. Multimodality imaging of a cardiac paraganglioma. *Radiol Case Rep.* (2016) 11:277–81. doi: 10.1016/j.radcr.2016.08.002
20. Tomasian A, Lai C, Ruehm S, Krishnam MS. Cardiovascular magnetic resonance and PET-CT of left atrial paraganglioma. *J Cardiovasc Magn Reson.* (2010) 12:1. doi: 10.1186/1532-429X-12-1
21. Alghamdi AA, Sheth T, Manowski Z, Djoleto OF, Bhatnagar G. Utility of cardiac CT and MRI for the diagnosis and preoperative assessment of cardiac paraganglioma. *J Card Surg.* (2009) 24:700–1. doi: 10.1111/j.1540-8191.2009.00857.x
22. Thomas D, Grant FD, Kwong R, Nose V, Di Carli MF, Dorbala S. Multimodality imaging of an unusual case of cardiac paraganglioma. *J Nucl Cardiol.* (2009) 16:644–7. doi: 10.1007/s12350-009-9067-z
23. McGann C, Tazelaar H, Cho SR, Al-Saghir Y, Shean F, Young W, et al. In vivo detection of encapsulated intracardiac paraganglioma by delayed gadolinium enhancement magnetic resonance imaging. *J Cardiovasc Magn Reson.* (2005) 7:371–5. doi: 10.1081/jcmr-200053642
24. Michałowska AM, ćwikła JB, Konka M, Kolasińska-ćwikła A, Januszewicz A, Michałowska I, et al. Eleven-year follow-up of cardiac paraganglioma in a patient with SDHD C11X gene mutation. *Kardiol Pol.* (2021) 79:1276–7. doi: 10.33963/KP.a2021.0085
25. Huot Daneault A, Desaulniers M, Beauregard JM, Beaulieu A, Arsenault F, April G, et al. Highly symptomatic progressing cardiac paraganglioma with intracardiac extension treated with 177Lu-DOTATATE: a case report. *Front Endocrinol (Lausanne).* (2021) 12:705271. doi: 10.3389/fendo.2021.705271
26. Wu C, Yang X, Zhang H, Song Y. Cardiac paraganglioma with sulfur subunit B gene mutation: a case report. *Eur Heart J Case Rep.* (2021) 5:ytab025. doi: 10.1093/ehjcr/ytab025
27. Almenieir N, Karls S, Derbekyan V, Lisbona R. Nuclear imaging of a cardiac paraganglioma. *J Nucl Med Technol.* (2017) 4:247–8. doi: 10.2967/jnmt.116.182212

28. Dhanasopon AP, Shemin RJ, Yeh MW. Cardiac paraganglioma presenting as gestational hypertension. *Surgery.* (2010) 147:459–61. doi: 10.1016/j.surg.2008.08.018
29. Yuan WQ, Wang WQ, Su TW, Chen HT, Shi ZW, Fang WQ, et al. A primary right atrium paraganglioma in a 15-year-old patient. *Endocrine.* (2007) 32:245–8. doi: 10.1007/s12020-007-9019-9
30. Sheehy N, Kulke MH, Van den Abbeele AD. F-18 FDG PET/CT in the diagnosis and management of a pericardiac paraganglioma. *Clin Nucl Med.* (2008) 33:545–6. doi: 10.1097/RLU.0b013e31817dea57
31. Chan EY, Ali A, Umana JP, Nguyen DT, Hamilton DJ, Graviss EA, et al. Management of primary cardiac paraganglioma. *J Thorac Cardiovasc Surg.* (2020) S0022-5223:32704–5. doi: 10.1016/j.jtcvs.2020.09.100
32. Taïeb D, Jha A, Treglia G, Pacak K. Molecular imaging and radionuclide therapy of pheochromocytoma and paraganglioma in the era of genomic characterization of disease subgroups. *Endocr Relat Cancer.* (2019) 26:R627–52. doi: 10.1530/ERC-19-0165
33. Jalil ND, Pattou FN, Combemale F, Chapuis Y, Henry JF, Peix JL, et al. Effectiveness and limits of preoperative imaging studies for the localisation of pheochromocytomas and paragangliomas: a review of 282 cases. French association of surgery (AFC), and the French association of endocrine surgeons (AFCE). *Eur J Surg.* (1998) 164:23–8. doi: 10.1080/110241598750004913
34. Van Der Horst-Schrivers AN, Jager PL, Boezen HM, Schouten JP, Kema IP, Links TP. Iodine-123 metaiodobenzylguanidine scintigraphy in localising phaeochromocytomas–experience and meta-analysis. *Anticancer Res.* (2006) 26:1599–604.
35. Timmers HJ, Chen CC, Carrasquillo JA, Whatley M, Ling A, Havekes B, et al. Comparison of 18F-fluoro-L-DOPA, 18F-fluoro-deoxyglucose, and 18F-fluorodopamine PET and 123I-MIBG scintigraphy in the localization of pheochromocytoma and paraganglioma. *J Clin Endocrinol Metab.* (2009) 94:4757–67. doi: 10.1210/jc.2009-1248
36. Ayala-Ramirez M, Feng L, Habra MA, Rich T, Dickson PV, Perrier N, et al. Clinical benefits of systemic chemotherapy for patients with metastatic pheochromocytomas or sympathetic extra-adrenal paragangliomas: insights from the largest single-institutional experience. *Cancer.* (2012) 118:2804–12. doi: 10.1002/cncr.26577
37. Tanabe A, Naruse M, Nomura K, Tsuiki M, Tsumagari A, Ichihara A. Combination chemotherapy with cyclophosphamide, vincristine, and dacarbazine in patients with malignant pheochromocytoma and paraganglioma. *Horm Cancer.* (2013) 4:103–10. doi: 10.1007/s12672-013-0133-2
38. Khan MF, Datta S, Chisti MM, Movahed MR. Cardiac paraganglioma: clinical presentation, diagnostic approach and factors affecting short and long-term outcomes. *Int J Cardiol.* (2013) 166:315–20. doi: 10.1016/j.ijcard.2012.04.158
39. Chen G, Wang J, Weinberg L, Robinson C, Ho T, Lin W, et al. Anaesthetic management of cardiac phaeochromocytoma: a case series. *Int J Surg Case Rep.* (2018) 51:134–8. doi: 10.1016/j.ijscr.2018.08.019

Conflict of Interest: The authors declare that the research was conducted in the absence of any commercial or financial relationships that could be construed as a potential conflict of interest.

Publisher's Note: All claims expressed in this article are solely those of the authors and do not necessarily represent those of their affiliated organizations, or those of the publisher, the editors and the reviewers. Any product that may be evaluated in this article, or claim that may be made by its manufacturer, is not guaranteed or endorsed by the publisher.

frontiers | Frontiers in Medicine

TYPE Case Report
PUBLISHED 04 August 2022
DOI 10.3389/fmed.2022.967531

OPEN ACCESS

EDITED BY
Gaurav Malviya,
University of Glasgow, United Kingdom

REVIEWED BY
Majid Assadi,
Bushehr University of Medical Sciences, Iran
Domenico Albano,
University of Brescia, Italy

*CORRESPONDENCE
Jiong Cai
jiong_cai@163.com
Pan Wang
1298178828@qq.com
Dandan Li
807442003@qq.com

†These authors have contributed equally to this work

SPECIALTY SECTION
This article was submitted to Nuclear Medicine, a section of the journal Frontiers in Medicine

RECEIVED 13 June 2022
ACCEPTED 05 July 2022
PUBLISHED 04 August 2022

CITATION
Hu X, Xiong W, Li S, Li X, Cai J, Wang P and Li D (2022) Case report: Thoracic and lumbar plasma cell myeloma mimicking hemangiomas on MRI and ^{18}F-FDG PET/CT.
Front. Med. 9:967531.
doi: 10.3389/fmed.2022.967531

Case report: Thoracic and lumbar plasma cell myeloma mimicking hemangiomas on MRI and ^{18}F-FDG PET/CT

Xianwen Hu[1†], Wei Xiong[2†], Shun Li[1], Xue Li[1], Jiong Cai[1*], Pan Wang[1*] and Dandan Li[3*]

[1]Affiliated Hospital of Zunyi Medical University, Department of Nuclear Medicine, Zunyi, China, [2]Yinjiang Autonomous County People's Hospital, Department of Medical Imaging, Yinjiang, China, [3]Zunyi Hospital of Traditional Chinese Medicine, Department of Obstetrics, Zunyi, China

Plasma cell myeloma (PCM) is a malignant clonal disease of abnormal proliferation of plasma cells, which is the second most common hematological malignancy after leukemia. PCM often diffuses and involves the bones of the whole body, especially the spinal column, ribs, skull, pelvis, and other axial bones and flat bones. Herein, we present a 55-year-old man who came to the hospital seeking medical help for low-back pain and numbness in his lower limbs. Computed tomography (CT) was performed because the clinician suspected that the patient had a herniated disc, and the results showed that the 7th thoracic vertebrae and the 3rd lumbar vertebrae showed a low density of bone destruction with "honeycombing" changes. Magnetic resonance imaging (MRI) showed that the corresponding lesions presented long T1 and long T2 signals, and the lesions were significantly enhanced in contrast-enhanced T1WI sequences, and fluoro18-labeled deoxyglucose positron emission tomography/computed tomography (^{18}F-FDG PET/CT) showed mild radioactive uptake in the lesions. Based on these imaging findings, the patient was considered for a diagnosis of hemangiomas, and surgery was performed because the affected vertebra was pressing on the spinal cord. However, intraoperative frozen section examination showed that the patient had plasma cell myeloma. Our case study suggests that PCM involving a single thoracic and lumbar spine is rare and should be considered as one of the imaging differential diagnoses of hemangiomas. Moreover, the diagnosis of PCM is difficult when the number of lesions is small, especially when the plasma cell ratio is within the normal reference range in laboratory tests.

KEYWORDS

plasma cell myeloma, hemangioma, PET/CT, magnetic resonance imaging, fluoro18-labeled deoxyglucose

10.3389/fmed.2022.967531

Case description

A 55-year-old male patient presented to our hospital for more than half a year due to lower-back pain and numbness of both lower extremities. Physical examination showed that the muscle strength of both lower extremities of the patient was weakened, the lower back suffered percussion pain, and there were no positive signs in the rest of the body. The hemogram, bone marrow examination, and tumor marker values of the patient were all within the normal reference range. Imaging examinations were performed because clinicians suspected he had a lumbar disc herniation. CT showed that the patient's 7^{th} thoracic vertebral body, right vertebral arch, and 3^{rd} lumbar vertebral body had low-density bone destruction, showing "fence-like" or "honeycombing" changes (as shown in Supplementary Figure 1), which presented as uneven low T1 and high T2 signals on magnetic resonance imaging (MRI), and a contrast-enhanced scan showed marked enhancement of the lesions (as shown in Figure 1). ^{18}F-FDG PET/CT showed a mild FDG concentration in the 7^{th} thoracic and 3^{rd} lumbar vertebrae, with a maximum standard uptake value (SUVmax) of 4 and 4.5, respectively, as shown in Figure 2. Based on negative laboratory results and imaging findings that simulated the "fence-like" or "honeycombing" appearance of hemangioma, the patient was considered for a diagnosis of hemangioma preoperatively. Because the diseased vertebral body has a wedge-shaped flattening and compresses the spinal cord backward, surgical treatment is necessary in order to relieve its compression symptoms. Under general anesthesia, the patient received "posterior percutaneous 3^{rd} lumbar vertebral balloon dilatation kyphoplasty, and posterior 7^{th} thoracic vertebra vertebroplasty plus posterior 7^{th} thoracic vertebral adnexectomy, spinal canal exploration and decompression, and posterior screw rod system internal fixation." The diseased tissue removed surgically was sent for biopsy; HE staining showed the diffuse distribution of round or oval plasma cells in the tumor. Immunohistochemistry showed positive expression of tumor cells CD56, CD79a, CD138, Kappa, MUM1, CD38, Vimentin, and Lambda was weakly positive, but CD20, CD3, CK, EMA, LCA, and ALK were negative (as shown in Figure 3). Postoperatively, the patient received 10 local radiotherapy sessions over a 2-week period, each dose of approximately 30 Gy. The patient's condition was stable, and no progress was found in the follow-up for 2 years through imaging examinations. A recent X-ray examination is shown in Supplementary Figure 2.

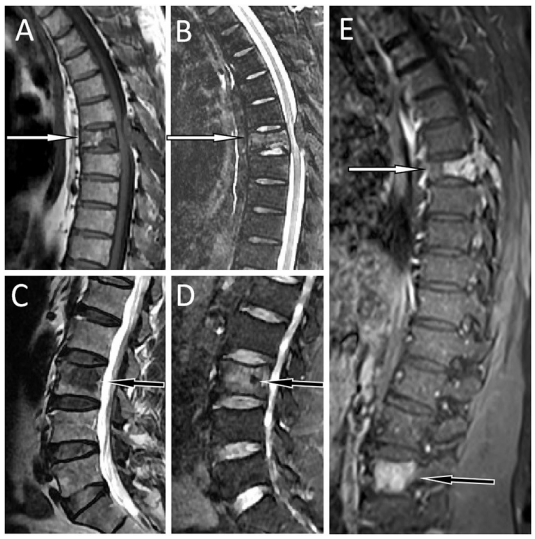

FIGURE 1
MRI showed abnormal signal shadows in the 7th thoracic (T7) and adnexa vertebrae [**(A)** T1WI; **(B)** T2WI fat suppression sequence; white arrows] and the 3rd lumbar vertebrae [**(C)** T1WI; **(D)** T2WI fat suppression sequence; black arrows]. Besides, The T7 vertebrae became wedge-shaped, suggesting a pathological compression fracture. T1WI contrast enhancement showed obvious homogeneous enhancement of the lesions **(E)**. T7, the white arrow; L3, the black arrow.

Discussion

Plasmacytoma is a B-cell monoclonal malignant tumor characterized by abnormal proliferation of plasma cells, accounting for about 10% of hematological malignancies (1). The etiology of the disease is unclear, but a study has found that it is closely related to herpes viruses in dendritic cells cultured from patients with myeloma, as well as to long-term exposure to industrial and agricultural toxins, ionizing radiation, chronic infection, advanced age, male sex, obesity, and family history of hematologic malignancies (2). Studies have shown that the occurrence of PCM is related to cytogenetic abnormalities, including 1q21 gene amplification, 17p deletion, and IgH rearrangement, and (t 4; 14), (t 14; 16), (t 14; 20) are considered high-risk factors (3–5). PCM is more common in the elderly, with a median age of 68 years at diagnosis, and only 35% of patients younger than 65 years at diagnosis (6). PCM often pervades the whole body bones, especially the spinal column, ribs, skull, pelvis, and other axial bones and flat bones, which is mainly manifested as progressive lytic bone destruction, which can lead to pathological fracture with the progression of the disease, and patients often come to the hospital for medical help because of bone pain (7, 8). Moreover, PCM can cause abnormal hematopoietic function, anemia, hypercalcemia, abnormal renal function, and repeated infections may appear (9). The clinical diagnosis of PCM mainly includes serological examination, bone marrow puncture, and biopsy. The proportion of monoclonal plasma cells in bone marrow $\geq$ 10% or clear biopsy evidence indicating bone or soft tissue plasma cell tumor (i.e., extramedullary plasma cell tumor) is the necessary condition for the diagnosis of MM, and only

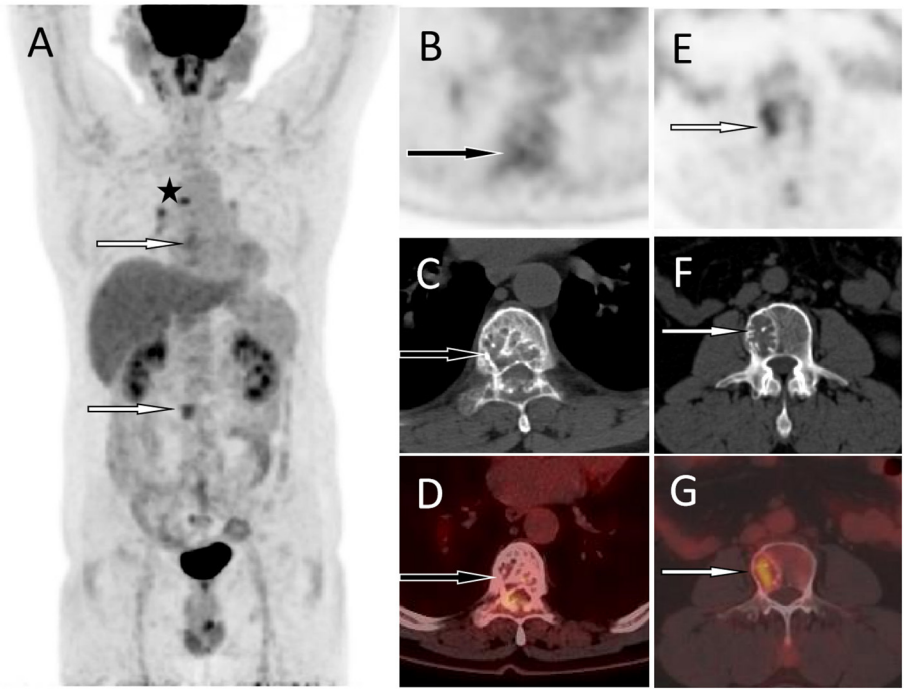

FIGURE 2
^{18}F-FDG PET/CT was then performed to assess the nature of the lesion and the patient's systemic condition. The MIP **(A)** showed mild radiation uptake in the T7 area (the black arrow) and increased FDG uptake in the L3 lesion area (the white arrow). In addition, there is radioactive uptake of lymph nodes in the mediastinum (the asterisk arrow), which are pathologically confirmed as inflammatory. The axial figures at the T7 level [**(B)** PET; **(C)** CT; **(D)** PET/CT fusion] showed the destruction of bone density in the vertebral body and adnexa, presenting a "fence-like" change, with a slight increase in FDG uptake and an SUVmax of 3.0 (black arrows). An axial map at the L3 level [**(E)** PET; **(F)** CT; **(G)** PET/CT fusion] showed destruction of bone density in the right portion of the vertebral body with increased FDG uptake and SUVmax of 4.5 (white arrows). Based on these imaging findings, the patient was considered to have hemangiomas. Based on pathological and immunohistochemical findings, the patient was confirmed to have plasma cell myeloma.

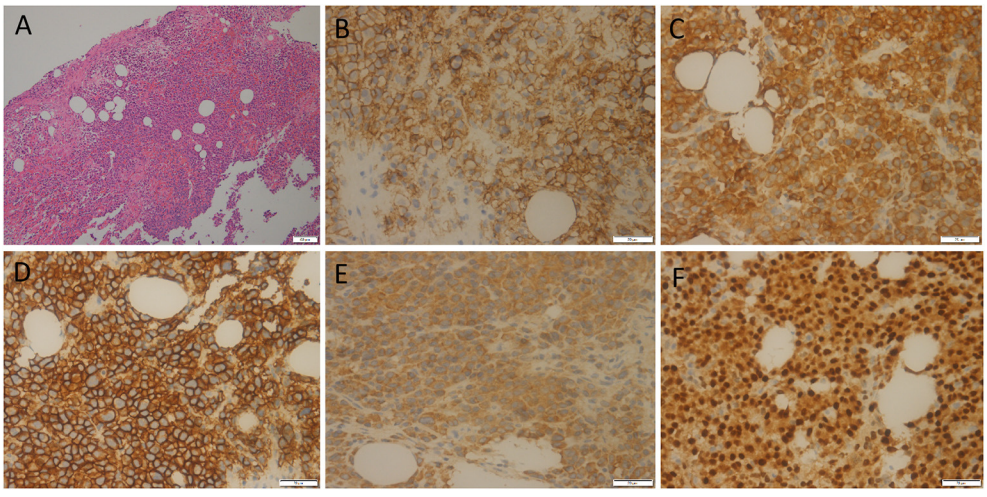

FIGURE 3
HE staining showed the diffuse distribution of round or oval plasma cells in the tumor **(A)**. Immunohistochemistry showed positive expression of tumor cells CD56 **(B)**, CD79a **(C)**, CD138 **(D)**, Kappa **(E)**, and MUM1 **(F)**.

3–5% of MM patients with bone marrow plasma cell proportion <10% (10). The results of the bone marrow examination in our case were all within the normal reference range, which is relatively rare.

Imaging examinations are of great significance to the localization of PCM, the extent of involvement, and the formulation of treatment plans, especially CT, MRI, and PET/CT. On CT, PCM mainly manifests as punch-like, moth-eaten, or granular low-density bone destruction areas, and some patients only show osteoporosis-like changes (11). Vertebral PCMs have different MRI appearances at different ages due to changes in the ratio of red and yellow bone marrow components. On T1WI, the area of bone destruction or bone marrow infiltration is a clearly demarcated low signal against the high signal of bone marrow fat, and contrast-enhanced T1WI scans showed mild to moderate inhomogeneous enhancement; on T2WI, the lack of contrast with a bone marrow fat signal often leads to unclear lesions; on T2WI, fat suppression due to the signal of fat was suppressed, and the high signal of the lesion was clearly displayed (12). MRI diffusion-weighted imaging (DWI) is a non-invasive method that can reflect the diffusion of water molecules in living tissues, which has a high sensitivity and specificity for the detection of bone marrow lesions in patients with PCM, and, by measuring, apparent diffusion coefficient (ADC) value can indirectly and quantitatively evaluate the damage degree of bone marrow lesions (13). Due to the infiltration and accumulation of malignant plasma cells to replace normal bone marrow tissue, the extracellular space is reduced, and the movement of water molecules is blocked, resulting in a decrease in the ADC value of PCM lesions so as to differentiate PCM from other benign lesions such as hemangioma (14). The metabolism of PCM tissue is relatively strong, and the glycolysis of normal tissue cells is significantly lower than that of the lesion. Therefore, the lesion tissue will take up a large amount of ^{18}F-FDG, which shows a large amount of radioactive concentration during PET/CT imaging (15). Compared with CT and MRI, PET/CT can better display the lesion volume and metabolic activity of patients with PCM, and has higher sensitivity and specificity in the detection of extramedullary infiltration of PCM (16–18). Moreover, PET/CT also plays an important role in the efficacy evaluation after treatment and prognosis of patients with PCM, and studies have suggested that the metabolic activity of lesions, the volume of high metabolic lesions, and extramedullary infiltration are all related factors affecting the survival (19–21). In addition to FDG, ^{68}ga-pentixafor, ^{11}C-choline, and ^{11}C-methionine were also used as PET tracers in plasma cell myeloma detection studies and showed a higher detection rate than FDG (22–24).

Spinal PCM should be differentiated from metastases, vertebral tuberculosis, hemangioma, etc. Metastatic bone tumors are more common in middle-aged and elderly people, and usually have primary tumors, which are mostly osteolytic destruction of the posterior vertebral body, with unclear boundaries and irregular shapes, often involving the vertebral arch and forming paravertebral soft tissue masses (25). Spinal tuberculosis is mostly irregular osteolytic destruction, the intervertebral space between the diseased vertebral bodies narrows and disappears, the vertebral bodies are embedded in each other, and paravertebral cold abscesses and bone bridge formation may also appear. On MRI, the diseased vertebral body usually shows an inhomogeneous low signal on T1WI and a high signal on T2WI, and the paravertebral abscess shows annular enhancement on an enhanced scan (26). The typical CT manifestations of vertebral hemangioma are decreased bone density of the affected vertebral body, with mesh or honeycomb changes, and slight swelling and thinning of the bone cortex. Two-dimensional reconstruction shows "fence-like" or "honeycombing" of the affected vertebral body, and the lesions may invade half or the entire vertebral body or accessories, with occasional paravertebral or intraspinal soft tissue masses, and non-contrast-enhanced scans; the tumor was significantly enhanced due to the presence of more vascular components (27, 28). Our patient showed "fence-like" low-density bone destruction on CT, with obvious homogeneous enhancement on enhanced MRI, and mild radioactive uptake on PET/CT, which overlapped with the imaging features of hemangioma and was misdiagnosed, which overlapped with the imaging features of hemangioma and was misdiagnosed.

The main treatment of PCM includes anti-myeloma drugs, bone-targeted drug therapy, local radiotherapy, and chemotherapy, while surgery is usually not recommended for patients with a definite diagnosis of PCM because the optimal timing of chemoradiation may be missed (29). However, when the tumor destroys the bone and causes a fracture, surgery should be performed as soon as possible when the patient has spinal cord compression with neurological symptoms, as surgery can relieve the tumor's compression on the spinal cord and avoid further aggravation of spinal cord injury caused by compression (30). At the same time, the development of individualized diagnosis and treatment plans for PCM patients with different conditions is helpful for the improvement of the patient's condition. The prognosis of patients with PCM is poor, and the literature reports that the 2- and 3-year survival rates of PCM patients with spinal cord involvement are 58 and 50%, respectively (31). Our patient has been followed up for 2 years without disease progression.

In conclusion, PCM of a single thoracic and lumbar spine is rare, and its imaging manifestations can be simulated as vertebral hemangioma, which should be used as one of its differential diagnoses. Individualized treatment plans are feasible for patients with vertebral PCM, especially those with spinal cord compression. Local radiotherapy after surgical resection of the lesion may improve the prognosis of single thoracic and lumbar PCM.

Data availability statement

The original contributions presented in the study are included in the article/Supplementary material, further inquiries can be directed to the corresponding authors.

Ethics statement

Written informed consent was obtained from the individual(s) for the publication of any potentially identifiable images or data included in this article.

Author contributions

JC and PW: funding acquisition. DL: investigation. SL: methodology. XH and WX: writing–original draft. XH, XL, and JC: writing–review and editing. All authors contributed to the article and approved the submitted version.

Funding

This study was funded by the National Natural Science Foundation of the People's Republic of China, NSFC (Grant No. 81571712), Zunyi Medical College Research Start Fund 2018ZYFY03, and QianKeHe platform talents [2017] (Grant No. 5733-035).

Conflict of interest

The authors declare that the research was conducted in the absence of any commercial or financial relationships that could be construed as a potential conflict of interest.

Publisher's note

All claims expressed in this article are solely those of the authors and do not necessarily represent those of their affiliated organizations, or those of the publisher, the editors and the reviewers. Any product that may be evaluated in this article, or claim that may be made by its manufacturer, is not guaranteed or endorsed by the publisher.

Supplementary material

The Supplementary Material for this article can be found online at: https://www.frontiersin.org/articles/10.3389/fmed.2022.967531/full#supplementary-material

References

1. Kyle RA, Rajkumar SV. Multiple myeloma. *Blood.* (2008) 111:2962–72. doi: 10.1182/blood-2007-10-078022

2. Brown LM, Gridley G, Check D, Landgren O. Risk of multiple myeloma and monoclonal gammopathy of undetermined significance among white and black male United States veterans with prior autoimmune, infectious, inflammatory, and allergic disorders. *Blood.* (2008) 111:3388–94. doi: 10.1182/blood-2007-10-121285

3. Walker BA, Wardell CP, Murison A, Boyle EM, Begum DB, Dahir NM, et al. APOBEC family mutational signatures are associated with poor prognosis translocations in multiple myeloma. *Nat Commun.* (2015) 6:6997. doi: 10.1038/ncomms7997

4. Ross FM, Chiecchio L, Dagrada G, Protheroe RKM, Stockley DM, Harrison CJ, et al. The t(14;20) is a poor prognostic factor in my eloma but is associated with long-term stable disease in monoclonal gammopathies of undetermined significance. *Haematologica.* (2010) 95:1221–5. doi: 10.3324/haematol.2009.016329

5. Specht K, Haralambieva E, Bink K, Kremer M, Mandl-Weber S, Koch I, et al. Different mechanisms of cyclin D1 overexpression in multiple myeloma revealed by fluorescence *in situ* hybridization and quantitative analysis of mRNA levels. *Blood.* (2004) 104:1120–6. doi: 10.1182/blood-2003-11-3837

6. Palumbo A, Avet-Loiseau H, Oliva S, Lokhorst HM, Goldschmidt H, Rosinol L, et al. Revised international staging system for multiple myeloma: a report from international myeloma working group. *J Clin Oncol.* (2015) 33:2863–9. doi: 10.1200/JCO.2015.61.2267

7. Dores GM, Landgren O, McGlynn KA, Curtis RE, Linet MS, Devesa SS. Plasmacytoma of bone, extramedullary plasmacytoma, and multiple myeloma: incidence and survival in the United States, 1992-2004. *Br J Haematol.* (2009) 144:86–94. doi: 10.1111/j.1365-2141.2008.07421.x

8. Faria KM, Ribeiro ACP, Brandão TB, Silva WG, Lopes MA, Pereira J, et al. Radiographic patterns of multiple myeloma in the jawbones of patients treated with intravenous bisphosphonates. *J Am Dent Assoc.* (2018) 149:382–91. doi: 10.1016/j.adaj.2017.12.028

9. Cowan AJ, Allen C, Barac A, Basaleem H, Bensenor I, Curado MP, et al. Global burden of multiple myeloma: a systematic analysis for the global burden of disease study 2016. *JAMA Oncol.* (2018) 4:1221–7. doi: 10.1001/jamaoncol.2018.2128

10. Rajkumar SV, Dimopoulos MA, Palumbo A, Blade J, Merlini G, Mateos MV, et al. International myeloma working group updated criteria for the diagnosis of multiple myeloma. *Lancet Oncol.* (2014) 15:e538–48. doi: 10.1016/S1470-2045(14)70442-5

11. Pierro A, Posa A, Astore C, Sciandra M, Tanzilli A, Petrosino A, et al. Whole-body low-dose multidetector-row CT in multiple myeloma: guidance in performing, observing, and interpreting the imaging findings. *Life.* (2021) 11:1320. doi: 10.3390/life11121320

12. Sommer G, Klarhöfer M, Lenz C, Scheffler K, Bongartz G, Winter L. Signal characteristics of focal bone marrow lesions in patients with multiple myeloma using whole body T1W-TSE, T2W-STIR and diffusion-weighted imaging with background suppression. *Eur Radiol.* (2011) 21:857–62. doi: 10.1007/s00330-010-1950-0

13. Treitl KM, Ricke J, Baur-Melnyk A. Whole-body magnetic resonance imaging (WBMRI) vs. whole-body computed tomography (WBCT) for myeloma imaging and staging. *Skeletal Radiol.* (2022) 51:43–58. doi: 10.1007/s00256-021-03799-4

14. Dutoit JC, Verstraete KL. Whole-body MRI, dynamic contrast-enhanced MRI, and diffusion-weighted imaging for the staging of multiple myeloma. *Skeletal Radiol.* (2017) 46:733–50. doi: 10.1007/s00256-017-2609-6

15. Silva Y, Riedinger JM, Chrétien ML, Caillot D, Corre J. Guillen K, et al. Comparison between tumour metabolism derived from ^{18}F-FDG PET/CT and accurate cytogenetic stratification in newly diagnosed multiple myeloma patients. *Quant Imaging Med Surg.* (2021) 11:4299–309. doi: 10.21037/qims-21-85

16. Walker RC, Brown TL, Jones-Jackson LB, De Blanche L, Bartel T. Imaging of multiple myeloma and related plasma cell dyscrasias. *J Nucl Med.* (2012) 53:1091–101. doi: 10.2967/jnumed.111.098830

17. Tirumani SH, Sakellis C, Jacene H, Shinagare AB, Munshi NC, Ramaiya NH, et al. Role of FDG-PET/CT in extramedullary multiple myeloma: correlation of FDG-PET/CT findings with clinical outcome. *Clin Nucl Med.* (2016) 41:e7–13. doi: 10.1097/RLU.0000000000000902

18. Koppula B, Kaptuch J, Hanrahan CJ. Imaging of multiple myeloma: usefulness of MRI and PET/CT. *Semin Ultrasound CT MR.* (2013) 34:566–77. doi: 10.1053/j.sult.2013.05.006

19. Zamagni E, Cavo M. The role of imaging techniques in the management of multiple myeloma. *Br J Haematol.* (2012) 159:499–513. doi: 10.1111/bjh.12007

20. Bartel TB, Haessler J, Brown TL, Shaughnessy JD Jr, van Rhee F, Anaissie E, et al. F18-fluorodeoxyglucose positron emission tomography in the context of other imaging techniques and prognostic factors in multiple myeloma. *Blood.* (2009) 114:2068–76. doi: 10.1182/blood-2009-03-213280

21. Fonti R, Larobina M, Del Vecchio S, De Luca S, Fabbricini R, Catalano L, et al. Metabolic tumor volume assessed by ^{18}F-FDG PET/CT for the prediction of outcome in patients with multiple myeloma. *J Nucl Med.* (2012) 53:1829–35. doi: 10.2967/jnumed.112.106500

22. Pan Q, Cao X, Luo Y, Li J, Feng J, Li F. Chemokine receptor-4 targeted PET/CT with 68Ga-Pentixafor in assessment of newly diagnosed multiple myeloma: comparison to ^{18}F-FDG PET/CT. *Eur J Nucl Med Mol Imaging.* (2020) 47:537–46. doi: 10.1007/s00259-019-04605-z

23. Nanni C, Zamagni E, Cavo M, Rubello D, Tacchetti P, Pettinato C, et al. ^{11}C-choline vs. ^{18}F-FDG PET/CT in assessing bone involvement in patients with multiple myeloma. *World J Surg Oncol.* (2007) 5:68. doi: 10.1186/1477-7819-5-68

24. Lapa C, Kircher M, Da Via M, Schreder M, Rasche L, Kortüm KM, et al. Comparison of ^{11}C-Choline and ^{11}C-Methionine PET/CT in Multiple Myeloma. *Clin Nucl Med.* (2019) 44:620–4. doi: 10.1097/RLU.0000000000002638

25. Löfgren J, Mortensen J, Rasmussen SH, Madsen C, Loft A, Hansen AE, et al. A Prospective Study Comparing ^{99m}Tc-Hydroxyethylene-Diphosphonate Planar Bone Scintigraphy and Whole-Body SPECT/CT with ^{18}F-Fluoride PET/CT and ^{18}F-Fluoride PET/MRI for Diagnosing Bone Metastases. *J Nucl Med.* (2017) 58:1778–85. doi: 10.2967/jnumed.116.189183

26. Narlawar RS, Shah JR, Pimple MK, Patkar DP, Patankar T, Castillo M. Isolated tuberculosis of posterior elements of spine: magnetic resonance imaging findings in 33 patients. *Spine.* (2002) 27:275–81. doi: 10.1097/00007632-200202010-00015

27. Acosta FL Jr, Sanai N, Chi JH, Dowd CF, Chin C, Tihan T, et al. Comprehensive management of symptomatic and aggressive vertebral hemangiomas. *Neurosurg Clin N Am.* (2008) 19:17–29. doi: 10.1016/j.nec.2007.09.010

28. Teferi N, Abukhiran I, Noeller J, Helland LC, Bathla G, Ryan EC, et al. Vertebral hemangiomas: diagnosis and management. A single center experience. *Clin Neurol Neurosurg.* (2020) 190:105745. doi: 10.1016/j.clineuro.2020.105745

29. Akram H, Allibone J. Spinal surgery for palliation in malignant spinal cord compression. *Clin Oncol.* (2010) 22:792–800. doi: 10.1016/j.clon.2010.07.007

30. Kilciksiz S, Karakoyun-Celik O, Agaoglu FY, Haydaroglu A. A review for solitary plasmacytoma of bone and extramedullary plasmacytoma. *Sci World J.* (2012) 2012:895765. doi: 10.1100/2012/895765

31. Rades D, Veninga T, Stalpers LJ, Basic H, Rudat V, Karstens JH, et al. Outcome after radiotherapy alone for metastatic spinal cord compression in patients with oligometastases. *J Clin Oncol.* (2007) 25:50–6. doi: 10.1200/JCO.2006.08.7155

frontiers | Frontiers in Medicine

TYPE Case Report
PUBLISHED 11 August 2022
DOI 10.3389/fmed.2022.946477

OPEN ACCESS

EDITED BY
Silvia Taralli,
UOC di Medicina Nucleare, Dipartimento di Diagnostica per Immagini, Radioterapia Oncologica ed Ematologia, Fondazione Policlinico Universitario A. Gemelli (IRCCS), Italy

REVIEWED BY
Carmelo Caldarella,
Agostino Gemelli University Polyclinic (IRCCS), Italy
Yi Ji,
Sichuan University, China

*CORRESPONDENCE
Lei Kang
kanglei@bjmu.edu.cn

SPECIALTY SECTION
This article was submitted to Nuclear Medicine, a section of the journal Frontiers in Medicine

RECEIVED 14 June 2022
ACCEPTED 18 July 2022
PUBLISHED 11 August 2022

CITATION
Qiu Y, Chen Z, Yang Q, Huang W, Song L, Fan Y and Kang L (2022) Case report: A rare case of retroperitoneal kaposiform hemangioendothelioma with spinal involvement without abnormal platelet count in ^{18}F-FDG PET/CT.
Front. Med. 9:946477.
doi: 10.3389/fmed.2022.946477

Case report: A rare case of retroperitoneal kaposiform hemangioendothelioma with spinal involvement without abnormal platelet count in ^{18}F-FDG PET/CT

Yongkang Qiu, Zhao Chen, Qi Yang, Wenpeng Huang, Lele Song, Yan Fan and Lei Kang*

Department of Nuclear Medicine, Peking University First Hospital, Beijing, China

Kaposiform hemangioendothelioma (KHE) is a rare vascular neoplasm that mostly appears in infancy or early childhood. Most KHE occurred on the limbs and trunk with cutaneous lesions. Approximately 12% of KHE patients manifested as deep masses and spinal involvement is extremely rare. KHE may develop into life-threatening thrombocytopenia and consumptive coagulopathy, known as the Kasabach-Merritt phenomenon (KMP), especially in patients with retroperitoneal involvement. The thrombocytopenia is usually severe, with a median platelet count of 21 $\times$ 10^9/L at the initial presentation of KMP. Here, firstly we described a case of a 13-month-old girl with KHE who presented the movement limitation of the lower extremity caused by spinal involvement with a normal platelet count. ^{18}F-fluorodeoxyglucose-positron emission tomography/CT (^{18}F-FDG PET/CT) showed mildly elevated metabolism in the lesion, suggesting a probably low-grade malignant tumor. Then the patient was diagnosed with KHE by biopsy. After 6-month sirolimus monotherapy, the size of the retroperitoneal lesion was reduced significantly and the patient showed improvement in clinical symptoms. This case demonstrated the advantage of ^{18}F-FDG PET/CT in the evaluation of disease activity in KHE and the possibility of using ^{18}F-FDG PET/CT to guide therapy and prognostication.

KEYWORDS

kaposiform hemangioendothelioma, kasabach-merritt phenomenon, spinal involvement, sirolimus, PET/CT

Introduction

Kaposiform hemangioendothelioma (KHE) is a rare vascular neoplasm that mostly appears in infancy or early childhood. The pathogenesis of KHE has not yet been discovered (1). The main pathological features of KHE are dysregulation of angiogenesis and lymphangiogenesis. The histologic hallmark of KHE is infiltrating, defined and

confluent nodules of neoplastic spindled endothelial cells involving multiple planes of tissue, and the clusters of spindled tumor cells exhibit multiple slit-like vascular lumina, containing red blood cells (2). KHE can be classified into superficial, mixed, and deep lesions based on depth. Approximately 12% of KHE patients manifested as deep masses (3). The manifestations of KHE are variable, ranging from cutaneous lesions with variable performance to deep masses without cutaneous signs. KHE can be accompanied by a life-threatening complication Kasabach-Merritt phenomenon (KMP), which is characterized by thrombocytopenia, hypofibrinogenemia, and clotting factor consumption (3). Intrathoracic and retroperitoneal lesions are more likely to develop KMP because they are more expansive and infiltrative.

There is very little published research on ^{18}F-fluorodeoxyglucose-positron emission tomography/CT (^{18}F-FDG PET/CT) in KHE. Herein we report a case of retroperitoneal KHE with lower extremity mobility limitation caused by spinal involvement without abnormal platelet count. ^{18}F-FDG PET/CT scan helped to find the retroperitoneal lesion with mildly elevated metabolism, which suggested low disease activity.

Case description

A 13-month-old girl presented with lower extremity mobility limitation for 10 months. Left lower extremity weakness was first noted at 3 months of age, followed by pain when the left leg was straightened or extended. In the suspicion of bone disease, she underwent a non-contrast-enhanced CT scan that showed a pelvic mass with the destruction of the adjacent bone. Laboratory tests were normal and no obvious skin lesions were observed. The patient was diagnosed with immune thrombocytopenia at 7-month age, and the minimum platelet count was 38×10^9/L. But her platelet counts gradually return to normal without special treatment. The patient performed bone puncture and flow cytometry to rule out hematological diseases.

To assess the patient's whole-body condition and metabolically characterize the lesion, ^{18}F-FDG PET/CT examination was further performed. It revealed unevenly mildly increased metabolic uptake within the already known mass in the left retro-peritoneum. The boundary of the lesion is not clear, with an approximate size of 3.3 cm × 2.5 cm and SUVmax of 1.7 (**Figures 1A,D**). L4, L5, and left iliac bone showed mixed lytic and sclerotic changes, SUVmax of 1.8 (**Figures 1B,C,E,F**). Left psoas, iliopsoas, erector spinae, and gluteus medius were enlarged when compared to contralateral side muscles, as also evident at a subsequent contrast-enhanced CT scan. Contrast-enhanced CT scan showed the ill-defined lesion (**Figure 2A**) and rich blood vessels in the mass (**Figure 2B**). There were no other abnormal CT features or ^{18}F-FDG Uptake. Then the patient underwent a fine-needle biopsy of the retroperitoneal mass. Photomicrograph of the specimen showed there are many irregular hemangioma-like tumor cell nodules in the lesion, containing a large number of red blood cells (**Figures 3A,B**). The tumor cells were positive for Vimentin, CD31 (**Figure 3C**), CD34, ERG, SMA, and D2-40 (**Figure 3D**). Ki-67 staining showed the proportion of the positive tumor cells was about 1–2%. Upon pathologic examination with immunohistochemistry, KHE was diagnosed.

Then, sirolimus.8 mg/day monotherapy was started. Blood drug concentration and blood routine were monitored regularly. After 3-month sirolimus monotherapy, abdominal ultrasound suggested a reduction of the lesion. Meanwhile, the clinical symptoms and signs were recovered soon. She can stand for about 20 s. Blood drug concentration showed a mildly low level (6.2 ng/ml), so the dose of sirolimus changed to 1 mg/day. After 6-month sirolimus monotherapy, the retroperitoneal mass was reduced by 80% (**Figure 4**) and the clinical symptoms almost disappeared. The patient is still receiving sirolimus monotherapy and regular follow-up. During sirolimus treatment, there were no obvious adverse reactions or abnormal laboratory tests. The patient's platelet count has remained at normal levels since treatment. There are no new clinical signs and symptoms.

Discussion

Kaposiform hemangioendothelioma is a rare vascular neoplasm that mostly appears in infancy or early childhood. KHE is a kind of intermediate tumor type with locally aggressive characteristics, which is characterized by dysregulation of angiogenesis and lymphangiogenesis. KHE may develop into life-threatening thrombocytopenia and consumptive coagulopathy, known as KMP. Approximately 12% of KHE patients manifested as deep masses (3). Intrathoracic and retroperitoneal lesions are more likely to develop KMP because they are more expansive and infiltrative.

Deep KHEs, especially visceral KHEs, are usually undetectable, easily missed clinically, and generally associated with high mortality. The co-existence of a vascular mass with prominent thrombocytopenia and coagulopathy, including hypofibrinogenemia, can make the diagnosis of KHE relatively straightforward. In patients with deep KHE without KMP, a definitive diagnosis often depends on biopsy because of the non-specific and vague symptoms. A definitive preoperative differential diagnosis between deep KHE and a malignant tumor (e.g., neuroblastoma or sarcoma) is also complex and challenging in patients with spine involvement. Imaging findings are significant for pre-treatment diagnosis, but a combination of clinical features, laboratory, and pathological

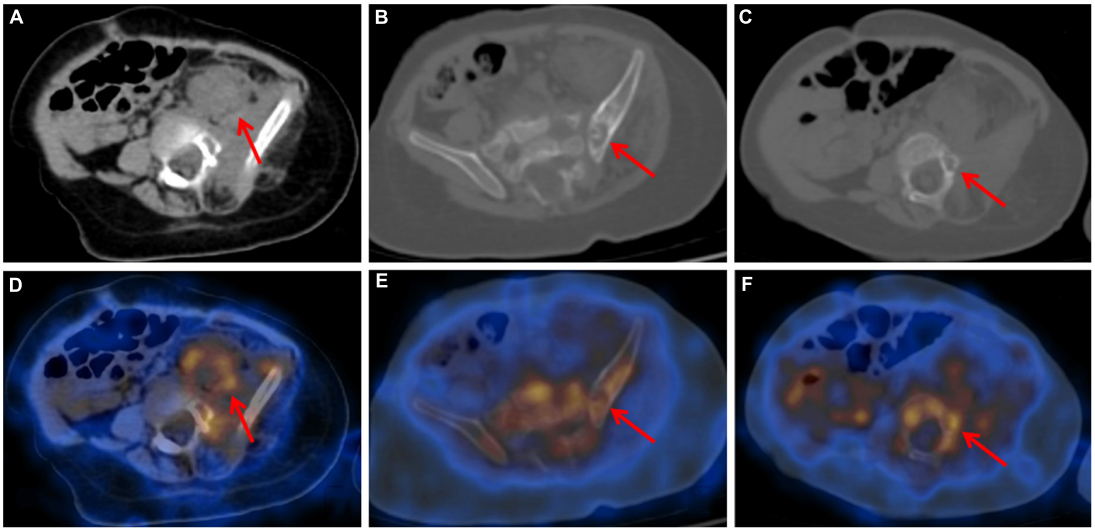

FIGURE 1
Axial CT **(A–C)** and fused PET/CT (**D–F**) images showed retroperitoneum mass with unevenly mildly increased metabolic uptake (**A,D**) and mixed lytic and sclerotic changes of left iliac bone (**B,E**) and L5 (**C,F**). Adjacent bones also presented mildly increased metabolic uptake.

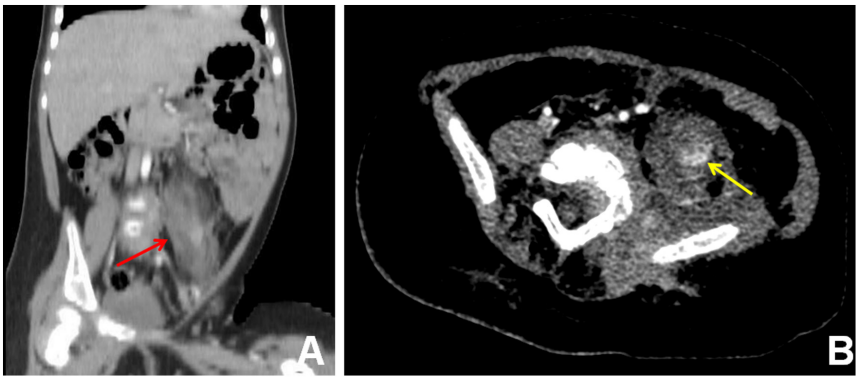

FIGURE 2
Contrast-enhanced CT scan, coronal view **(A)**, and axial view **(B)**, showed the ill-defined lesion of the retroperitoneum **(A)** (red arrow) and rich blood vessels **(B)** (yellow arrow) in the mass.

assessments are essential for diagnosis. KHE should be part of the differential diagnosis in an infant presenting with purpura and unexplained profound thrombocytopenia and coagulopathy.

In this case, ^{18}F-FDG PET/CT has played an important part. PET/CT showed a low metabolic activity within the retroperitoneal mass, which greatly helped physicians rule out a malignant tumor. After comprehensive consideration of the patient's PET/CT imaging and clinical findings, the patient was given sirolimus monotherapy rather than combination therapy. The good treatment response of the patient proved this judgment was feasible. There are few reports about ^{18}F-FDG PET/CT in KHE. Xu et al. (4) reported a 37-year-old woman with KHE in the sacrum, who showed intense ^{18}F-FDG accumulation. Another KHE associated with the lymphangiomatosis case involving mesentery and ileum demonstrated mild ^{18}F-FDG uptake in the lesion (5). This may indicate that many factors, such as age at disease onset, location, and disease activity can affect the functional pattern of KHE in PET/CT. In addition, the biopsy is frequently not possible or recommended in KHE with severe KMP, so accurate non-invasive examination becomes more important. PET/CT, which can reflect both morphological and functional characteristics, may be an ideal choice.

In this case, although the lesion was located in the retroperitoneum, the patient did not display any symptoms of KMP on admission: her platelet count was normal, and

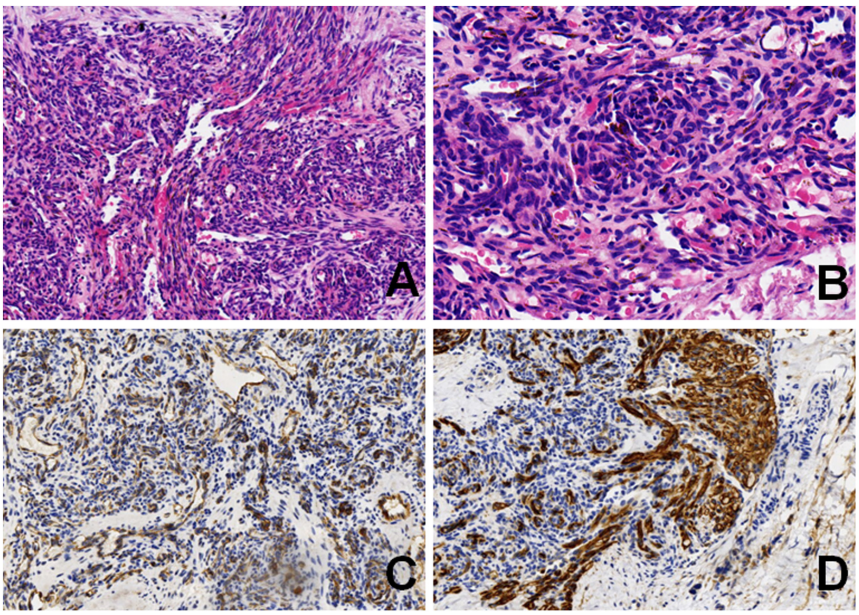

FIGURE 3
Photomicrograph showed irregular spindle tumor cell nodules in the lesion, containing a large number of red blood cells **(A)** (HE, original magnification × 10). Higher magnification showed a glomeruloid pattern of small central slit-like vessels **(B)** (HE, original magnification × 20). Neoplastic cells are positive for CD31 **(C)** (original magnification × 10), and D2-40 **(D)** (original magnification × 10).

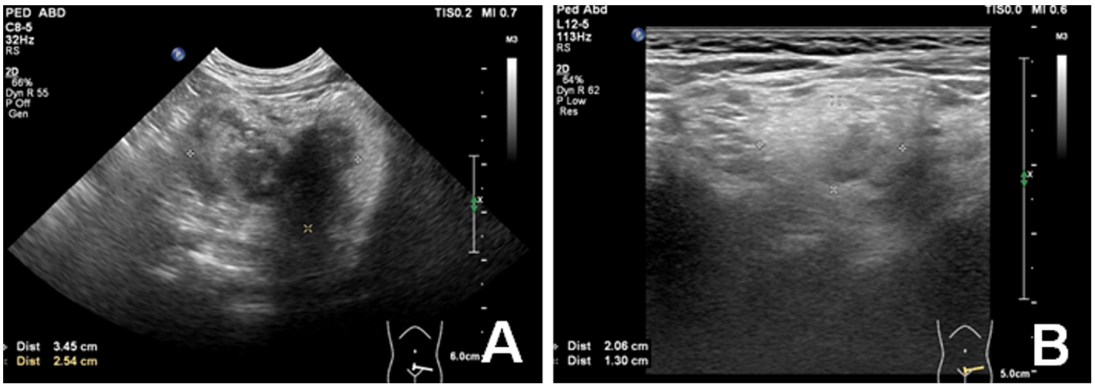

FIGURE 4
Ultrasound image showed a significant decreased (80%) volume of peritoneal mass before **(A)** and after 6-month Sirolimus monotherapy **(B)**.

no obvious skin lesions were observed. The patient was diagnosed with immune thrombocytopenia at 7-month age with a minimum platelet count of 38 × 10^9/L, which is consistent with previous research on KMP (3). According to her parent, her face and legs used to appear petechial hemorrhages. The patient's platelet counts gradually return to a normal level without any special treatment, and her skin lesions disappeared. We presume that this patient has a long disease duration (probably from birth) and her KHE lesion's activity decreased compared with the most active period. Imaging findings confirmed what we thought. ^{18}F-FDG PET/CT showed very mild uptake elevation of the retroperitoneal lesion, suggestive of low disease activity. In addition, sclerotic bone lesions and long-term symptoms suggested a long disease course. The basic pathophysiology of KMP is platelet trapping, activation, and consumption within the abnormal vascular structure. With reduced disease activity, the platelet count may return to a normal level but KHE lesions seldom spontaneously regress (6). It was reported that the signs and symptoms of congenital KHE with KMP may alleviate spontaneously, but the lesions would rebound accompanying severe KMP within the next few days or weeks (1). The incidence of KMP in KHE with deep lesions is probably underestimated because the platelet count may have returned to normal by the time the lesion is discovered.

The aggressive characteristics and destructive growth patterns of KHE can cause functional limitations and pain in joints and muscles, which may affect patients' abilities to perform routine daily activities (7). KMP usually causes acute pain at the tumor sites, and musculoskeletal disorders are frequently found in cases involving the extremities. Lesions in thoracic or retroperitoneal may cause scoliosis (8). Early diagnosis and aggressive treatment are important for these patients. Musculoskeletal disorders may cause by tumor infiltration of the muscles, connective tissues, and joint structures, which can lead to diffuse muscle fibrosis and joint contracture (9). Another cause of functional limitations or pain is local nerve compression. Some studies suggested in most patients, the muscle lesions were still present even after long-term treatment, which is often inconsistent with stabilization of lesions and/or hematological parameters (7, 10). In this case, ^{18}F-FDG PET/CT provided information about the glucose metabolism and morphology of muscles. Around the tumor, enlarged muscles and bone destruction were found with slight FDG uptake. The width of psoas on the affected side was 3.2 cm (SUVmax 1.4) whereas that on the healthy side was only 1.8 cm (SUVmax 0.9), suggesting the possibility of evasion of psoas and spine around the tumor. After 6-month sirolimus treatment, the patient's symptoms in her left leg had a remarkable improvement and almost disappeared. Thus, nerve compression may be the main cause of her symptom. Low activity of lesions and a rapidly shrinking mass correlated with her good prognosis.

The treatment options for KHE are not standardized due to the marked heterogeneity and rarity of KHE. Considering the low platelet level in patients with KHE and the unclear boundary of the lesion, surgical treatment is difficult. In 2013, a consensus treatment statement for KHE was published (11), but the recommendation is based on expert opinion rather than rigorous clinical studies. Pharmacological treatments have improved in recent years, possible options include vincristine, corticosteroids, sirolimus, interferon-α, etc. (1). Notably, an individualized treatment plan should be given to different patients. Monotherapy is usually not recommended in patients with KMP. In recent years, an increasing number of studies have reported the application of mTOR inhibitors sirolimus in KHE (12–14). It has shown good therapeutic results, and sirolimus therapy also exhibited a high response rate (94%) in patients who did not respond to corticosteroids or vincristine (15). According to previous reports, short-term prednisolone treatment plus sirolimus therapy was superior to sirolimus monotherapy in improving the signs and symptoms of active KHE with KMP (16). But for patients with milder symptoms or less activity, monotherapy may be sufficient. It may be the development direction of KHE treatment that comprehensive consideration of PET characteristics and clinical manifestations to develop a personalized treatment plan.

Conclusion

In conclusion, this case shows a rare deep KHE without an abnormal platelet count and with a good response to sirolimus monotherapy. This case demonstrated the advantage of ^{18}F-FDG PET/CT in the evaluation of disease activity in KHE and the possibility of using ^{18}F-FDG PET/CT to guide therapy and prognostication.

Data availability statement

The original contributions presented in this study are included in the article/supplementary material. Further inquiries can be directed to the corresponding author.

Ethics statement

The study was approved by the Institutional Review Board of Peking University First Hospital. Written informed consent was obtained from the minor's legal guardian for the publication of any potentially identifiable images or data included in this article.

Author contributions

YQ: acquisition and analysis of the work, draft the manuscript, imaging data collection, and analysis. WH and ZC: manuscript editing. QY and LS: formal analysis and resources. LK and YF: supervision and writing—review and editing. All authors met the requirements for authorship for the submitted version and agreed to its submission.

Funding

This study was funded by the Beijing Science Foundation for Distinguished Young Scholars (JQ21025) and the Peking University Medicine Fund of Fostering Young Scholars' Scientific & Technological Innovation (BMU2022PY006).

Conflict of interest

The authors declare that the research was conducted in the absence of any commercial or financial relationships that could be construed as a potential conflict of interest.

Publisher's note

References

1. Ji Y, Chen S, Yang K, Xia C, Li L. Kaposiform hemangioendothelioma: current knowledge and future perspectives. *Orphanet J Rare Dis.* (2020) 15:39. doi: 10.1186/s13023-020-1320-1

2. Putra J, Gupta A. Kaposiform haemangioendothelioma: a review with emphasis on histological differential diagnosis. *Pathology.* (2017) 49:356–62. doi: 10.1016/j.pathol.2017.03.001

3. Ji Y, Yang K, Peng S, Chen S, Xiang B, Xu Z, et al. Kaposiform haemangioendothelioma: clinical features, complications and risk factors for kasabach-merritt phenomenon. *Br J Dermatol.* (2018) 179:457–63. doi: 10.1111/bjd.16601

4. Xu H, Song L, Duan J. 18f-Fdg Pet/Ct findings in a woman with kaposiform hemangioendothelioma in the sacrum. *Clin Nucl Med.* (2022) 47:e353–4. doi: 10.1097/rlu.0000000000004000

5. Dong A, Zhang L, Wang Y, He T, Zuo C. Abdominal kaposiform hemangioendothelioma associated with lymphangiomatosis involving mesentery and ileum: a case report of Mri, Ct, and 18f-Fdg Pet/Ct Findings. *Medicine.* (2016) 95:e2806. doi: 10.1097/md.0000000000002806

6. O'Rafferty C, O'Regan GM, Irvine AD, Smith OP. Recent advances in the pathobiology and management of kasabach-merritt phenomenon. *Br J Haematol.* (2015) 171:38–51. doi: 10.1111/bjh.13557

7. Schaefer BA, Wang D, Merrow AC, Dickie BH, Adams DM. Long-term outcome for kaposiform hemangioendothelioma: a report of two cases. *Pediatr Blood Cancer.* (2017) 64:284–6. doi: 10.1002/pbc.26224

8. Qiu T, Yang K, Dai S, Chen S, Ji Y. Case report: kaposiform hemangioendothelioma with spinal involvement. *Front Pediatr.* (2021) 9:600115. doi: 10.3389/fped.2021.600115

9. Ji Y, Yang K, Chen S, Peng S, Lu G, Liu X. Musculoskeletal complication in kaposiform hemangioendothelioma without kasabach-merritt phenomenon: clinical characteristics and management. *Cancer Manag Res.* (2018) 10:3325–31. doi: 10.2147/cmar.S171223

10. Enjolras O, Mulliken JB, Wassef M, Frieden IJ, Rieu PN, Burrows PE, et al. Residual lesions after kasabach-merritt phenomenon in 41 patients. *J Am Acad Dermatol.* (2000) 42(2 Pt 1):225–35. doi: 10.1016/s0190-9622(00)90130-0

11. Drolet BA, Trenor CC III, Brandão LR, Chiu YE, Chun RH, Dasgupta R, et al. Consensus-derived practice standards plan for complicated kaposiform hemangioendothelioma. *J Pediatr.* (2013) 163:285–91. doi: 10.1016/j.jpeds.2013.03.080

12. Boccara O, Puzenat E, Proust S, Leblanc T, Lasne D, Hadj-Rabia S, et al. The effects of sirolimus on kasabach-merritt phenomenon coagulopathy. *Br J Dermatol.* (2018) 178:e114–6. doi: 10.1111/bjd.15883

13. Zhang G, Chen H, Gao Y, Liu Y, Wang J, Liu XY. Sirolimus for treatment of kaposiform haemangioendothelioma with kasabach-merritt phenomenon: a retrospective cohort study. *Br J Dermatol.* (2018) 178:1213–4. doi: 10.1111/bjd.16400

14. Lackner H, Karastaneva A, Schwinger W, Benesch M, Sovinz P, Seidel M, et al. Sirolimus for the treatment of children with various complicated vascular anomalies. *Eur J Pediatr.* (2015) 174:1579–84. doi: 10.1007/s00431-015-2572-y

15. Peng S, Yang K, Xu Z, Chen S, Ji Y. Vincristine and sirolimus in the treatment of kaposiform haemangioendothelioma. *J Paediatr Child Health.* (2019) 55:1119–24. doi: 10.1111/jpc.14370

16. Ji Y, Chen S, Zhou J, Yang K, Zhang X, Xiang B, et al. Sirolimus plus prednisolone vs sirolimus monotherapy for kaposiform hemangioendothelioma: a randomized clinical trial. *Blood.* (2022) 139:1619–30. doi: 10.1182/blood.2021014027

frontiers | Frontiers in Medicine

TYPE Case Report
PUBLISHED 23 September 2022
DOI 10.3389/fmed.2022.1023804

OPEN ACCESS

EDITED BY
Natale Quartuccio,
Azienda Ospedaliera Ospedali Riuniti Villa Sofia Cervello, Italy

REVIEWED BY
Guozhu Hou,
Chinese Academy of Medical Sciences and Peking Union Medical College, China
Kenneth Y. Y. Kok,
Universiti Brunei Darussalam, Brunei
Yue Chen,
Southwest Medical University, China

*CORRESPONDENCE
Pan Wang
1298178828@qq.com
Jiong Cai
jiong_cai@163.com
Dandan Li
807442003@qq.com

SPECIALTY SECTION
This article was submitted to Nuclear Medicine, a section of the journal Frontiers in Medicine

RECEIVED 20 August 2022
ACCEPTED 01 September 2022
PUBLISHED 23 September 2022

CITATION
Hu X, Li X, Yang C, Li D, Cai J and Wang P (2022) Kimura disease, a rare cause of inguinal lymphadenopathy: A case report.
Front. Med. 9:1023804.
doi: 10.3389/fmed.2022.1023804

Kimura disease, a rare cause of inguinal lymphadenopathy: A case report

Xianwen Hu[1], Xue Li[1], Changwei Yang[1], Dandan Li[2]*, Jiong Cai[1]* and Pan Wang[1]*

[1]Department of Nuclear Medicine, Affiliated Hospital of Zunyi Medical University, Zunyi, China, [2]Department of Obstetrics, Zunyi Hospital of Traditional Chinese Medicine, Zunyi, China

Kimura's disease (KD) is a rare chronic granulomatous disease of unknown etiology that mainly involves damage to lymph nodes, soft tissues, and salivary glands. The clinical symptoms are mainly painless subcutaneous soft tissue masses, often involving head and neck lymph nodes and salivary glands, and are mainly characterized by diffuse eosinophilic infiltration, lymphocyte, and vascular proliferation. There are few reports in the literature that KD affects only inguinal lymph nodes. We report in this study a 41-year-old male patient who presented to the hospital for medical help with soft tissue masses in the groin. Magnetic resonance imaging (MRI) showed multiple abnormal soft tissue nodules around the iliac vessels in the left groin, and a contrast-enhanced scan showed obvious homogeneous enhancement. Diffusion-weighted imaging showed limited movement of water molecules and showed an obvious high signal. Fluoro18-labeled deoxyglucose positron emission tomography/computed tomography (^{18}F-FDG PET/CT) was recommended for further evaluation of the patient's general condition, and the results showed that except for the radioactive uptake in the lesions in the left groin region, no obvious abnormality was found in the rest of the body. Based on these imaging findings, the patient was first suspected to have malignant lesions, and then the patient underwent histopathological examination, which was confirmed to be KD. Our case study suggests that KD affects only the inguinal lymph nodes is rare and should be considered as one of the imaging differential diagnoses for lymphadenopathy such as lymphoma, metastases, and Castleman's disease.

KEYWORDS

Kimura's disease, inguinal lymphadenopathy, PET/CT, magnetic resonance imaging, flfluoro18-labeled deoxyglucose

Case description

A 41-year-old man came to our hospital for medical help because of the discovery of groin masses for over 1 month. Physical examination revealed that two soft tissue nodules with a length of about 1.0 cm were palpable in the left inguinal region, which was tough in quality, with good mobility and no obvious tenderness. No obvious positive signs were seen in other parts of the body. The blood routine results revealed that the eosinophil count was increased, with a value of 0.78×10^9/L, and the rest leukocyte and platelet counts were all within the normal reference value range. His immunoglobulin (Ig) E level was slightly elevated, with a value of 204 IU/ml (the reference value was less than 165 IU/ml), and IgG, IgM, and IgA were all within the normal reference range. Magnetic resonance imaging (MRI) was recommended for the nature of these soft tissue masses, which showed isointensity with muscle tissue on T1WI and T2WI (as shown in **Figure 1**). Diffusion-weighted imaging (DWI) showed hyperintensity, and a contrast-enhanced scan showed obvious homogeneous enhancement, which was considered as an enlarged lymph node, but the benign and malignant lesions could not be determined. To further systematically evaluate the patient's whole-body condition, the patient underwent ^{18}F-FDG PET/CT examination (as shown in **Figure 2**), of which results showed that there were multiple nodules with increased radioactivity uptake of different sizes in the left inguinal region, with maximum standard uptake value (SUVmax) ranging from 4.5 to 5.3, and no obvious abnormal radioactive uptake foci were found in the rest of the body. The lesion was limited and surgical resection was feasible for this patient, so he underwent left groin mass excision under local anesthesia. Postoperative pathological and immunohistochemical examination (as shown in **Figure 3**) of the excised mass showed that it was an eosinophilic lymphogranuloma, that is, Kimura's disease (KD), and the gene test result was wild type. Based on the established KD diagnosis, the patient received additional oral prednisone for 1 year postoperatively. The patient was followed up by regular telephone calls for 3 years, and there was no sign of recurrence.

Discussion

Kimura disease (KD), also known as eosinophilic lymphogranulomatosis, is a rare benign chronic lymphoproliferative disorder originating in the dermis, subcutaneous tissue, and lymph nodes, which is more common in Asian adult men (1, 2). KD often occurs in the head and neck lymph nodes, easily involving the salivary glands, and rarely occurs in the inguinal lymph nodes (3, 4). At present, the etiology of KD is not clear, which may be related to allergic reactions caused by candida albicans, parasites or viruses, arthropod bite, endocrine disorders, autoimmune diseases that change the regulatory T-cell immune response, or induce IgE-induced type I hypersensitivity, resulting in the release of eosinophils such as interleukin-4 and interleukin-5, which eventually leads to the deposition of eosinophils in the diseased tissue (5, 6). The disease lacks characteristic clinical manifestations and usually presents as single or multiple painless masses in the affected area, a few may be accompanied by skin itching, and unilateral disease is more common (7). The patient we present is a middle-aged male with unilateral painless lymphadenopathy with elevated eosinophils on laboratory tests, consistent with features of KD, but our patient presented with only inguinal lymph node involvement, which is rare.

Imaging examinations including CT, MRI, and PET/CT play an important role in the localization and characterization of KD. On CT, the swollen lymph nodes involved are more uniform in density, and there are few low-density cystic necrosis areas and high-density calcifications (3). One study has divided KD into two types according to the CT findings of the lesions, namely nodular type with clear edge and uniform density and diffuse swelling type with unclear edge and infiltration of surrounding subcutaneous fat (8). The main manifestations of nodular type are homogeneous isomuscular signal on T1WI, slightly high-to-high signal on T2WI and DWI. Diffuse swelling type is mainly manifested as inhomogeneous hypointense on T1WI with a relatively blurred boundary of the lesion, and uneven iso-to-high signal on T2WI, and contrast-enhanced scans show different degrees of enhancement (4). Our patient presented as soft tissue masses with well-defined borders and uniform density/signal, no cystic necrosis or calcification, and contrast-enhanced scan showed obvious uniform enhancement, consistent with nodular type KD. There are currently few PET/CT studies on KD, and a previous study (9) showed a SUVmax of 4.0–4.5 for KD lesions, which are consistent with our patient (SUVmax of 4.5–5.3).

The location of the lymph nodes in the groin area is superficial, and lymphadenopathy is one of the common clinical signs, and the etiology includes infectious and tumorous lesions. KD involving inguinal lymph nodes mainly needs to be differentiated from lymphoma, lymph node tuberculosis, metastases, and giant lymph node hyperplasia (Castleman disease, CD). Lymphoma has a short course of disease, with fever, weight loss in a short period of time, and other cachexia, most of which are bilateral and multiregional. The lymph nodes in the affected area often tend to fuse and show mild to moderate homogeneous enhancement after contrast enhancement (3, 10). ^{18}F-FDG PET/CT has been widely used in the diagnosis, staging, and evaluation of the degree of malignancy of lymphoma. According to the pathological nature of lymphoma, it can show different degrees

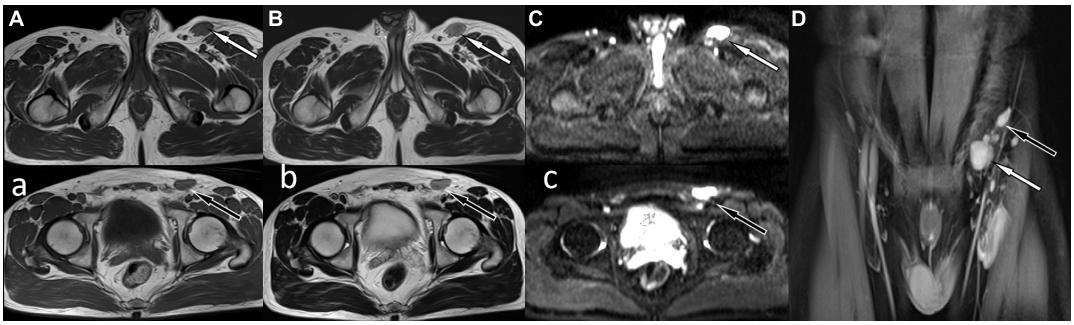

FIGURE 1
Magnetic resonance imaging (MRI) showed abnormal soft tissue nodules around the iliac vessels in the left groin, T1WI sequence was isointense with muscle tissue **(A,a)** white arrow levels the plane of the greater trochanter, black arrow levels the plane of the femoral head), and T2WI was slightly hyperintense **(B,b)**. Diffusion-weighted imaging showed obvious high signal **(C,c)**, and contrast-enhanced scan showed obvious homogeneous enhancement **(D)**.

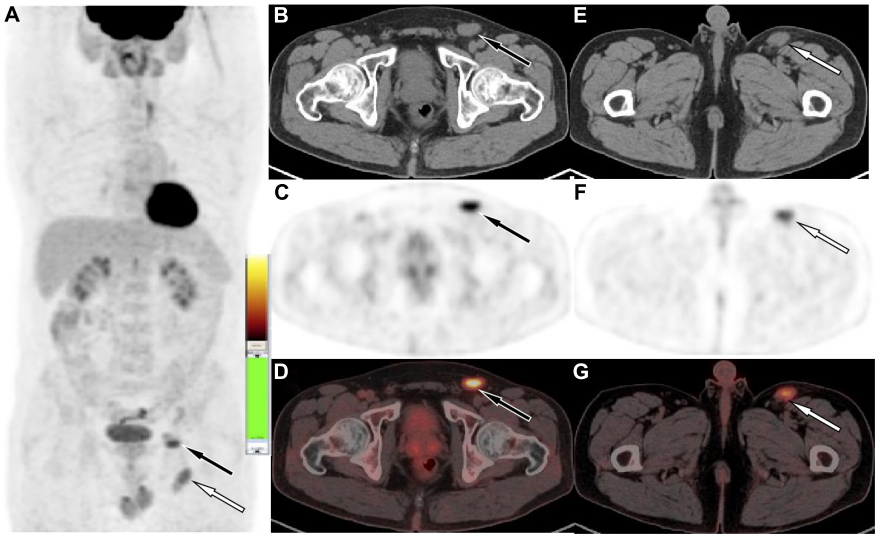

FIGURE 2
Fluoro18-labeled deoxyglucose positron emission tomography/computed tomography (^{18}F-FDG PET/CT) of the patient, the maximum intensity projection [MIP, **(A)**] showed multiple mild to moderate radioactive uptake foci in the left inguinal region (white arrow levels the plane of the greater trochanter, black arrow levels the plane of the femoral head). The axial figures in the left inguinal region at the femoral head level [**(B)** CT; **(C)** PET; **(D)** PET/CT fusion] and greater trochanter level [**(E)** CT; **(F)** PET; **(G)** PET/CT fusion] showed soft tissue nodules with radioactive uptake, with SUVmax of 5.3 (black arrow) and 4.5 (white arrow), respectively.

of radioactive uptake. Based on our case and previous reports, the radioactive uptake of KD is similar to that of indolent lymphoma, making it difficult to differentiate (9, 11). Lymph node tuberculosis often has clinical manifestations of low fever, fatigue, night sweats, and increased erythrocyte sedimentation rate, which is more common in young people, and more secondary or associated with tuberculosis. MRI showed uneven signals in the long T1 and T2 of the lesion lymph nodes, and contrast-enhanced scan showed thick-walled annular enhancement, easy adhesion and fusion, and a "multilocular sign" with relative specificity (12). On ^{18}F-FDG PET/CT images, lymphatic tuberculosis often showed lymphadenopathy with heterogeneous density, low-density necrosis, and/or high-density calcification foci. Active lymphatic tuberculosis often showed high radiation uptake, and the central necrotic area showed radiation distribution defect (13). Inguinal lymph node metastasis is one of the common metastatic routes of abdominal and pelvic malignant tumors. It is characterized by enlarged lymph nodes, uneven density or signal, which can be fused into masses, and lymph nodes with cystic necrosis show thin-walled heterogeneous enhancement on contrast-enhanced scans (14). Lymph node metastases have similar biological characteristics to primary tumors and the metabolic activity of most malignant tumors is significantly increased, so lymph node

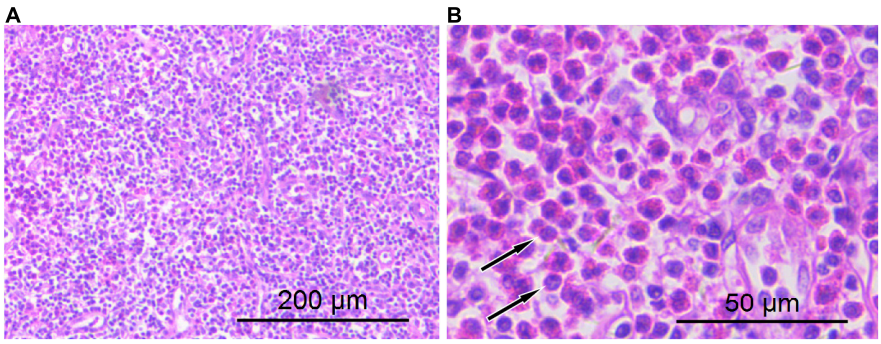

FIGURE 3
Hematoxylin–eosin staining showed lymphocyte proliferation in the lesions with diffuse eosinophil infiltration [**(A)** 100 × magnification; **(B)** 400 × magnification arrows indicate eosinophilic microabscesses].

metastases show high uptake of ^{18} F-FDG. Furthermore, ^{18}F-FDG PET/CT imaging has high sensitivity and specificity for the diagnosis of lymph node metastases, especially for small lymph nodes with no obvious changes in size, shape, and density (15). Castleman disease can occur in any site with lymph nodes, and it is rare in the groin. MRI plain scan showed that the lesions were isointense on T1WI, hyperintensity on T2WI and DWI, relatively uniform in texture, rare in necrosis, and uniform on T1WI-enhanced signal. In some cases, obviously thickened and tortuous feeding vessels with flow void signal were seen in or around the lesions, and radial or fissure-like unenhanced areas may also occasionally be seen within the lesion, which may be thickened hyalinized collagen fibers (16). The metabolism of CD in ^{18}F-FDG PET/CT was slightly increased, and delayed imaging showed no significant changes. If the SUVmax of the diseased lymph nodes were increased, which indicated that the lesion was evolving and might develop into lymphoma (17). Moreover, angiolymphoid hyperplasia with eosinophilia (ALHE), hemangioma, etc., are also one of the rare causes of inguinal lymphadenopathy. ALHE is more common in young women, often presenting as a single subcutaneous mass with clear edges, erythematous, brittle skin, easy to bleed, eosinophils, and elevated serum IgE are rare, and most of them are not accompanied by lymphadenopathy, which can be differentiated from KD (18). Hemangiomas are often seen with round phleboliths, which are not difficult to differentiate. Our patient presented with multiple enlarged lymph nodes confined to the left groin with homogeneous density or signal, marked homogeneous enhancement on contrast-enhanced scan, moderate uptake of ^{18}F-FDG, which partially overlapped with the imaging findings of CD and indolent lymphoma, combined with laboratory findings of elevated eosinophil counts, making the diagnosis of KD possible.

The diagnosis of KD still requires histopathological examination, including extensive lymphoid follicle-like structures are seen in the lesions, and a large number of eosinophils infiltrate the lymphoid follicles and the formation of eosinophilic microabscesses are the characteristic manifestations of the diagnosis of this disease (7). The treatment of KD currently mainly includes surgical resection, glucocorticoid therapy, radiotherapy, and chemotherapy, which is sensitive to glucocorticoid therapy and chemotherapy, but it is prone to recurrence after drug withdrawal. A previous study revealed that the combination of surgical resection and postoperative radiotherapy can reduce the local recurrence rate of KD (19). Our patient had a good prognosis after combined glucocorticoid therapy after surgical resection of the lesion, and no disease recurrence has been found in the 3-year follow-up.

Conclusion

Kimura's disease affects only the inguinal lymph nodes is rare and should be considered as one of the imaging differential diagnoses for lymphadenopathy such as lymphoma, metastases, and Castleman's disease. Combined glucocorticoid therapy after surgical resection of the lesion can reduce local recurrence in patients with KD.

Data availability statement

The original contributions presented in this study are included in the article/supplementary material, further inquiries can be directed to the corresponding authors.

Ethics statement

Written informed consent was obtained from the individual(s) for the publication of any potentially identifiable images or data included in this article.

Author contributions

JC and PW: funding acquisition. DL: investigation. XL and CY: methodology. XH: writing-original draft. XH, PW, and JC: writing-review and editing. All authors contributed to the article and approved the submitted version.

Funding

This study was funded by the National Natural Science Foundation of China, NSFC (grant number 81571712), Zunyi Medical College Research Start Fund 2018ZYFY03, and QianKeHe platform talents [2017] (grant number 5733-035).

Conflict of interest

The authors declare that the research was conducted in the absence of any commercial or financial relationships that could be construed as a potential conflict of interest.

Publisher's note

References

1. Deshpande AH, Nayak S, Munshi MM, Bobhate SK. Kimura's disease, diagnosis by aspiration cytology. *Acta Cytol.* (2002) 46:357–63.

2. Ohta N, Fukase S, Suzuki Y, Ito T, Yoshitake H, Aoyagi M. Increase of Th2 and Tc1 cells in patients with Kimura's disease. *Auris Nasus Larynx.* (2011) 38:77–82. doi: 10.1016/j.anl.2010.03.011

3. Zhang R, Ban XH, Mo YX, Lv MM, Duan XH, Shen J, et al. Kimura's disease: the CT and MRI characteristics in fifteen cases. *Eur J Radiol.* (2011) 80:489–97. doi: 10.1016/j.ejrad.2010.09.016

4. Park SW, Kim HJ, Sung KJ, Lee JH, Park IS. Kimura disease: CT and MR imaging findings. *AJNR Am J Neuroradiol.* (2012) 33:784–8. doi: 10.3174/ajnr.A2854

5. Zhang G, Li X, Sun G, Cao Y, Gao N, Qi W. Clinical analysis of Kimura's disease in 24 cases from China. *BMC Surg.* (2020) 20:1. doi: 10.1186/s12893-019-0673-7

6. Okura T, Miyoshi K, Irita J, Enomoto D, Nagao T, Kukida M, et al. Kimura's disease associated with membranous nephropathy with IgG4 and phospholipase A2 receptor-positive staining of the glomerular basement membrane. *Intern Med.* (2014) 53:1435–40. doi: 10.2169/internalmedicine.53.2042

7. Chen H, Thompson LD, Aguilera NS, Abbondanzo SL. Kimura disease: a clinicopathologic study of 21 cases. *Am J Surg Pathol.* (2004) 28:505–13. doi: 10.1097/00000478-200404000-00010

8. Gopinathan A, Tan TY. Kimura's disease: imaging patterns on computed tomography. *Clin Radiol.* (2009) 64:994–9. doi: 10.1016/j.crad.2009.07.003

9. Yu M, Wang Z, Zhao J, Wu F. Lymphadenopathy Due to Kimura's Disease Mimicking Lymphoma on FDG PET/CT. *Clin Nucl Med.* (2019) 44:299–300. doi: 10.1097/RLU.0000000000002474

10. Park JS, Jin W, Ryu KN, Won KY. Bilateral asymmetric superficial soft tissue masses with extensive involvement of both upper extremities: demonstration of Kimura's disease by US and MRI (2008: 12b). *Eur Radiol.* (2009) 19:781–6. doi: 10.1007/s00330-008-1059-x

11. Khalaf M, Abdel-Nabi H, Baker J, Shao Y, Lamonica D, Gona J. Relation between nodule size and 18F-FDG-PET SUV for malignant and benign pulmonary nodules. *J Hematol Oncol.* (2008) 1:13. doi: 10.1186/1756-8722-1-13

12. Yang Z, Sone S, Min P, Li F, Maruyama Y, Watanabe T, et al. [Distribution and contrast enhanced CT appearance of abdominal tuberculous lymphadenopathy]. *Nihon Igaku Hoshasen Gakkai Zasshi.* (1997) 57:567–71.

13. Lefebvre N, Argemi X, Meyer N, Mootien J, Douiri N, Sferrazza-Mandala S, et al. Clinical usefulness of (18)F-FDG PET/CT for initial staging and assessment of treatment efficacy in patients with lymph node tuberculosis. *Nucl Med Biol.* (2017) 50:17–24. doi: 10.1016/j.nucmedbio.2017.04.003

14. King AD, Tse GM, Ahuja AT, Yuen EH, Vlantis AC, To EW, et al. Necrosis in metastatic neck nodes: diagnostic accuracy of CT, MR imaging, and US. *Radiology.* (2004) 230:720–6. doi: 10.1148/radiol.2303030157

15. Yang S, Liu C, Li C, Hua K. Nomogram predicting lymph node metastasis in the early-stage cervical cancer. *Front Med.* (2022) 9:866283. doi: 10.3389/fmed.2022.866283

16. Zhao S, Wan Y, Huang Z, Song B, Yu J. Imaging and clinical features of Castleman Disease. *Cancer Imaging.* (2019) 19:53. doi: 10.1186/s40644-019-0238-0

17. Chen S, Song L, Xie X, Han X, Cheng B. A case of abdominal mesenteric Castleman's disease with left renal cell carcinoma and stomach leiomyoma. *Hell J Nucl Med.* (2016) 19:285–8.

18. Zou A, Hu M, Niu B. Comparison between Kimura's disease and angiolymphoid hyperplasia with eosinophilia: case reports and literature review. *J Int Med Res.* (2021) 49:3000605211040976. doi: 10.1177/03000605211040976

19. Ye P, Wei T, Yu GY, Wu LL, Peng X. Comparison of local recurrence rate of three treatment modalities for kimura disease. *J Craniofac Surg.* (2016) 27:170–4. doi: 10.1097/SCS.0000000000002337

frontiers | Frontiers in Medicine

TYPE Case Report
PUBLISHED 10 October 2022
DOI 10.3389/fmed.2022.1002663

OPEN ACCESS

EDITED BY
Natale Quartuccio,
Azienda Ospedaliera Ospedali Riuniti Villa Sofia Cervello, Italy

REVIEWED BY
Francesco Giammarile,
International Atomic Energy Agency, Austria
Carmelo Caldarella,
Fondazione Policlinico Universitario A. Gemelli IRCCS, Italy

*CORRESPONDENCE
Makoto Taninokuchi Tomassoni
makoto.taninokuchi@studio.unibo.it

†These authors have contributed equally to this work and share first authorship

SPECIALTY SECTION
This article was submitted to Nuclear Medicine, a section of the journal Frontiers in Medicine

RECEIVED 25 July 2022
ACCEPTED 21 September 2022
PUBLISHED 10 October 2022

CITATION
Taninokuchi Tomassoni M, Cattabriga A, Gaudiano C, Ciccarese F, Corcioni B, Bianchi L, Schiavina R, Brunocilla E and Golfieri R (2022) Dynamic FDG PET/CT on bladder paraganglioma: A case report. *Front. Med.* 9:1002663. doi: 10.3389/fmed.2022.1002663

Dynamic FDG PET/CT on bladder paraganglioma: A case report

Makoto Taninokuchi Tomassoni[1*†], Arrigo Cattabriga[1†], Caterina Gaudiano[1], Federica Ciccarese[1], Beniamino Corcioni[1], Lorenzo Bianchi[2,3], Riccardo Schiavina[2,3], Eugenio Brunocilla[2,3] and Rita Golfieri[1]

[1]Department of Radiology, IRCCS Azienda Ospedaliero Universitaria di Bologna, Bologna, Italy, [2]Division of Urology, IRCCS, Azienda Ospedaliero Universitaria di Bologna, Bologna, Italy, [3]University of Bologna, Bologna, Italy

Paraganglioma (PGL) is characterized by equivocal clinical manifestations and arriving to a suspicion might be challenging. Nevertheless, diagnostic imaging and nuclear medicine are a fundamental part of the diagnosis and management of this particular neuroendocrine tumor (NET). We herein report a rare case of bladder paraganglioma with unusual onset and typical PET/CT characteristics that led to its recognition.

KEYWORDS

bladder paraganglioma, bladder cancer, FDG PET/CT, nuclear medicine, radiology

Introduction

Bladder paraganglioma (BPG) is a neuroendocrine tumor originating from the chromaffin tissue of the bladder wall, more specifically from the sympathetic nervous system embedded in the muscle layer. Belonging to the category of extra-adrenal pheochromocytoma, it accounts for 0.06% of all bladder tumors and 1% of overall paragangliomas (1–3) and it's therefore considered a very rare yet severe condition as it could lead to hypertensive crisis during handling and mobilization (4).

More than one-third of BPGs are malignant and may be either non-functioning or functioning, the latter usually presenting with micturitional attacks, consisting of a variety of symptoms during urination, such as palpitations, headache, fainting and visual disturbances. Nevertheless, almost 30% of patients affected by BPG do not present with any specific symptoms. Consequently, medical imaging plays an important role in order to achieve an early diagnosis (5–7).

Ultrasound (US), computed tomography (CT), and magnetic resonance imaging (MRI) are important to identify, localize and morphologically describe the tumor. BPGs are submucosal hypervascular lesions that in up to 40% of cases are located in the bladder dome (8–10). Cystoscopy is substantially limited, mostly being able to exclude mucosal involvement, typical of urothelial lesions, whilst biopsy is contraindicated since could unleash a hypertensive episode in patients without the correct medical treatment (11).

Lastly, nuclear medicine studies are essential to evaluate the functional pattern of the lesion and to exclude metastases. ^{123}I-MIBG is a guanidine analog similar to

noradrenaline that, when administered, is stored in the adrenergic cells of paragangliomas that are equipped with noradrenaline transporters and can be used in nuclear medicine exams. On the other hand, BPGs express somatostatin receptors, that bounds to ^{68}Ga-DOTANOC, a somatostatin analog used in nuclear medicine imaging (12, 13). ^{18}F-FDOPA is an amino acid analog that, once decarboxylated to ^{18}F-dopamine, is stored in secretory vesicles of PGL cells (14).

While both ^{123}I-MIBG SPECT/CT and ^{68}Ga-DOTANOC PET/CT are routinely used for the diagnosis of NETs and, in particular, paragangliomas, it has been demonstrated that ^{68}Ga-DOTANOC PET/CT is superior to ^{123}I-MIBG SPECT/CT in providing valuable information for staging extra-adrenal PGL (15). Therefore, ^{68}Ga-DOTANOC PET/CT should be considered as the first-line investigation study for nuclear medicine diagnosis of PGLs (16).

Nevertheless, in not-specialized centers, this particular radionuclide might not be available.

In this case, dynamic FDG PET/CT could be used in addition to other clinical and imaging data in order to reach a correct diagnosis, as PGLs show a typical pattern with early uptake of FDG and wash-out in the delayed 1-h acquisition phase, taking into account the risk of false negative results (17, 18).

We herein present the case of a patient affected by BPG with non-specific symptoms that were further investigated with radiological and nuclear medicine imaging.

Case report

A 59-years-old male with no pathological history presented to the Emergency Room with 12-h acute urinary retention. Laboratory tests were normal, except for a small reduction of red blood cells (4.2 million/ml), hematocrit (38.9%) and hemoglobin 13.5 g/dl.

After Foley catheter positioning, it was documented significative hematuria with clots emission. The patient was therefore admitted to the urology department of our hospital and a CT Urography was performed, demonstrating

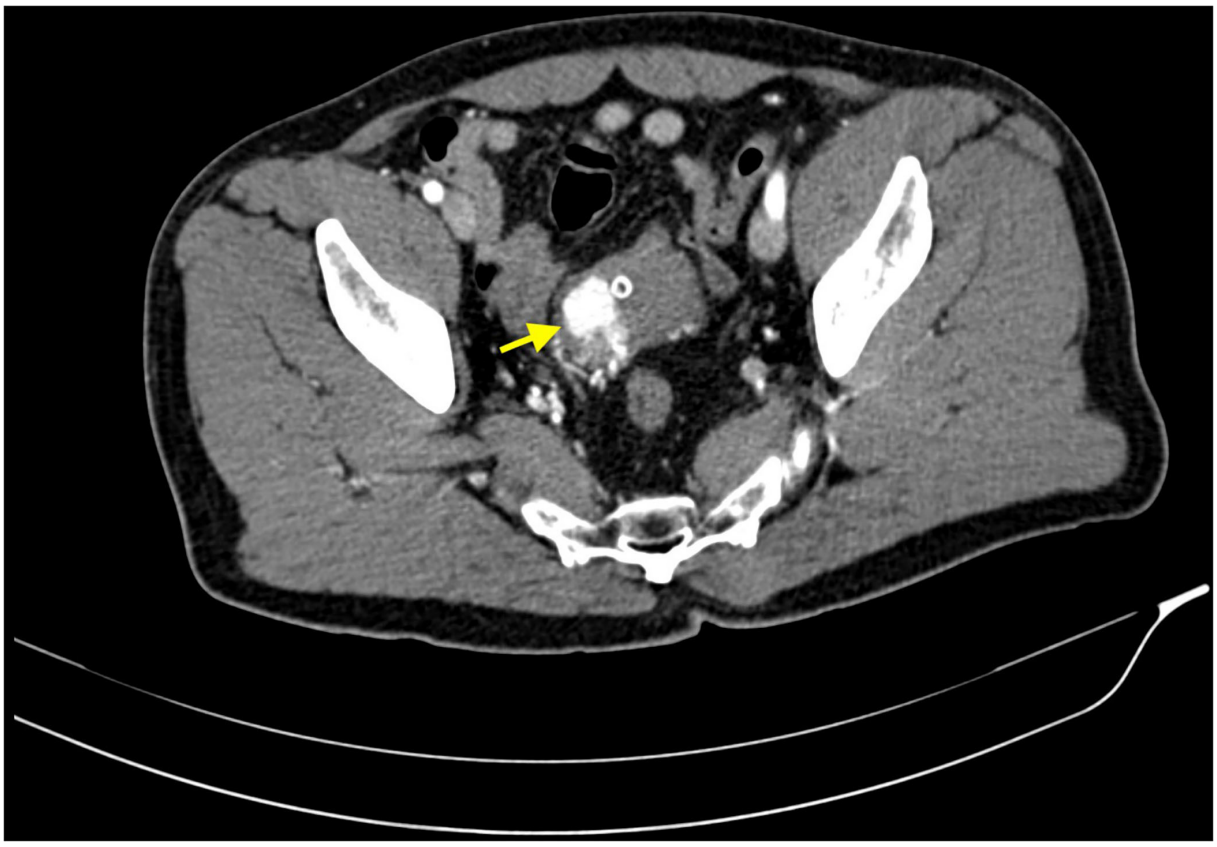

FIGURE 1
CT scan acquired in arterial phase, after intravenous administration of iodinated contrast media. This image shows a highly vascular lesion within the right wall of the bladder dome (yellow arrow). Some small feeding arteries are appreciable too. The bladder is empty due to urinary catheterization *via* Foley catheter.

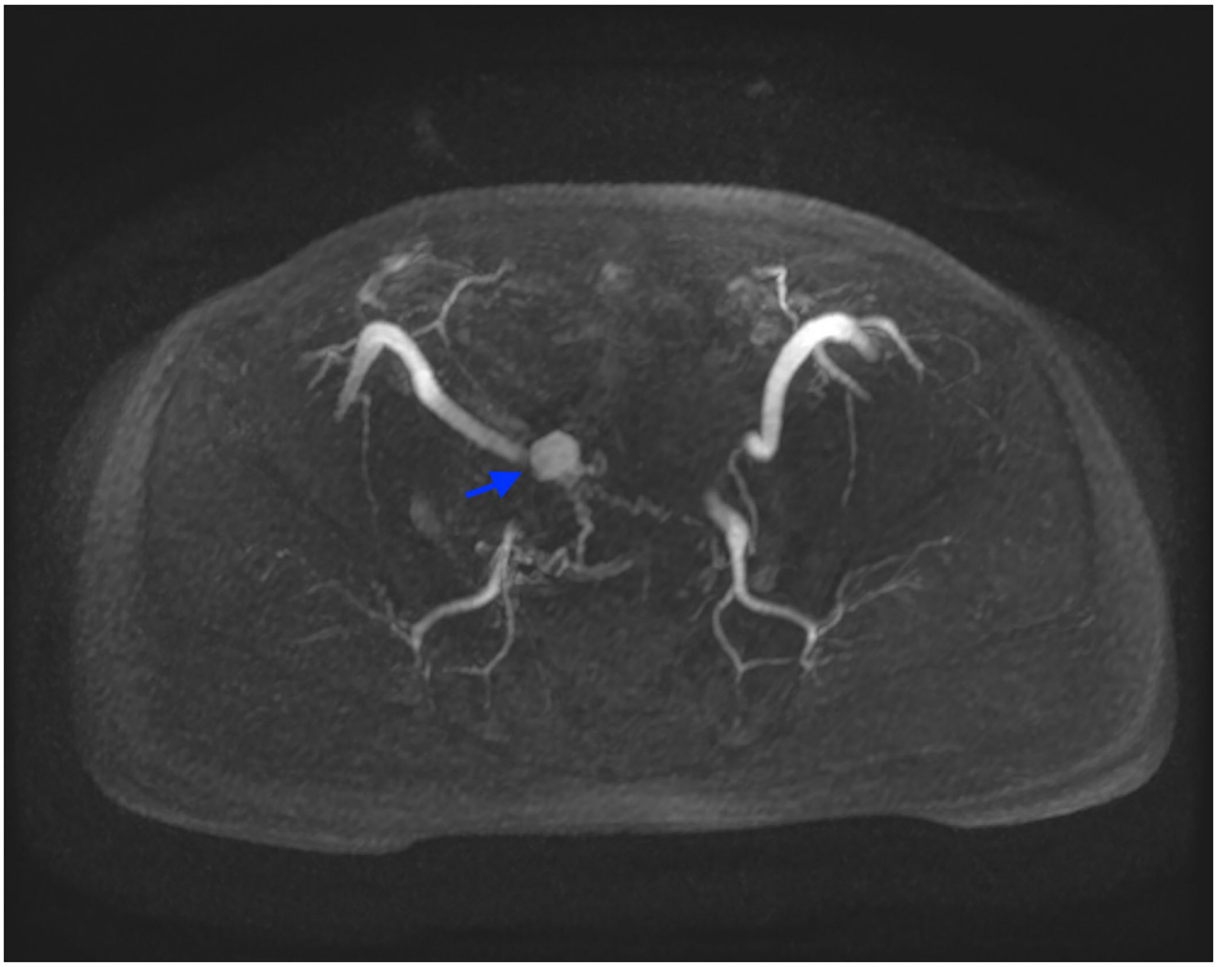

FIGURE 2
MRI angiography, axial LAVA sequence acquired in arterial phase after administration of intravenous contrast media, with Maximum Intensity Projection reformatting. This image depicts the highly vascularized lesion and its feeding vessels (blue arrow).

a significantly contrast-enhanced bladder nodule fed by thin arterial vessels originating from both left and right hypogastric arteries (Figure 1). It was concluded that these findings were suggestive both of a neoplasm or a vascular arteriovenous malformation. Consequently, further examinations were needed.

The patient underwent abdominal Ultrasonography, to determine whether the lesion was a solid neoplasm (hyperechogenic) or a vascular formation (hypo-anechogenic). The US documented a solid lesion protruding into the bladder wall, characterized by an intense Color-Doppler signal, suggestive of solid hyper-vascular neoplasm. On the same day, a cystoscopy was performed, showing a posterolateral voluminous protruding mass, without any mucosal involvement; therefore, the appearance was not typical for urothelial carcinoma.

The findings of CT-scan and US, showing a solid hyper-vascular lesion of the bladder dome, suggested the suspicion of BPG. The patient subsequently underwent MRI angiography, that clearly depicted the lesion and its multiple afferent feeding arteries, confirming the findings described on CT-scan (Figure 2).

Nuclear medicine studies were thus performed to confirm the suspicion and to decide the best therapeutical workflow. PET/CT images where acquired with a field of view (FOV) extended from the vertex to the roots of the lower limbs, the slice thickness was 3.27 mm. In particular, FDG PET showed an early intense FDG uptake with a complete washout after 60 min (Figures 3, 4). This radio-nuclear pattern, along with the previous radiological findings, were consistent for Bladder Paraganglioma. Additionally, FDG PET did not show any further pathological radionuclide uptake.

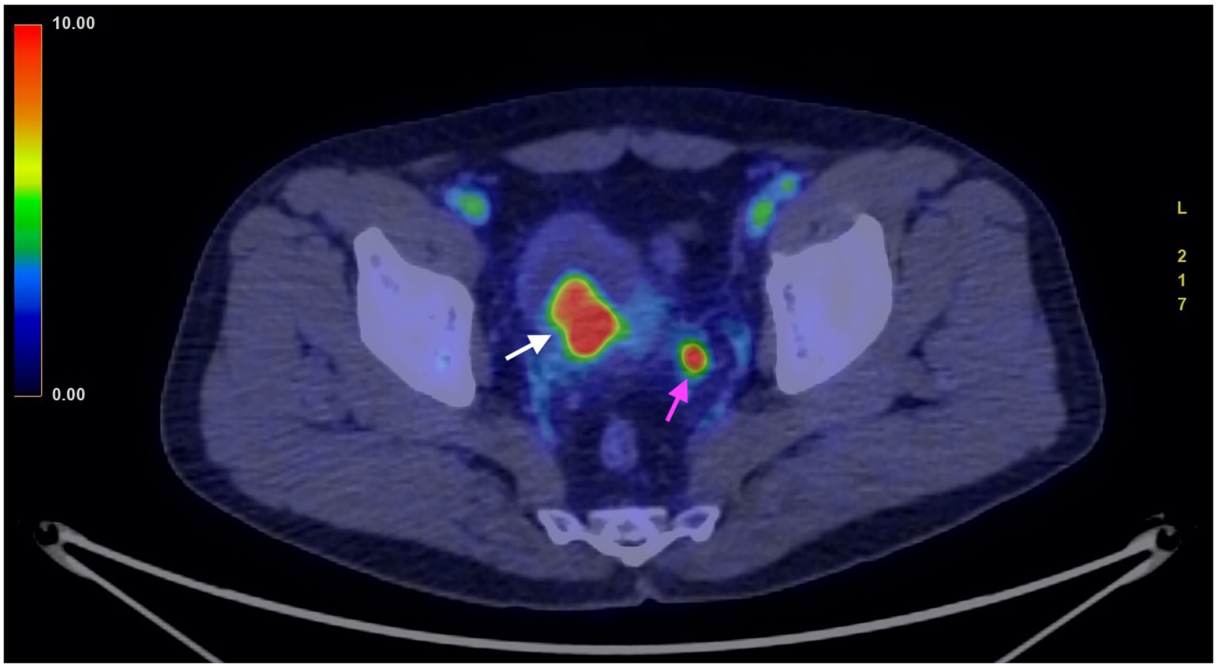

FIGURE 3
FDG PET/CT (image fusion technique) acquired in an early phase, 3 min after administration of the ^{18}FDG. The image shows intense uptake of the ^{18}FDG by the tumor (white arrow). The smaller high uptake spot on the left corresponds to physiological collection of urine within the ureter (purple arrow).

To determine whether the described lesion was a functioning or a non-functioning BPG, urinary and blood metanephrines were evaluated, with values consistent for non-functioning tumor.

After proper premedication with α-blockers drugs, the patient underwent transurethral resection (TURB) and pathological report confirmed the clinical-radiological suspicion.

Four and twelve months follow up with CT scan and 1 year follow up with FDG PET/CT didn't show any signs of tumor relapse.

Discussion

Although bladder cancer is one of the most frequent neoplasms, BPG accounts only for 0.06% of the totality of bladder tumors (19, 20). Despite being very uncommon, BPG must be included in the differential diagnosis, mostly because its management should be different from that of urothelial carcinoma, considering the high risk of hypertensive crisis after biopsy and during surgical resection. Whilst cystoscopy and urinary cytology are considered the main tools for urothelial carcinoma identification diagnosis, radiology and nuclear medicine are considered essential for telling BPG apart (21, 22).

In this case, the patient presented with hematuria and urinary retention, symptoms non-specific for BPG but more suggestive for aggressive urothelial carcinoma. A preliminary CT-scan with a delayed urographic phase suggested the presence either of a vascular malformation or a hypervascular solid tumor, situated on the bladder dome, where 40% of PGLs are usually found and could give a suspicion (8–10).

This clinical case shows three important elements to consider during the diagnostical workflow in bladder cancer and in particular BPGs.

First of all, the combination of radiological and nuclear medicine imaging techniques with laboratory tests (urinary metanephrines) led to the diagnosis of non-functioning BPG, granting the patient the chance to avoid a radical cystectomy while undergoing a curative, less invasive, procedure (TURB).

Secondly, ultrasound confirms to be the most useful first-level, cost-effective and non-invasive approach that can however provide some extra-information integrating more complex, second level, imaging techniques such as CT-scan and that might therefore help to choose the following steps.

Lastly, while ^{68}Ga-DOTANOC PET/CT is considered the best nuclear medicine exam for the identification and diagnosis of BPGs yet, many centers would not have the chance to routinely perform this kind of exam. In this case dynamic FDG PET-CT (by far more accessible and commonly performed)

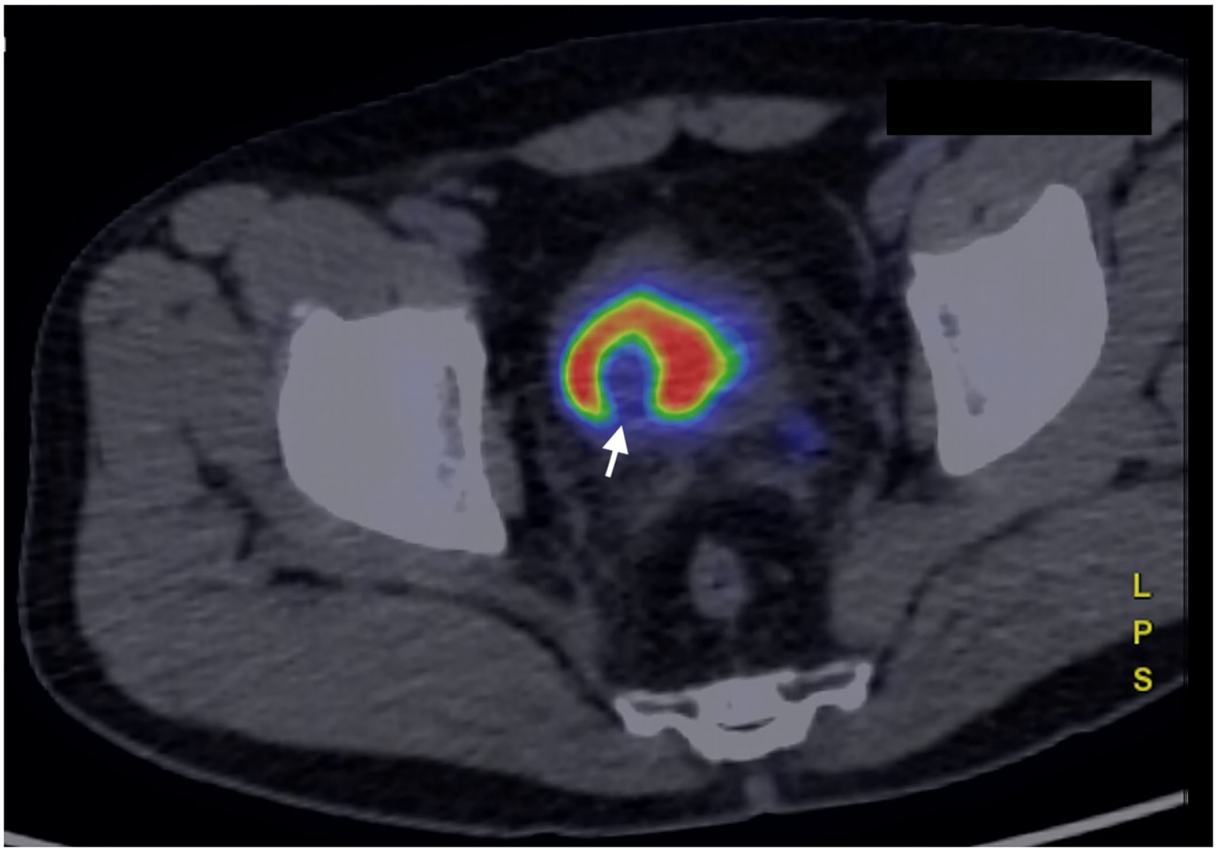

FIGURE 4
FDG PET/CT (image fusion technique) acquired in a late phase, 60 min after administration of the ^{18}FDG. The bladder lesion is characterized by complete washout of the ^{18}FDG, that collects in the urine, within the bladder (white arrow).

might integrate the radiological techniques and confirm the suspicion of paraganglioma.

Conclusion

In the presented case, taking into account the impossibility to perform ^{68}Ga-DOTANOC PET/CT or ^{123}I-MIBG SPECT/CT, accurate interdisciplinary communication and integration of radiological imaging with dynamic FDG PET/CT ensured an early diagnosis and prompt treatment of urinary bladder paraganglioma.

Data availability statement

The original contributions presented in the study are included in the article/supplementary material, further inquiries can be directed to the corresponding author.

Author contributions

MTT and AC: data collection and drafting the article. CG: conception of the work and critical revision of the article. FC, BC, LB, RS, EB, and RG: final approval of the version to be published. All authors contributed to the article and approved the submitted version.

Funding

The work reported in this publication was funded by the Italian Ministry of Health, RC-2022-2773395.

Conflict of interest

The authors declare that the research was conducted in the absence of any commercial or financial relationships that could be construed as a potential conflict of interest.

Publisher's note

References

1. Zhai H, Ma X, Nie W, Li H, Peng C, Li X, et al. Paraganglioma of the urinary bladder: a series of 22 cases in a single center. *Clin Genitourin Cancer.* (2017) 15:e765–71. doi: 10.1016/j.clgc.2017.03.010

2. Alanee S, Williamson SR, Gupta NS. A rare case of non-functioning bladder paraganglioma treated with robotic assisted partial cystectomy. *Urol Case Rep.* (2019) 26:100950. doi: 10.1016/j.eucr.2019.100950

3. Romano IJ, Gentile F, Lippolis A. Postmicturition syndrome: a neglected syndrome dangerous for the bladder and the heart. *J Am Soc Hypertens.* (2018) 12:589–93. doi: 10.1016/j.jash.2018.06.008

4. Lazareth H, Cohen D, Vasiliu V, Tinel C, Martinez F, Grünfeld JP, et al. Paraganglioma of the bladder in a kidney transplant recipient: a case report. *Mol Clin Oncol.* (2017) 6:553–5. doi: 10.3892/mco.2017.1182

5. Boyer AC, Jafri SZ, Jafri SM, Amin MB. Neuroendocrine carcinoma of the urinary bladder: a retrospective study of CT findings. *Abdom Imaging.* (2013) 38:870–6. doi: 10.1007/s00261-012-9971-6

6. Gkikas C, Ram M, Tsafrakidis P. Urinary bladder paraganglioma and concomitant metastatic lung cancer. A case report. *Urol Case Rep.* (2016) 5:17–9. doi: 10.1016/j.eucr.2015.12.002

7. Leestma JE, Price EB Jr. Paraganglioma of the urinary bladder. *Cancer.* (1971) 28:1063–73. doi: 10.1002/1097-0142 1971 28:4<1063::AID-CNCR2820280433>3.0.CO;2-R

8. Qin J, Zhou G, Chen X. Imaging manifestations of bladder paraganglioma. *Ann Palliat Med.* (2020) 9:346–51. doi: 10.21037/apm.2020.03.09

9. Pahwa HS, Kumar A, Srivastava R, Rai A. Unsuspected pheochromocytoma of the urinary bladder: reminder of an important clinical lesson. *BMJ Case Rep.* (2012) 2012:bcr2012006377. doi: 10.1136/bcr-2012-006377

10. Kalliath L, Karthikeyan D, Ramakrishna B, Kripesh G, Chandran N. Non-functional urinary bladder paraganglioma with negative Ga-DOTA-NOC PET/CT uptake. *Egypt J Radiol Nucl Med.* (2021) 52:286. doi: 10.1186/s43055-021-00671-2

11. Rode J, Bentley A, Parkinson C. Paraganglial cells of urinary bladder and prostate: potential diagnostic problem. *J Clin Pathol.* (1990) 43:13–6. doi: 10.1136/jcp.43.1.13

12. Milardovic R, Corssmit EP, Stokkel M. Value of ^{123}I-MIBG scintigraphy in paraganglioma. *Neuroendocrinology.* (2010) 91:94–100. doi: 10.1159/000242499

13. Reubi JC, Waser B, Schaer JC, Laissue JA. Somatostatin receptor sst1-sst5 expression in normal and neoplastic human tissues using receptor autoradiography with subtype-selective ligands. *Eur J Nucl Med.* (2001) 28:836–46. doi: 10.1007/s002590100541

14. Helali M, Moreau M, Le Fèvre C, Heimburger C, Bund C, Goichot B, et al. ^{18}F-FDOPA PET/CT combined with MRI for gross tumor volume delineation in patients with skull base paraganglioma. *Cancers (Basel).* (2019) 11:54. doi: 10.3390/cancers11010054

15. Kroiss A, Shulkin BL, Uprimny C, Frech A, Gasser RW, Url C, et al. ^{68}Ga-DOTATOC PET/CT provides accurate tumour extent in patients with extraadrenal paraganglioma compared to ^{123}I-MIBG SPECT/CT. *Eur J Nucl Med Mol Imaging.* (2015) 42:33–41. doi: 10.1007/s00259-014-2892-6

16. Singh D, Shukla J, Walia R, Vatsa R, Paul N, Chhabra A, et al. Role of ^{68Ga}DOTANOC PET/computed tomography and ^{1311}MIBG scintigraphy in the management of patients with pheochromocytoma and paraganglioma: a prospective study. *Nucl Med Commun.* (2020) 41:1047–59. doi: 10.1097/MNM.0000000000001251

17. Lewington V, Lambert B, Poetschger U, Sever ZB, Giammarile F, McEwan AJB, et al. ^{123}I-mIBG scintigraphy in neuroblastoma: development of a SIOPEN semi-quantitative reporting, method by an international panel. *Eur J Nucl Med Mol Imaging.* (2017) 44:234–41. doi: 10.1007/s00259-016-3516-0

18. van Berkel A, Vriens D, Visser EP, Janssen MJR, Gotthardt M, Hermus ARMM, et al. Metabolic subtyping of pheochromocytoma and paraganglioma by ^{18}F-FDG pharmacokinetics using dynamic PET/CT scanning. *J Nucl Med.* (2019) 60:745–51. doi: 10.2967/jnumed.118.216796

19. Sung H, Ferlay J, Siegel RL, Laversanne M, Soerjomataram I, Jemal A, et al. Global cancer statistics 2020: GLOBOCAN estimates of incidence and mortality worldwide for 36 cancers in 185 countries. *CA Cancer J Clin.* (2021) 71:209–49. doi: 10.3322/caac.21660

20. Xu DF, Chen M, Liu YS, Gao Y, Cui XG. Non-functional paraganglioma of the urinary bladder: a case report. *J Med Case Rep.* (2010) 4:216. doi: 10.1186/1752-1947-4-216

21. Cicione A, Cantiello F, Damiano R. Cistectomia nel carcinoma non muscolo invasivo della vescica: quando e come (rigida o flessibile) [Cystoscopy in non-muscle-invasive bladder cancer: when and how (rigid or flexible)]. *Urologia.* (2013) 80 Suppl 21:11–5. doi: 10.5301/RU.2013.10858

22. Lenis AT, Lec PM, Chamie K, Mshs MD. Bladder cancer: a review. *JAMA.* (2020) 324:1980–991. doi: 10.1001/jama.2020.17598

frontiers | Frontiers in Medicine

TYPE Case Report
PUBLISHED 01 November 2022
DOI 10.3389/fmed.2022.1024008

OPEN ACCESS

EDITED BY
Gaurav Malviya,
University of Glasgow, United Kingdom

REVIEWED BY
Guozhu Hou,
National Cancer Center, Cancer Hospital, Chinese Academy of Medical Sciences and Peking Union Medical College, China
Pilar Paredes,
Hospital Clinic of Barcelona, Spain

*CORRESPONDENCE
Zhi-Jun Pei
pzjzml1980@taihehospital.com

SPECIALTY SECTION
This article was submitted to Nuclear Medicine, a section of the journal Frontiers in Medicine

RECEIVED 20 August 2022
ACCEPTED 30 September 2022
PUBLISHED 01 November 2022

CITATION
Zeng D-B, Chang C, Liu X-S, Gao Y, Wang Y-L and Pei Z-J (2022) Magnetic resonance imaging and ^{18}F-fludeoxyglucose positron emission tomography/computed tomography findings of retroperitoneal clear cell carcinoma with an unknown primary site: A case report. *Front. Med.* 9:1024008. doi: 10.3389/fmed.2022.1024008

Magnetic resonance imaging and ^{18}F-fludeoxyglucose positron emission tomography/computed tomography findings of retroperitoneal clear cell carcinoma with an unknown primary site: A case report

Dao-Bing Zeng[1], Chan Chang[2], Xu-Sheng Liu[1], Yan Gao[1], Ya-Lan Wang[1] and Zhi-Jun Pei[1]*

[1]Department of Nuclear Medicine, Taihe Hospital, Hubei University of Medicine, Shiyan, China, [2]Department of Respiratory and Critical Care Medicine, Taihe Hospital, Hubei University of Medicine, Shiyan, China

Herein, we report a case of retroperitoneal clear cell carcinoma (RCCC) with an unknown primary site that was confirmed *via* pathology. A 46-year-old man presented with low-grade fever, hyperhidrosis, and nightly fatigue that had occurred for the last 20 days. His weight had decreased significantly within the past 2 months (approximately 12 kg). On abdominal ultrasound, a mass was observed near the left renal hilum. In addition, enhanced magnetic resonance imaging (MRI) of the abdomen revealed a retroperitoneal nodular mass; however, no abnormalities in either kidney or adrenal glands were observed. ^{18}F-fludeoxyglucose positron emission tomography/computed tomography (^{18}F-FDG PET/CT) demonstrated an intensely FDG-avid retroperitoneal mass, the maximum standardized uptake value (SUVmax) was 19.6. On March 8, 2021, left retroperitoneal lesion resection, retroperitoneal lymph node dissection, and double kidney exploration were performed under general anesthesia. A post-operative pathological examination revealed Poorly differentiated clear cell carcinoma (left retroperitoneal) and metastatic lymph nodes. Immunohistochemical findings showed that the tumor originated from the kidney. At 6-month follow-up, reexamination of the patient revealed retroperitoneal lesion recurrence; however, no abnormalities were observable *via* enhanced computed tomography (CT) of both kidneys. To our knowledge, there have been no previous reports of RCCC of unknown origin.

KEYWORDS

^{18}F-FDG PET/CT, MRI, clear cell carcinoma, retroperitoneum, kidney, pathology

Introduction

Approximately 80% of all primary renal cell carcinomas are clear cell carcinomas, making them the most common pathological type of renal cell carcinoma (1). Nonetheless, reports of retroperitoneal clear cell carcinoma (RCCC) are extremely rare. There have been no previous reports on this subject in the literature. Herein, we report a case of RCCC that was pathologically confirmed. Although immunohistochemistry suggested the carcinoma was renal in origin, no obvious abnormality was found *via* imaging or the surgical exploration of both kidneys.

Manuscript formatting

Headings

Case presentation

A 46-year-old male who had experienced fever of unknown cause for the past 20 days presented with fever at night, night sweats, and a slight sense of fatigue. After sweating, the patient's body temperature returned to normal in the morning. A routine blood examination at an external hospital revealed elevated C-reactive protein and ESR levels of 28.0 mg/L (normal value 0–10 mg/L) and 25.0 mm/h (normal value 0–15 mm/h), respectively. Abdominal color ultrasound and enhanced computed tomography (CT) findings suggested retroperitoneal space-occupying lesions. The patient had no known history of malignancy. After admission, a magnetic resonance imaging (MRI) of the upper abdomen was performed. MRI findings indicative of the retroperitoneal mass were as follows (**Figure 1**). In addition, MRI suggested that retroperitoneal mass may be a metastatic tumor.

A whole body ^{18}F-fludeoxyglucose positron emission tomography/computed tomography (^{18}F-FDG PET/CT) (**Figure 2**) was performed to identify primary malignancy, PET/CT images demonstrated a retroperitoneal soft tissue density mass with Significantly increased FDG activity (SUVmax: 19.6), and revealed a lymph node adjacent to the mass with elevated FDG uptake (SUVmax: 7.9).^{18}F-FDG PET/CT did not detect potential tumors in other parts of the body. After imaging, the patient underwent a percutaneous biopsy guided by color ultrasound. A percutaneous retroperitoneal mass biopsy revealed a poorly differentiated carcinoma with immunohistochemical findings indicating it may have been renal in origin. Four weeks later, left retroperitoneal lesion resection, retroperitoneal lymph node dissection, and double kidney exploration were performed under general anesthesia. A post-operative pathological examination (**Figure 3A**) indicated clear cell carcinoma (left retroperitoneal) and metastatic lymph nodes. The following immunohistochemical findings (**Figure 3B**) suggested the carcinoma was renal in origin: Ki-67 (approximately 30% +), PAX8 (+), CK8 (+), vimentin (+), and PLAP (weak +). No abnormalities were found on imaging and intraoperative exploration of both kidneys in this case. On 6-month follow-up, abdominal enhanced CT revealed retroperitoneal lesion recurrence (**Figure 4**); however, there remained no obvious abnormality in either kidney.

Discussion

In this case, RCCC revealed extremely high FDG metabolic activity, which may be related to its pathological grade. The metabolic activity of FDG in renal clear cell carcinoma is related to pathological grade (2). Takahashi et al. found that highgrade clear cell renal cell carcinoma (ccRCC) showed higher metabolism than low-grade ccRCC, and high-grade on pathological nuclear grading was the most significant predictive value of SUV (3). According to the histological subtypes and the grade, high-grade ccRCC showed higher SUV than normal kidney tissues; in contrast, low-grade ccRCC did not show differences in the SUV when compared with normal kidney tissues (3). To explore the potential parameters from pre-operative ^{18}F-FDG PET/CT that might associate with the World Health Organization/the International Society of Urological Pathology (WHO/ISUP) grade in ccRCC, Zhao Y. et al. revealed metabolic parameters of primary tumor SUVmax was significantly different between any two of the four different WHO/ISUP grades, except those between the WHO/ISUP grade 3 and grade 4. The optimal cutoff values to predict high WHO/ISUP grade for SUVmax was 4.15 (4). WHO/ISUP system is a universal RCC grading system. The higher the nuclear grading, the worse the tumor differentiation, the higher the invasiveness, and the worse the prognosis of patients. Therefore, the possible reason for the high SUVmax value of this patient is related to the low differentiation of the tumor.

Remarkably, In this case, no abnormalities were found in either kidney *via* imaging or surgical exploration, findings that are likely suggestive of retroperitoneal renal tumor metastasis. Cancer of unknown primary site (CUPS) refers to primary tumors that cannot be detected by clinical, imaging, endoscopic, or other standard examination methods. CUPS accounting for 2.3–5% of all malignant tumors, of which nearly 80% can be presumed to be primary tumors *via* immunohistochemistry, molecular typing, genotype analysis, or other methods. In the remaining 20% of tumors, the origin of primary tissue cannot be determined (5, 6).

The pathogenesis of CUPS tumors is still unclear, Currently, two hypotheses have been formulated to describe their development. The first hypothesis states that all tumors have primary foci; however, the primary

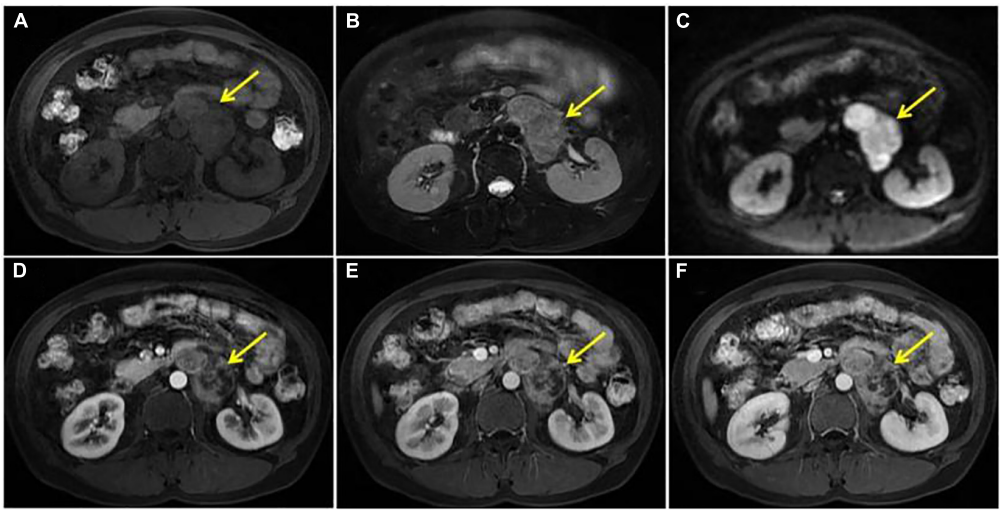

FIGURE 1
Magnetic resonance imaging (MRI) findings. Low signal on T1WI and heterogeneously high signal on T2WI [**(A,B)**, arrows], and high signal on axial diffusion-weighted imaging [DWI, B600; **(C)**, arrow] indicate the presence of a retroperitoneal mass. Axial early arterial and portal venous post-contrast T1-weighted fat-suppressed imaging findings indicating a heterogeneously enhanced mass are shown [**(D,E)**, arrows]; Retroperitoneal mass enhancement is more obvious in the delayed post-contrast T1-weighted fat-suppressed image [**(F)**, arrow].

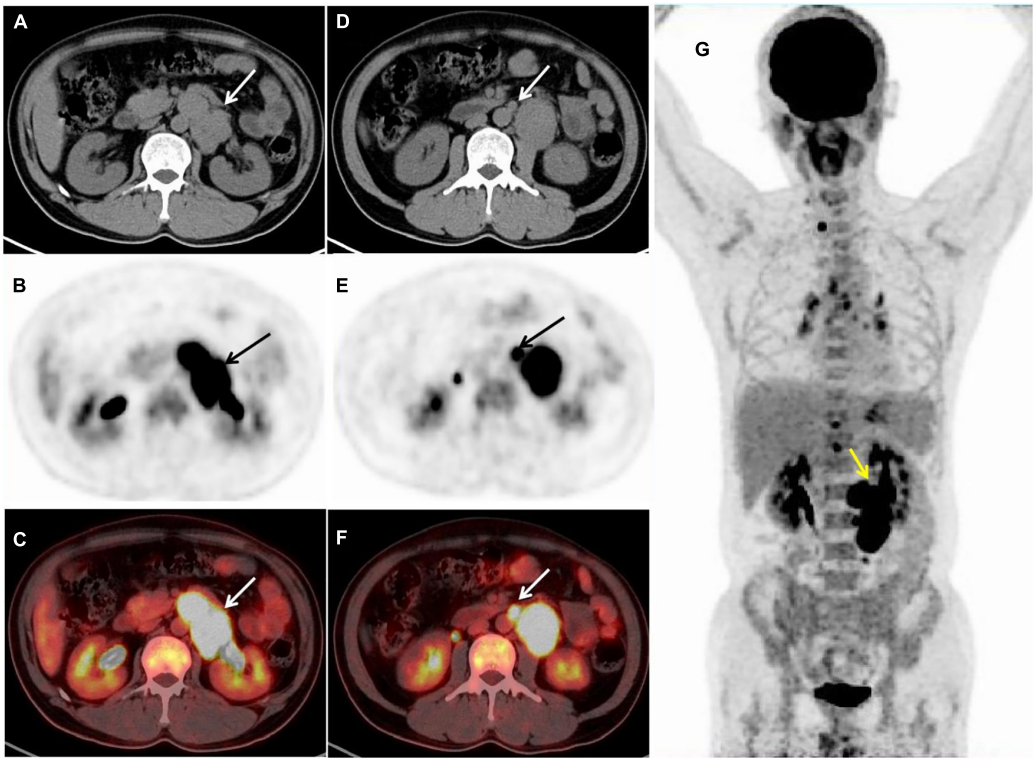

FIGURE 2
Whole body ^{18}F-fludeoxyglucose positron emission tomography/computed tomography (^{18}F-FDG PET/CT) as a screen for primary malignancy. An axial computed tomography (CT) image demonstrating a retroperitoneal soft tissue density mass at the level of the left hilum is shown in **(A)** (arrow). PET **(B)**, fused PET/CT images **(C)**, and a maximum intensity projection (MIP) image **(G)** revealing significantly increased FDG activity in the left retroperitoneal mass (arrow) are shown. An axial CT image **(D)** reveals the presence of a lymph node adjacent to the mass (arrow), while PET **(E)** and fused **(F)** images show significant uptake of FDG by the retroperitoneal lymph node.

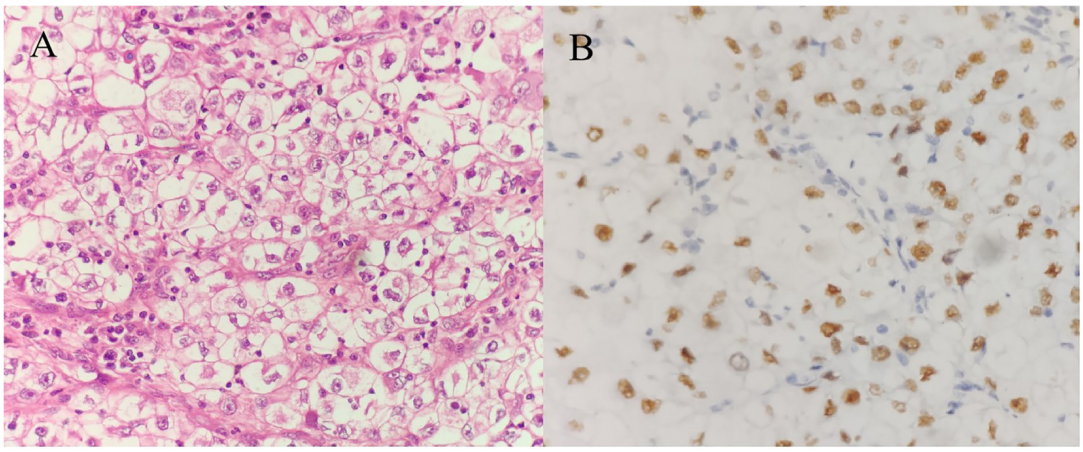

FIGURE 3
Pathological and immunohistochemical (IHC) findings. Post-operative pathological findings **(A)** reveal clear cell carcinoma (left retroperitoneal),the large polygonal tumor cells with transparent cytoplasm are arranged in a nest like manner, and the stroma is rich in small blood vessels. IHC findings **(B)**:Pax8 immunohistochemical staining of tumor cells is positive, indicating its renal origin.

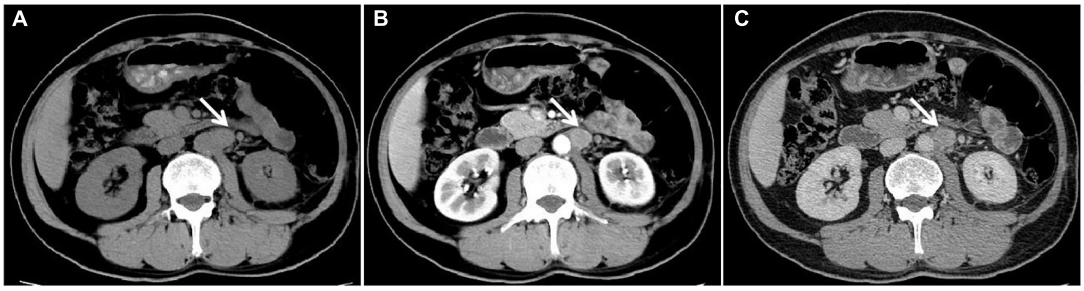

FIGURE 4
Abdominal enhanced computed tomography (CT) findings at 6-month follow-up. Axial images from non-enhanced CT **(A)** to CT enhanced in arterial phase **(B)** and venous phase **(C)**. Non-enhanced CT **(A)** reveals the presence of a soft tissue density nodule in the surgical area (left para-abdominal aorta), CT enhanced in arterial phase **(B)** moderately enhanced nodules in the operative area, and decreased enhancement in venous phase **(C)**. No obvious abnormalities in either kidney are shown.

foci in CUPS tumors are too small or difficult to be detectable *via* existing clinical methods. As disease progresses or the accuracy of detection methods improves, primary foci will be found. The other hypothesis suggests that CUPS are a special type of tumors that exist independently (without primary foci) but are biologically similar (7).

Based on the clinical characteristics of CUPS tumors, patients are often referred for symptoms and signs related to metastases. To improve the diagnosis and evaluation of the tumors, it is important to obtain clues indicative of their primary tissue, therefore, it is necessary to comprehensively evaluate the patient's history, tumor markers, imaging findings, and the tumor's pathological type, immunohistochemistry, and gene expression profile and so on. Most tumors with unknown primary foci are adenocarcinomas (60%) and undifferentiated carcinomas (30%), while squamous cell carcinomas and/or transitional cell carcinomas (5–8%), neuroendocrine tumors (2–4%) and sarcomas (about 1%) are relatively rare (7, 8). The most commonly observed metastatic tumors with unknown primary foci are head and neck tumors, breast cancer, prostate cancer, pancreatic and biliary system primary tumors. The most common sites of metastasis include the lymph nodes, bone, liver, and lung (8). No prior case of RCCC with an unknown primary site has been reported in the literature.

Large prospective clinical trials will be needed if we want to obtain conclusive evidence needed to improve treatment options for patients with tumors of unknown primary origin. According to current diagnosis and treatment guidelines, if a primary tumor can be reasonably presumed, the patient should be treated according to the specifications formulated for the presumed primary tumor, and the patient's prognosis comparable to that of those with the specific type of primary

tumor (7, 9). If no presumption can be made, patient prognosis varies and treatment includes empiric chemotherapy, palliative chemotherapy, and other supportive care. With the development of targeted therapy, successful cases of targeted therapy selected according to the molecular classification of tumors with unknown primary foci have been reported; however, no large-scale cohort study assessing the effectiveness of targeted therapy has reached a definitive conclusion (10–14). Immune checkpoint inhibitors have also been used to treat tumors of unknown primary origin, but only a subset of patients who have tumors with specific biological markers benefit from immunotherapy (15).

The diagnosis of occult tumors and those with an unknown clinical primary site comes with difficulties and challenges. Therefore, it is crucial to carefully read the film, take each patient's history, obtain comprehensive laboratory results, and perform imaging and pathological examinations when evaluating such patients. PET/CT facilitates the whole-body assessment of patients. Some primary tumors may remain undetectable by PET/CT, but to transfer mode, scope, metabolic activity for overall evaluation, guiding the follow-up treatment measures, which have important significance, is also the primary focal unknown tumors guidelines recommended by the important assessment tool.

Data availability statement

The original contributions presented in this study are included in the article/supplementary material, further inquiries can be directed to the corresponding author.

Ethics statement

Written informed consent was obtained from the individual(s) for the publication of any potentially identifiable images or data included in this article.

Author contributions

D-BZ conceived the project and wrote the manuscript. D-BZ, CC, and X-SL performed image post-processing and editing. D-BZ, YG, and Y-LW participated in the discussion and language editing. Z-JP reviewed the manuscript. All authors contributed to the article and approved the submitted version.

Conflict of interest

The authors declare that the research was conducted in the absence of any commercial or financial relationships that could be construed as a potential conflict of interest.

Publisher's note

All claims expressed in this article are solely those of the authors and do not necessarily represent those of their affiliated organizations, or those of the publisher, the editors and the reviewers. Any product that may be evaluated in this article, or claim that may be made by its manufacturer, is not guaranteed or endorsed by the publisher.

References

1. Escudier B, Porta C, Schmidinger M, Rioux-Leclercq N, Bex A, Khoo V, et al. Renal cell carcinoma: ESMO clinical practice guidelines for diagnosis, treatment and follow-up†. *Ann Oncol.* (2019) 30:706–20. doi: 10.1093/annonc/mdz056

2. Liu Y. The place of FDG PET/CT in renal cell carcinoma: value and limitations. *Front Oncol.* (2016) 6:201. doi: 10.3389/fonc.2016.00201

3. Takahashi M, Kume H, Koyama K, Nakagawa T, Fujimura T, Morikawa T, et al. Preoperative evaluation of renal cell carcinoma by using 18F-FDG PET/CT. *Clin Nucl Med.* (2015) 40:936–40. doi: 10.1097/RLU.0000000000000875

4. Zhao Y, Wu C, Li W, Chen X, Li Z, Liao X, et al. 2-[18F]FDG PET/CT parameters associated with WHO/ISUP grade in clear cell renal cell carcinoma. *Eur J Nucl Med Mol Imaging.* (2021) 48:570–9. doi: 10.1007/s00259-020-04996-4

5. Olivier T, Fernandez E, Labidi-Galy I, Dietrich PY, Rodriguez-Bravo V, Baciarello G, et al. Redefining cancer of unknown primary: is precision medicine really shifting the paradigm? *Cancer Treat Rev.* (2021) 97:102204. doi: 10.1016/j.ctrv.2021.102204

6. Moran S, Martinez-Cardús A, Boussios S, Esteller M. Precision medicine based on epigenomics: the paradigm of carcinoma of unknown primary. *Nat Rev Clin Oncol.* (2017) 14:682–94. doi: 10.1038/nrclinonc.2017.97

7. Fizazi K, Greco FA, Pavlidis N, Pentheroudakis G, Esmo Guidelines Committee. Cancers of unknown primary site: ESMO clinical practice guidelines for diagnosis, treatment and follow-up. *Ann Oncol.* (2015) 26(Suppl. 5):v133–8. doi: 10.1093/annonc/mdv305

8. Qaseem A, Usman N, Jayaraj JS, Janapala RN, Kashif T. Cancer of unknown primary: a review on clinical guidelines in the development and targeted management of patients with the unknown primary site. *Cureus.* (2019) 11:e5552. doi: 10.7759/cureus.5552

9. Tomuleasa C, Zaharie F, Muresan MS, Pop L, Fekete Z, Dima D, et al. How to diagnose and treat a cancer of unknown primary site. *J Gastrointestin Liver Dis.* (2017) 26:69–79. doi: 10.15403/jgld.2014.1121.261.haz

10. Asakura H, Takashima H, Mitani M, Haba R, Seo R, Yokoe K, et al. Unknown primary carcinoma, diagnosed as inflammatory breast cancer,and successfully treated with trastuzumab and vinorelbine. *Int J Clin Oncol.* (2005) 10:285–8. doi: 10.1007/s10147-005-0485-x

11. Chung JH, Ali SM, Davis J, Robstad K, McNally R, Gay LM, et al. Poorly differentiated malignant neoplasm lacking lung markers harbors an EML4-ALK rearrangement and responds to crizotinib. *Case Rep Oncol.* (2014) 7:628–32. doi: 10.1159/000367780

12. Tan DS, Montoya J, Ng QS, Chan KS, Lynette O, Sakktee Krisna S, et al. Molecular profiling for druggable genetic abnormalities in carcinoma of unknown primary. *J Clin Oncol.* (2013) 31:e237–9. doi: 10.1200/JCO.2012.44.3937

13. Yamada T, Ohtsubo K, Ishikawa D, Nanjo S, Takeuchi S, Mouri H, et al. Cancer of unknown primary site with epidermal growth factor receptor mutation for which gefitinib proved effective. *Gan To Kagaku Ryoho.* (2012) 39:1291–4.

14. Yamada T, Ohtsubo K, Ishikawa D, Nanjo S, Takeuchi S, Mouri H, et al. Putative lung adenocarcinoma with epidermal growth factor receptor mutation presenting as carcinoma of unknown primary site: a case report. *Medicine.* (2018) 97:e9942. doi: 10.1097/MD.0000000000009942

15. Gröschel S, Bommer M, Hutter B, Budczies J, Bonekamp D, Heining C, et al. Integration of genomics and histology revises diagnosis and enables effective therapy of refractory cancer of unknown primary with PDL1 amplification. *Cold Spring Harb Mol Case Stud.* (2016) 2:a001180. doi: 10.1101/mcs.a001180

frontiers | Frontiers in Medicine

TYPE Case Report
PUBLISHED 03 November 2022
DOI 10.3389/fmed.2022.1019964

OPEN ACCESS

EDITED BY
Gaurav Malviya,
University of Glasgow, United Kingdom

REVIEWED BY
Chentian Shen,
Shanghai Jiao Tong University, China
Lucia Baratto,
Stanford University, United States
Sharjeel Usmani,
Kuwait Cancer Control Center, Kuwait

*CORRESPONDENCE
Lei Kang
kanglei@bjmu.edu.cn

†These authors have contributed equally to this work

SPECIALTY SECTION
This article was submitted to Nuclear Medicine, a section of the journal Frontiers in Medicine

RECEIVED 15 August 2022
ACCEPTED 07 September 2022
PUBLISHED 03 November 2022

CITATION
Zhang Y, Huang W, Li L, Qiu Y, Jiao H, Chen Z, Yang Q, Song L and Kang L (2022) Retroperitoneal alveolar rhabdomyosarcoma intruding into spinal canal: A case report and literature review.
Front. Med. 9:1019964.
doi: 10.3389/fmed.2022.1019964

Retroperitoneal alveolar rhabdomyosarcoma intruding into spinal canal: A case report and literature review

Yongbai Zhang[1†], Wenpeng Huang[1†], Liming Li[2], Yongkang Qiu[1], Hao Jiao[1], Zhao Chen[1], Qi Yang[1], Lele Song[1] and Lei Kang[1*]

[1]Department of Nuclear Medicine, Peking University First Hospital, Beijing, China, [2]Department of Radiology, The First Affiliated Hospital of Zhengzhou University, Zhengzhou, China

Background: Rhabdomyosarcoma (RMS) is the most frequent soft sarcoma in children and adolescents. Alveolar rhabdomyosarcoma (ARMS) is a relatively rare subtype that is characterized by aggressive behavior and an unsatisfactory prognosis. An ARMS can arise anywhere but most commonly occurs at extremity sites with a very small fraction in the retroperitoneum. The utility of 2-Deoxy-2-[fluorine-18]-fluoro-D-glucose (^{18}F-FDG) positron emission tomography combined with computed tomography (PET/CT) remains to be established in ARMS.

Case Report: A 3-year-old female child was accidentally found with a large left upper abdominal mass for a day. CT examination indicated a huge soft tissue mass in the left retroperitoneum extending superiorly to the level of the left hilus renalis and inferiorly to the left acetabulum in the pelvic cavity, with intrusion into the lumbar foramens. ^{18}F-FDG PET/CT found a mass in the left retroperitoneum from the level of T12 to the left acetabulum, with the maximum standardized uptake value (SUV_{max}) of about 7.0, and a CT value of about 39 HU, invading the left L3-5 intervertebral foramina and protruding into the spinal canal, with unclear boundary with the spinal cord. Retroperitoneal tumor resection and the repair operation of vascular exploration were performed. An ARMS was confirmed by postoperative biopsy, immunohistochemical staining, and genetic detection with the rupture of the fork head in rhabdomyosarcoma (FKHR). The patient received chemotherapy and was in a good condition with no recurrence and obvious complications.

Conclusion: Retroperitoneal ARMS is rare and indicates a poor outcome with the potential to involve vital organs and intrude into the spinal canal. Accurate diagnosis and staging using PET/CT would contribute to better risk stratifications and appropriate treatment individually.

KEYWORDS

alveolar rhabdomyosarcoma, ^{18}F-FDG, PET/CT, retroperitoneum, spinal canal intrusion, case report

Introduction

Rhabdomyosarcoma (RMS), which is derived from primary mesenchymal cells that differentiate into skeletal muscle, is a type of high-grade rare malignant tumor with an incidence of 4.6 cases per million (1, 2). RMS is usually classified into four histologic subtypes: embryonal rhabdomyosarcoma (ERMS), alveolar rhabdomyosarcoma (ARMS), pleomorphic rhabdomyosarcoma, and sclerosing/spindle cell rhabdomyosarcoma (3). An ARMS is a relatively rare subcategory with a prevalence of about 20–25% of all RMS, compared with ERMS of 50–60% (4). It is more aggressive and has a more unsatisfactory prognosis than other subtypes (5). The ARMS most commonly occurs at extremity sites and sometimes in the head and/or neck or torso, while ERMS typically occurs in the head and neck (6). However, retroperitoneal ARMS is extremely rare and has poor outcomes accompanied by the large tumor volume and frequent involvement of vital organs, leading to difficult resection when it is diagnosed (7). Due to the specific anatomical location, retroperitoneal, especially paraspinal, ARMS shows the potential to infiltrate the vertebrae and protrude into the spinal canal (8, 9).

2-Deoxy-2-[fluorine-18]-fluoro-D-glucose (^{18}F-FDG) positron emission tomography combined with computed tomography (PET/CT) is an imaging technology illustrating detailed metabolic and functional molecular information and the precise anatomical region of the lesion (10). It is used in evaluating different tumors and represents an extremely promising investigation method for the diagnosis, staging, and prognosis of rhabdomyosarcoma. Herein, we described a rare case with retroperitoneal ARMS invading the intervertebral foramen and intruding into the spinal canal, and we reviewed the available literature on retroperitoneal ARMS.

Case presentation

A 3-year-old female was accidentally found with a large left upper abdominal mass for a day. By physical examination, a smooth, hard, painless, and firm mass of about 14 cm in the left upper abdomen was found. Laboratory test showed increased fibrinogen of 4.08 g/L (reference range 2–4 g/L), neuron-specific enolase (NSE) of 79.90 ng/mL (reference range 15.6–17 ng/mL), and tumor abnormal protein (TAP) of 135.60 (reference range 1–121). An ultrasound showed a solid mass of about 13.8 × 10.4 cm in the left upper abdomen, with an unclear boundary with the left kidney. Blood flow signal could be observed using the color doppler flow imaging (CDFI) technique (Figure 1).

Contrast-enhanced CT examination indicated a huge soft tissue mass, measuring 12.3 × 7.4 cm at the larger section, in the left retroperitoneum extending superiorly to the level of the left hilus renalis and inferiorly to the left acetabulum in the pelvic cavity, with intrusion into the lumbar foramens, compression and squeezing of the left kidney and left abdominal bowel, local compression and stenosis of the inferior vena cava, and the abdominal aorta was displaced to the right side by compression (Figure 2). The tissue mass showed mottling calcification, cystic degeneration, and necrosis. The patient was injected with 0.1 mCi/kg of ^{18}F-FDG after 6 h of fasting, and PET/CT images were acquired 60 min later. The tissue mass with a high FDG uptake was found using ^{18}F-FDG PET/CT in the left retroperitoneum from the level of T12 to the left acetabulum, with the maximum standardized uptake value (SUV_{max}) of about 7.0 and a CT value of about 39 HU. The tumor invaded the left L3-5 intervertebral foramina and protruded into the spinal canal, with an unclear boundary with the spinal cord (Figure 3). The abdominal cavity and retroperitoneum showed enlarged lymph nodes, with a SUV_{max} of about 6.4 and the largest size of about 2.0 × 3.0 cm. No obvious abnormal FDG uptake was observed in the lung and bone.

Retroperitoneal tumor resection and vascular repairing operation were performed 10 days after admission. The tumor was found to extend superiorly to the left hilus renalis, rightwards to cross the spine, and inferiorly to the level of the internal inguinal ring. It surrounded the abdominal aorta, the left iliac vessel, and the inferior vena cava, while locally infiltrating and growing in the inferior vena cava. After vessel clamping, the inferior vena cava segment invaded by the tumor was resected. Since the patient's family refused artificial vascular replacement, the inferior vena cava, at the level of the left and right iliac artery branches, and the left and right iliac veins were ligated. Histological results showed small round malignant cell with characteristic alveolar structures (Figures 4A,B). Immunohistochemical staining revealed myogenin (+), LCA (–), EMA (–), AE1/AE3 (–), Syn + (partly), NSE (–), CD99 (–), Fli-1 (–), Ki-67 (+60%), PAX-8 (+), CD56 (+), CgA (foci+), Desmin (+), Myo D1 (+), WT-1 (+), PD-1, S-100 (–), and PAX-5 (+). Fluorescence *in situ* hybridization revealed fork head in rhabdomyosarcoma (FKHR) rupture (Figure 4C). The final diagnosis was confirmed as ARMS with TNM stage 3 and IRS stage III, and the level of risk was high. Then, the patient received chemotherapy comprising vincristine, dactinomycin, and cyclophosphamide (VAC therapy) with supportive treatments to alleviate adverse reactions to chemotherapy. A combination of vincristine and irinotecan (VI) was administered 1 month later, and VAC was repeated 2 months later. The patient has survived for 9 months since the initial diagnosis with no recurrence and obvious complications.

Discussion

Rhabdomyosarcoma is the most common extracranial solid tumor in the pediatric population after neuroblastoma and

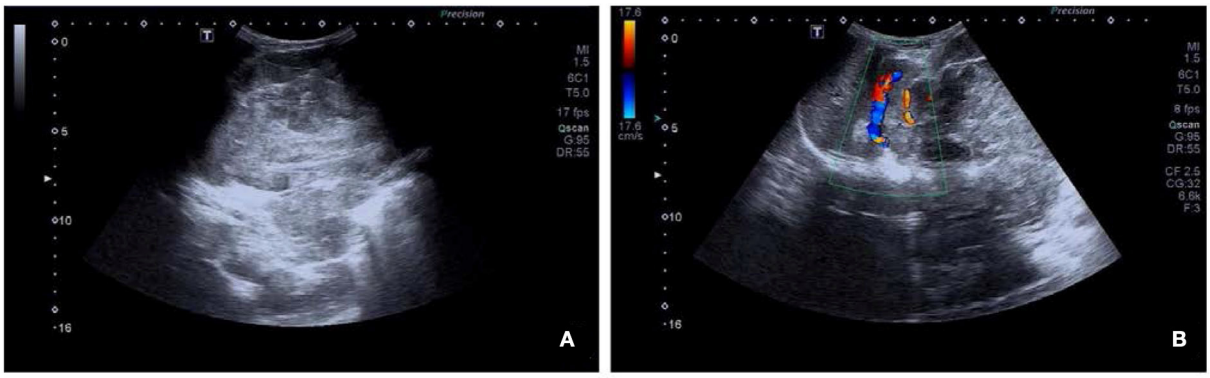

FIGURE 1
Ultrasound images of retroperitoneal alveolar rhabdomyosarcoma (ARMS). **(A)** A heterogeneous hypoechoic area of about 13.8 × 10.4 cm in the left upper abdomen, with an unclear boundary with the left kidney. **(B)** Blood flow signal observed using color doppler flow imaging (CDFI).

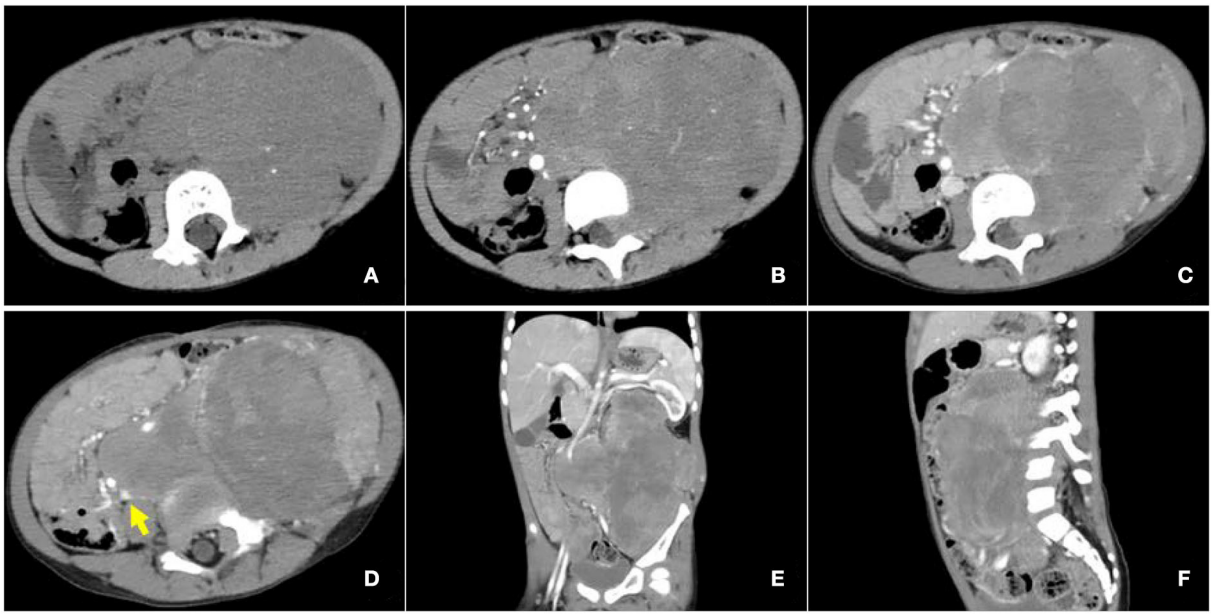

FIGURE 2
Enhanced computed tomography (CT) images of retroperitoneal ARMS. **(A)** A plain image with a CT attenuation value of about 47 HU; mottling calcification existing within the mass; **(B)** Arterial phase image with a CT attenuation value of about 50 HU; the mass supplied by branches of superior and inferior mesenteric arteries and areas of cystic degeneration and necrosis without enhancement existing within the mass; **(C–F)** venous phase image with a CT attenuation value of about 65 HU. Left renal vein reflux could be observed in the mass. The mass invaded the lumbar intervertebral foramen and compressed the left kidney, left abdominal bowel, and the inferior vena cava, and the abdominal aorta was also compressed and displaced to the right. The arrow illustrates the involvement of the inferior vena cava.

Wilms tumor (8). A total of 63% of RMS occur in children under 10 years old, and the incidence rate reaches the peak between 2 and 5 years old (11). ARMS is a relatively rare subtype with a poor prognosis, of which the estimated 10-year overall survival (OS) rate is 29.4% compared with 52.1% in the nonalveolar type (12). The retroperitoneum is not the typical primary site of RMS, with ∼8% of the incidence of all sites (13). Approximately, 20% of the patients present with distant metastatic disease at diagnosis, and lung, bone, and bone marrow are the commonly involved sites (6, 14).

We searched the literature in the PubMed database from 1997 to 2022 using the keywords containing alveolar rhabdomyosarcoma and retroperitoneal. In total, 5 available case reports were found. We summarize the case reports in Table 1 (7, 8, 15–17). Of these cases, male children seem to be the more vulnerable group, which is consistent with overall incidence

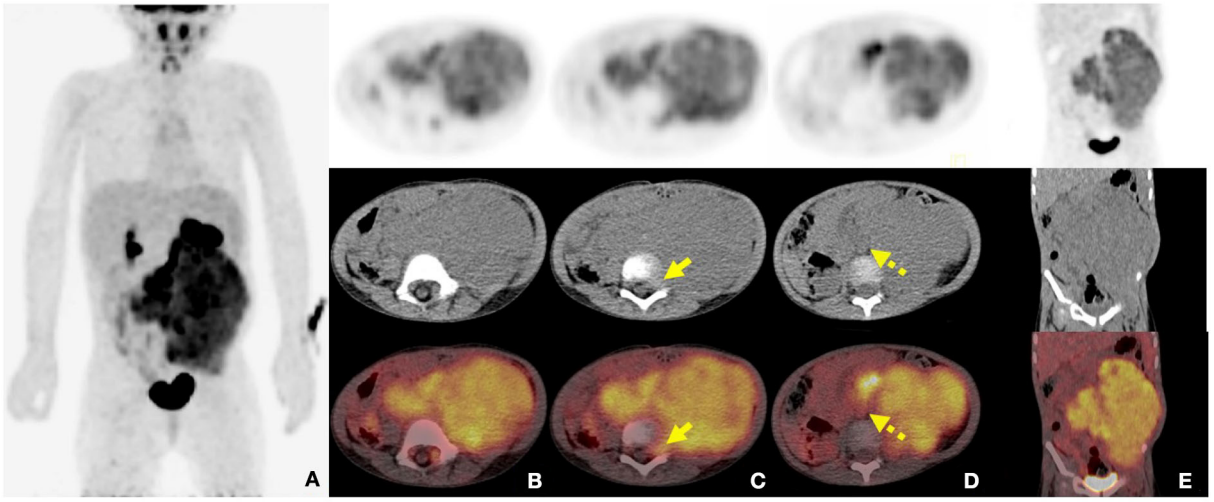

FIGURE 3
2-Deoxy-2-[fluorine-18]-fluoro-D-glucose (^{18}F-FDG) positron emission tomography combined with computed tomography (PET/CT) images of retroperitoneal ARMS. **(A)** The whole-body maximum density projection showing hypermetabolic areas in the left retroperitoneum; **(B)** The axial images showing the concentrated distribution of radioactivity in soft tissue mass, with maximum standardized uptake value (SUV_{max}) of about 7.0, the maximum layer of 8.8 × 10.3 cm, and a CT value of about 39 HU; **(C)** The axial images showing invasion of the left L3-5 intervertebral foramen and protrusion into the spinal canal, with unclear boundary with the spinal cord (short arrows); **(D)** The axial images showing the involved retroperitoneal lymph nodes (dash arrows); **(E)** The coronal image showing the lesion extending from the level T12 to the left acetabulum.

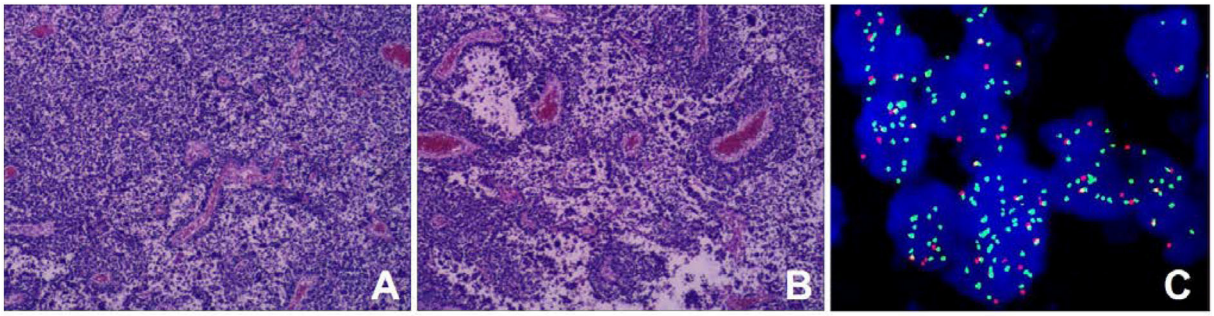

FIGURE 4
Histopathological results. **(A)** Tumor cells were round or oval with hyperchromatic nuclei and nuclear fission (HE staining); **(B)** Cells forming patterns resembling pulmonary alveoli, and fibrous vascular tissue between the alveoli (HE stain) [magnification (A,B) ×100]; **(C)** The fork head in rhabdomyosarcoma (FKHR) gene rupture was positive (fluorescence *in situ* hybridization) [magnification ×1000].

(male:female ratio of 1.51, 95% confidence interval (CI): 1.27–1.80) (18). Clinical symptoms are variable, depending on the size and location of the retroperitoneal mass and the presence or absence of distant metastases. The tumor squeezing certain organs can cause relevant performance, and the huge mass often invades vital organs such as the kidneys, aorta, inferior vena cava, and bilateral iliac vessels. However, patients can sometimes present with a mass and no notable symptom similar to the case we described here, causing a delay in diagnosis. It should be noticed that retroperitoneal ARMS appeared to have the potential to infiltrate the vertebrae and extend into the spinal canal. This could provide opportunities for tumors to invade the intervertebral foramen and spread to the spinal cord and even the brain as reported in the case study 2 (8). Thus, it argues for more attention on the careful and precise detection of the tumor intruding into the spinal canal and metastatic to the central nervous system.

Alveolar rhabdomyosarcoma recurrently, of ∼80%, harbors chromosomal translocations including a *t*(2;13)(q35;q14) or a *t*(1;13)(p36;q14), which can generate fusion genes PAX3- and PAX7-FOXO1 respectively. And proteins produced by these fusion genes can function as oncoproteins promoting the proliferation and apoptosis of tumor cells (6, 19). The diagnosis of ARMS requires histology and molecular pathology studies of

TABLE 1 Characteristics of patients with retroperitoneal alveolar rhabdomyosarcoma (ARMS) in the literature review.

Case	Authors	Patient sex	Age	Primary sites	Clinical symptom	Local invasion	Distant metastatic	Image methods	Management	Prognosis
1	Ito et al. (7)	M	11 years	Retroperitoneum	Back pain	Adventitia of the aortic wall	None	MRI	Surgery + chemotherapy + radiotherapy	Alive at 12 month
2	Kline et al. (8)	M	14 months	Right retroperitoneum	Mass and irritability	Spinal canal	Bone marrow, lung and leptomeningeal metastatic	CT, MRI	Surgery + chemotherapy	Died after 2 month
3	Mariko Kinoshita et al. (17)	M	3 years	Retroperitoneum	Abdominal distention and constipation	Pleural space	Liver and multiple lymph nodes	^{18}F-FDG PET/CT	Chemotherapy + radiotherapy	Alive at 22 month
4	Lugen Chen et al. (15)	M	13 years	Right retroperitoneum	Skin rash, petechiae, and ecchymoses over lower extremities and abdominal pain	–	Lymph nodes and bone marrow metastatic	CT	Chemotherapy	Alive at 8 month
5	Michiyuki Hakozaki et al. (16)	M	10 years	Left reniportal-retroperitoneal, groin and left gluteus maximus	Pain in the left buttock	–	Diffuse bone metastatic	CT	Surgery + chemotherapy + radiotherapy + peripheral blood stem cell transplantation	Died after 21 month

MRI, magnetic resonance imaging; —, No details in the report.

10.3389/fmed.2022.1019964

the tumor tissue (6). ARMS is typically composed of densely packed, small, and round cells aggregating in areas at the edges of fibrous septa forming structures such as pulmonary alveoli (1, 20). Immunohistochemical markers include myogenic markers such as MyoD (myf3) or myogenin (myf4), myosin, myoglobin, muscle-specific actin, or desmin (21).

Medical imaging provides noninvasive methods which are essential for the evaluation of patients with ARMS. The sonographic feature of ARMS is substantive hypoechoic or complex-echoic mass. CDFI shows rich and disorderly color blood flow signals within the mass. It often appears as an equal or a slightly low-density mass in plain CT, with unclear borders. The tumors usually grow rapidly, and necrosis, as well as cystic degeneration, can be seen in the lesions as a result of the insufficient blood supply. Enhanced CT scan shows heterogeneous enhancement and sometimes rim-like enhancement. Areas without enhancement are tissues with necrosis and cystic degeneration. Hemorrhage and calcification occur rarely, but mottling calcification was observed in this case. Moreover, CT can detect adjacent bone involvement but ARMS frequently destroy the bone. PET/CT reveals increased glucose metabolism of ARMS. As an advanced technology, PET/CT could provide more information about the lesions than conventional imaging detection methods. ^{18}F-FDG PET/CT imaging is useful for initial assessment, monitoring treatment response, and detection of recurrences with better accuracy for identifying primary sites, lymphatic involvement, and distant metastases (22, 23). Local lymph node metastasis has been considered a strong prognostic factor, calling for an emphasis on desirable detection modalities of lymphatic involvement (24). Compared with conventional imaging techniques, such as ultrasound, CT, and magnetic resonance imaging (MRI), PET/CT performs better in detecting lymph nodal metastasis with higher sensitivity and specificity (25). ^{18}F-FDG PET/CT can estimate the function and nature of nodes through the level of glucose metabolism in tissues and can help with accurate localization of the involved lymph nodes. In a prospective study by Völker et al. (25), the detection of involved lymph nodes using ^{18}F-FDG PET/CT reached a sensitivity of 93%, whereas conventional imaging modalities were only 36%. Ricard et al. (26) reported that ^{18}F-FDG PET/CT found 19 involved lymph nodes in 4 patients vs. 12 nodes by MRI and CT, and therefore, the results of PET/CT led to alteration of the lymph node staging and treatment strategies in some patients. Our case also observed similar advantages of PET/CT for discovering retroperitoneal lymphatic metastases, whereas negative in ultrasound and CT tests. The more accurate staging of regional lymph node involvement will benefit risk stratification and treatment decisions in patients with RMS. PET/CT also shows some potential superiorities in finding tumor invasion into the spinal canal. When evaluating the spinal canal involvement, all background tissues, including paraspinal musculature, vertebrae, spinal cord, nerve roots, and CSF, demonstrate relatively low metabolic activity using ^{18}F-FDG PET/CT, thus making it possible for differentiation between normal tissues and lesions (27, 28). PET/CT allows for the identification of soft-tissue involvement such as neural foramen invasion and epidural extension of tumor in malignant involvement of the spine (29). However, PET/CT is inferior to MRI when used to detect spinal cord involvement. In recent years, the integrated PET and MR (PET/MR) imaging modality has been rapidly developed with the combined superiorities of quantification of radioactive tracer metabolism provided by PET and outstanding soft tissue contrast by MR (30). The value of PET/MR in clinical applications remains to be established, and we hope this innovative technology will provide more accurate diagnosis and ultimately improve patient prognosis. In addition, a study illustrated that metabolic parameters obtained from baseline PET/CT were potential to select patients sensitive to treatment (31). Features of patients including unfavorable sites of the primary tumor, older patient age at initial presentation, the alveolar subtype, and regional lymph node involvement are considered to be poor prognostic factors for RMS (5, 32). Unfavorable sites include the prostate and bladder, cranial parameningeal sites, extremities, trunk, retroperitoneum, and other sites (13). Moreover, ^{18}F-FDG PET/CT may be an added prognostic predictor in RMS. High SUV_{max} value is more prevalent among patients with less favorable features including unfavorable primary sites, alveolar pathology, and high-risk group (33). A study found that during diagnosis, patients with SUV_{max} of <9 had an improved 3-year progression-free survival (62% of patients with SUV_{max} of <9 vs. 39% of patients with SUV_{max} of ≥ 9, $p = 0.02$) (34). In our case study, the SUV_{max} of 7.0 might be associated with the patient's favorable prognosis.

Retroperitoneal ARMS should be differentiated from neuroblastoma. Neuroblastoma is the most common extracranial solid tumor in the pediatric population and almost 70% of the patients have abdominal neuroblastoma (35, 36). Furthermore, neuroblastoma may arise from paraganglia and is likely to protrude into the spinal canal through the neural foramina. In addition to symptoms caused by the abdominal mass such as abdominal pain and fullness, patients usually present with elevated levels of vanillylmandelic acid (VMA) and homovanillic acid (HVA). The characteristic PET/CT findings of neuroblastoma in children include large size, mixed density with calcification, necrosis, and cystic degeneration, which specifically show peripheral hypermetabolic areas and central hypometabolic areas in the tumor, indicating central necrotic and cystic lesions. PET/CT is superior at revealing lymph nodes and distant organ metastases, which can provide an objective imaging basis for preoperative diagnosis and accurate staging of neuroblastoma in children, over conventional imaging. Calcification could be seen in almost 90% of cases, appearing as sandy, spotted, and mass shapes, which is a characteristic manifestation of neuroblastoma (37). ^{123}I-Metaiodobenzylguanidine (MIBG) plays an important role in

the diagnosis of neuroblastoma with an accumulation of MIBG in the lesions (38). However, the limited sensitivity of ^{123}I-MIBG needs to be improved. A prospective study by Piccardo et al. demonstrated that ^{18}F-3,4-dihydroxyphenylalanine (^{18}F-DOPA) PET/CT is more sensitive in detecting primary tumors, soft tissue metastases, and bone and bone marrow metastases than ^{123}I-MIBG (39). The diagnosis of neuroblastoma should be confirmed by biopsy. In this case, the diagnosis of ARMS was not definite until the results of postoperative histology distinguished it from neuroblastoma.

Overall, the cure rate of RMS could be increased with the improvements in risk stratifications and multimodal treatment including surgery, chemotherapy, and radiotherapy (40, 41). As for retroperitoneal RMS, surgery, especially radical resection, is the principal choice, with a longer median OS than palliative surgery and conservative treatment (18 vs. 6 months) (9).

Conclusion

Retroperitoneal ARMS is relatively rare and characterized by its unfavorable outcome with the potential to involve vital organs and intrude into the spinal canal, and even spread to CNS. It should be noted that the retroperitoneal mass may be misdiagnosed as neuroblastoma and a biopsy is necessary for the final diagnosis. Accurate staging using PET/CT would contribute to better risk stratifications and appropriate treatment individually.

Data availability statement

The original contributions presented in the study are included in the article/supplementary material, further inquiries can be directed to the corresponding author.

Ethics statement

Ethical review and approval was not required for the study on human participants in accordance with the local legislation and institutional requirements. Written informed consent from the patients/participants legal guardian/next of kin was not required to participate in this study in accordance with the national legislation and the institutional requirements. The study was approved by the Institutional Review Board at the First Affiliated Hospital of Zhengzhou University and Peking University First Hospital.

Author contributions

YZ manuscript drafting. WH acquisition and analysis of the work and imaging data collection and analysis. LL imaging data collection and analysis and resources collection. YQ and HJ manuscript editing. ZC, QY, and LS formal analysis and resource collection. LK supervision and writing-review and editing. All authors met the requirements for authorship for the submitted version and agreed to its submission.

Funding

This study was funded by the Beijing Science Foundation for Distinguished Young Scholars (JQ21025) and the Peking University Medicine Fund of Fostering Young Scholars' Scientific and Technological Innovation (BMU2022PY006).

Conflict of interest

The authors declare that the research was conducted in the absence of any commercial or financial relationships that could be construed as a potential conflict of interest. Written informed consent was obtained from the minor's legal guardian for the publication of any potentially identifiable images or data included in this article.

Publisher's note

References

1. Dziuba I, Kurzawa P, Dopierała M, Larque AB, Januszkiewicz-Lewandowska D. Rhabdomyosarcoma in children: current pathologic and molecular classification. *Polish J Pathol.* (2018) 69:20–32. doi: 10.5114/pjp.2018.75333

2. Ries LAG. *Cancer Incidence and Survival among Children and Adolescents: United States Seer Program, 1975–1995*. Bethesda: National Cancer Institute (1999).

3. Sbaraglia M, Bellan E, Dei Tos AP. The 2020 who classification of soft tissue tumours: news and perspectives. *Pathologica.* (2021) 113:70. doi: 10.32074/1591-951X-213

4. Sultan I, Qaddoumi I, Yaser S, Rodriguez-Galindo C, Ferrari A. Comparing adult and pediatric rhabdomyosarcoma in the surveillance, epidemiology and end results program, 1973–2005: an analysis of 2,600 patients. *J Clin Oncol.* (2009) 27:3391–7. doi: 10.1200/JCO.2008.19.7483

5. Kim JR, Yoon HM, Koh KN, Jung AY, Cho YA, Lee JS. Rhabdomyosarcoma in children and adolescents: patterns and risk factors of distant metastasis. *AJR Am J Roentgenol.* (2017) 209:409–16. doi: 10.2214/AJR.16.17466

6. Skapek SX, Ferrari A, Gupta AA, Lupo PJ, Butler E, Shipley J, et al. Rhabdomyosarcoma. *Nat Rev Dis Prim.* (2019) 5:1–19. doi: 10.1038/s41572-018-0051-2

7. Ito F, Watanabe Y, Harada T, Ando H, Seo T, Kaneko K, et al. Combined resection of abdominal aorta and inferior vena cava for retroperitoneal rhabdomyosarcoma invading the aortoiliac bifurcation. *J Pediatr Surg.* (1998) 33:1566–8. doi: 10.1016/S0022-3468(98)90501-2

8. Kline RM, Oseas RS, Jolley SG, Reyna TM, Erling MA, Sandberg AA, et al. Leptomeningeal metastasis from a paraspinal rhabdomyosarcoma with a Der(13)T(1;13)(Q23;Q32) in a 14-month-old boy. *Cancer Genet Cytogenet.* (1997) 98:97–101. doi: 10.1016/S0165-4608(96)00414-1

9. Wang T, Gao X, Yang J, Guo W, Wu Z, Tang L, et al. Treatment strategies and outcomes for spinal rhabdomyosarcoma: a series of 11 cases in a single center and review of the literature. *Clin Neurol Neurosurg.* (2020) 192:105729. doi: 10.1016/j.clineuro.2020.105729

10. Evens AM, Kostakoglu L. The role of Fdg-Pet in defining prognosis of hodgkin lymphoma for early-stage disease. *Hematol Am Soc Hematol Educ Prog.* (2014) 2014:135–43. doi: 10.1182/asheducation-2014.1.135

11. Menzies-Wilson R, Wong G, Das P. Case report: a rare case of middle-ear rhabdomyosarcoma in a 4-year-old boy. *F1000Res.* (2019) 8:1734. doi: 10.12688/f1000research.20558.2

12. Cecchetto G, Bisogno G, Treuner J, Ferrari A, Mattke A, Casanova M, et al. Role of surgery for nonmetastatic abdominal rhabdomyosarcomas: a report from the Italian and German soft tissue cooperative groups studies. *Cancer.* (2003) 97:1974–80. doi: 10.1002/cncr.11285

13. Maurer HM, Beltangady M, Gehan EA, Crist W, Hammond D, Hays DM, et al. The intergroup rhabdomyosarcoma study-I. A final report. *Cancer.* (1988) 61:209–20. doi: 10.1002/1097-0142(19880115)61:2<209::AID-CNCR2820610202>3.0.CO;2-L

14. Hawkins DS, Spunt SL, Skapek SX. Children's oncology group's 2013 blueprint for research: soft tissue sarcomas. *Pediatr Blood Cancer.* (2013) 60:1001–8. doi: 10.1002/pbc.24435

15. Chen L, Shah HO, Lin JH. Alveolar rhabdomyosarcoma with concurrent metastases to bone marrow and lymph nodes simulating acute hematologic malignancy. *J Pediatr Hematol Oncol.* (2004) 26:696–7. doi: 10.1097/01.mph.0000140654.50344.92

16. Hakozaki M, Hojo H, Tajino T, Yamada H, Kikuchi S, Kikuta A, et al. Therapeutic cytodifferentiation in alveolar rhabdomyosarcoma without genetic change of the Pax3-Fkhr chimeric fusion gene: a case study. *Hum Cell.* (2013) 26:149–54. doi: 10.1007/s13577-013-0067-6

17. Kinoshita M, Yamada A, Sawa D, Kamimura S, Miyachi M, Moritake H. Successful treatment of metastatic alveolar rhabdomyosarcoma with Mgmt gene promoter methylation by temozolomide-based combination chemotherapy. *Pediatr Blood Cancer.* (2018) 65:26750. doi: 10.1002/pbc.26750

18. Ognjanovic S, Linabery AM, Charbonneau B, Ross JA. Trends in childhood rhabdomyosarcoma incidence and survival in the United States, 1975–2005. *Cancer.* (2009) 115:4218–26. doi: 10.1002/cncr.24465

19. Marshall AD, Grosveld GC. Alveolar rhabdomyosarcoma: the molecular drivers of Pax3/7-Foxo1-induced tumorigenesis. *Skelet Muscle.* (2012) 2:25. doi: 10.1186/2044-5040-2-25

20. Rudzinski ER, Teot LA, Anderson JR, Moore J, Bridge JA, Barr FG, et al. Dense pattern of embryonal rhabdomyosarcoma, a lesion easily confused with alveolar rhabdomyosarcoma: a report from the soft tissue sarcoma committee of the children's oncology group. *Am J Clin Pathol.* (2013) 140:82–90. doi: 10.1309/AJCPA1WN7ARPCMKQ

21. Parham DM, Barr FG. Classification of rhabdomyosarcoma and its molecular basis. *Adv Anat Pathol.* (2013) 20:387–97. doi: 10.1097/PAP.0b013e3182a92d0d

22. Ben Arush MW, Bar Shalom R, Postovsky S, Militianu D, Haimi M, Zaidman I, et al. Assessing the use of Fdg-Pet in the detection of regional and metastatic nodes in alveolar rhabdomyosarcoma of extremities. *J Pediatr Hematol Oncol.* (2006) 28:440–5. doi: 10.1097/01.mph.0000212949.12856.02

23. Jadvar H, Gamie S, Ramanna L, Conti PS. Musculoskeletal system. *Semin Nucl Med.* (2004) 34:254–61. doi: 10.1053/j.semnuclmed.2004.06.002

24. Reboul-Marty J, Quintana E, Mosseri V, Flamant F, Asselain B, Rodary C, et al. Prognostic factors of alveolar rhabdomyosarcoma in childhood. An international society of pediatric oncology study. *Cancer.* (1991) 68:493–8. doi: 10.1002/1097-0142(19910801)68:3<493::AID-CNCR2820680308>3.0.CO;2-#

25. Völker T, Denecke T, Steffen I, Misch D, Schönberger S, Plotkin M, et al. Positron emission tomography for staging of pediatric sarcoma patients: results of a prospective multicenter trial. *J Clin Oncol.* (2007) 25:5435–41. doi: 10.1200/JCO.2007.12.2473

26. Ricard F, Cimarelli S, Deshayes E, Mognetti T, Thiesse P, Giammarile F. Additional benefit of F-18 Fdg Pet/Ct in the staging and follow-up of pediatric rhabdomyosarcoma. *Clin Nucl Med.* (2011) 36:672–7. doi: 10.1097/RLU.0b013e318217ae2e

27. Batouli A, Braun J, Singh K, Gholamrezanezhad A, Casagranda BU, Alavi A. Diagnosis of non-osseous spinal metastatic disease: the role of Pet/Ct and Pet/Mri. *J Neurooncol.* (2018) 138:221–30. doi: 10.1007/s11060-018-2794-8

28. Cook GJ, Maisey MN, Fogelman I. Normal variants, artefacts and interpretative pitfalls in pet imaging with 18-fluoro-2-deoxyglucose and carbon-11 methionine. *Eur J Nucl Med.* (1999) 26:1363–78. doi: 10.1007/s002590050597

29. Metser U, Lerman H, Blank A, Lievshitz G, Bokstein F, Even-Sapir E. Malignant involvement of the spine: assessment by 18f-Fdg Pet/Ct. *J Nucl Med.* (2004) 45:279–84.

30. Quick HH. Integrated Pet/Mr. *J Magn Reson Imag.* (2014) 39:243–58. doi: 10.1002/jmri.24523

31. Sa R, Liu D, Zhao H, Hou S, Lin Q, Guan F. Utility of [(18)F] fluorodeoxyglucose positron emission tomography/computed tomography for staging and therapy response evaluation in pediatric rhabdomyosarcoma: a case series and literature review. *Front Med.* (2020) 7:281. doi: 10.3389/fmed.2020.00281

32. Sun KK, Shen XJ. Small bowel metastasis from pulmonary rhabdomyosarcoma causing intussusception: a case report. *BMC Gastroenterol.* (2019) 19:71. doi: 10.1186/s12876-019-0990-4

33. El-Kholy E, El Nadi E, Hafez H, Ahmed S, Younes A, El-Kenanii N, et al. Added predictive value of 18f-Fdg Pet/Ct for pediatric rhabdomyosarcoma. *Nucl Med Commun.* (2019) 40:898–904. doi: 10.1097/MNM.0000000000001040

34. Casey DL, Wexler LH, Fox JJ, Dharmarajan KV, Schoder H, Price AN, et al. Predicting outcome in patients with rhabdomyosarcoma: role of [(18)F]fluorodeoxyglucose positron emission tomography. *Int J Radiat Oncol Biol Phys.* (2014) 90:1136–42. doi: 10.1016/j.ijrobp.2014.08.005

35. Abramowsky CR, Katzenstein HM, Alvarado CS, Shehata BM. Anaplastic large cell neuroblastoma. *Pediatr Dev Pathol.* (2009) 12:1–5. doi: 10.2350/07-04-0255.1

36. Duckett JW, Koop CE. Neuroblastoma. *Urol Clin North Am.* (1977) 4:285–95.

37. Patnaik S, Malempati AR, Uppin M, Susarla R. Rare mediastinal masses: imaging review. *J Cancer Res Ther.* (2021) 17:13–21. doi: 10.4103/jcrt.JCRT_587_19

38. Sharp SE, Gelfand MJ, Shulkin BL. Pediatrics: diagnosis of neuroblastoma. *Semin Nucl Med.* (2011) 41:345–53. doi: 10.1053/j.semnuclmed.2011.05.001

39. Piccardo A, Morana G, Puntoni M, Campora S, Sorrentino S, Zucchetta P, et al. Diagnosis, treatment response, and prognosis: the role of (18)F-Dopa Pet/Ct in children affected by neuroblastoma in comparison with (123)I-Mibg scan: the first prospective study. *J Nucl Med.* (2020) 61:367–74. doi: 10.2967/jnumed.119.232553

40. Karagiannis P, Guth N, Thoennissen GB, Bern C, Sperveslage J, Oschlies I, et al. Alveolar rhabdomyosarcoma confined to the bone marrow with no identifiable primary tumour using Fdg-Pet/Ct. *Clin Sarcoma Res.* (2015) 5:24. doi: 10.1186/s13569-015-0039-6

41. Weiss AR, Lyden ER, Anderson JR, Hawkins DS, Spunt SL, Walterhouse DO, et al. Histologic and clinical characteristics can guide staging evaluations for children and adolescents with rhabdomyosarcoma: a report from the children's oncology group soft tissue sarcoma committee. *J Clin Oncol.* (2013) 31:3226–32. doi: 10.1200/JCO.2012.44.6476

Frontiers in Medicine

Translating medical research and innovation into improved patient care

A multidisciplinary journal which advances our medical knowledge. It supports the translation of scientific advances into new therapies and diagnostic tools that will improve patient care.

Discover the latest Research Topics

See more →

Frontiers

Avenue du Tribunal-Fédéral 34
1005 Lausanne, Switzerland
frontiersin.org

Contact us

+41 (0)21 510 17 00
frontiersin.org/about/contact